Final Technical Report

Earthquake Frequency Statistics, Seismic Hazard, and the Mechanics of Faulting

USGS Award Number : 1434-94-G-2460
P.I.: Steven G. Wesnousky
Institution: University of Nevada, Reno
Address: Center for Neotectonic Studies
University of Nevada, Reno 89557
Tel: 702-784-1382
FAX: 702-784-1382
e-mail: stevew@seismo.unr.edu
Program Element: NEHRP-II.5

Research supported by the U.S. Geological Survey (USGS), Department of the Interior, under USGS award number 1434-94-G-2460. The views and conclusions contained in this document are those of the authors and should not be interpreted as necessarily representing the official policies, either expressed or implied, of the U.S. Government.

USGS Award Number : 1434-94-G-2460

TITLE: EARTHQUAKE FREQUENCY STATISTICS, SEISMIC HAZARD, AND THE MECHANICS OF FAULTING

P.I.: Steven G. Wesnousky
Institution: University of Nevada, Reno
Address: Center for Neotectonic Studies
University of Nevada, Reno 89557
Tel: 702-784-1382
FAX: 702-784-1382
e-mail: stevew@seismo.unr.edu

TECHNICAL ABSTRACT

We examined whether the shape of the magnitude-frequency distribution for strike-slip faults is described by the Gutenberg-Richter relationship (log(n)=a-bM) or the characteristic earthquake model, by analyzing a data set of faults from California, Mexico, Japan, New Zealand, China and Turkey. For faults within regional seismic networks, curves of the form logn/yr=a-bM, where n/yr is the number of events per year equal to magnitude M, are fit to the instrumental record of seismicity, and geological data are used to independently estimate the size and recurrence rate of the largest expected earthquakes that would rupture the total length of the fault. Extrapolation of instrumentally-derived curves to larger magnitudes agrees with geological estimates of the recurrence rate of the largest earthquakes for only four of the 22 faults if uncertainties in curve slope are considered, and significantly underestimates the geological recurrence rates in the remaining cases. Also, if we predict the seismicity of the faults as a function of fault length and slip rate, and the predicted seismicity is distributed in accord with the Gutenberg-Richter relationship, we find the predicted recurrence rate to be greater than the observed recurrence rates of smaller earthquakes along most faults. If individual fault zones satisfy the Gutenberg-Richter relationship over the long term, our observations imply that, during the recurrence interval of the largest expected earthquakes, the recurrence of lesser-sized events is not steady but, rather, strongly clustered in time. However, if the instrumental records provide an estimate of the long-term rate of small to moderate earthquakes along the faults, our observations imply that the faults generally exhibit a magnitude-frequency distribution consistent with the characteristic earthquake model. Also, we observe that the geometrical complexity of strike-slip faults is a decreasing function of cumulative strike-slip offset. The four faults we observe to be consistent with the Gutenberg-Richter relationship are among those characterized by the least amount of cumulative slip and greatest fault trace complexity. We therefore suggest that the ratio of the recurrence rate of small to large earthquakes along a fault zone may decrease as slip accumulates and the fault becomes smoother.

USGS Award Number : 1434-94-G-2460

TITLE: EARTHQUAKE FREQUENCY STATISTICS, SEISMIC HAZARD, AND THE MECHANICS OF FAULTING

P.I.: Steven G. Wesnousky
Institution: University of Nevada, Reno
Address: Center for Neotectonic Studies
University of Nevada, Reno 89557
Tel: 702-784-1382
FAX: 702-784-1382
e-mail: stevew@seismo.unr.edu

NON-TECHNICAL PROJECT SUMMARY

We use a global data set of strike-slip faults to examine the shape of the magnitude-frequency distribution along particular faults. Knowledge of the distribution is fundamental to making estimates of the future rate and size of earthquakes in seismic hazard analysis. It is well known that seismicity in a region is described by the Gutenburg-Richter relationship:

$$Log\ n = a\text{-}bM \qquad (1)$$

where n = number of events of magnitude M and a and b are empirical constants. The results of our study suggest that (1) is not true for individual faults.

INTRODUCTION

We have used a global data set of strike-slip faults to examine whether or not (a) the geometrical complexity of fault traces or (b) the shape of the magnitude-frequency distribution along particular faults is a function of the amount of cumulative strike-slip offset recorded by the faults. The motivation for (a) arises from earlier work of Wesnousky (1988) that suggested, on the basis of a small data set of faults primarily from California, that fault trace complexity decreases as a function of cumulative offset. The motivation for (b) stems from questions regarding whether or not seismicity along a single fault is described by the Gutenberg-Richter relationship:

$$Log\ n = a\text{-}bM \qquad (1)$$

where n = number of events of magnitude M and a and b are empirical constants (Ishimoto and Iida, 1939; Gutenberg and Richter, 1944). Catalogs of regional seismicity are typically well-described by the Gutenberg-Richter relationship (eq.(1)). The assumption that seismicity on a single fault also satisfies eq.(1) implies that there will be numerous lesser-size events in the time interval between the occurrence of the largest earthquakes on a fault (Fig. 1a). However, a number of studies have reported evidence to suggest that seismicity along faults does not satisfy eq.(1) across the entire magnitude range, but instead shows a greater frequency of occurrence of large earthquakes than would be expected from extrapolation of curves fit to the log-linear distribution of lesser-sized earthquakes (Wesnousky, Scholz and Matsuda., 1983; Schwartz and Coppersmith, 1984; Youngs and Coppersmith, 1985; Wesnousky, 1994). The concept now commonly referred to as the characteristic earthquake model of fault behavior (Fig. 1b). Determining whether it is the Gutenberg-Richter relationship or characteristic earthquake model that describes the seismicity along particular faults is problematic because historical records of seismicity are generally much shorter than the repeat time of the largest earthquake on a fault. However, the recurrence of the largest size events along a fault can be estimated independently with geologically determined paleoearthquake histories and fault slip rate data. Thus, in addition to examining the geometrical complexity of strike-slip faults, we combine instrumental records of seismicity with interpretation of paleoearthquake and fault slip rate data to examine the shape of the magnitude-frequency distribution for the global data set of strike-slip faults.

DATA AND ANALYSIS

Our analysis is limited to strike-slip faults that are (a) located within regional seismic networks, (b) have been the focus of fault slip rate or paleoearthquake studies, or (c) for which maps of sufficient detail exist to define discontinuities in fault trace that measure a kilometer or greater in width normal to fault strike. The faults considered are located in California, Mexico, New Zealand, Japan, China and Turkey. For convenience of presentation, the maps and a brief discussion of data bearing on the cumulative strike-slip offset and slip rate of each fault are placed in the Appendix. The location and size of steps in fault trace, measuring 1 km or more in width perpendicular to fault strike, are marked on the strip maps for each fault in Fig. A of the Appendix. Following the approach of Wesnousky (1988), we define the complexity of a fault trace as the number of observed steps per unit length of fault trace. Table 1 summarizes the data and references describing the length, cumulative strike-slip offset, slip rate and fault trace complexity for each fault. When uncertainty exists in defining the number of steps along a fault trace a range of values is listed for the number of steps and, hence, fault trace complexity. The smaller values of complexity reflect the number of clearly defined steps, and the larger values reflect the sum of both clearly defined and possible steps. Included as "possible steps" in some

cases are those steps located very close to the ends of faults that may be part of a fault splay or termination. The value of fault trace complexity is plotted versus cumulative strike-slip offset in Fig. 2. We defer discussion of the plot to the Discussion section of the paper.

It is only the faults listed in Table 2 and located in California, Japan, New Zealand, and Baja California that fall within regional seismic networks that have been recording for a relatively long period of time. The faults of southern California fall within the CIT-USGS network, which has been recording since 1932 (Given, Hutton and Jones, 1987). The epicentral distribution of seismicity for events of $M \geq 3$ for the period 1932-92 is shown in Fig. 3a within a polygon encompassing all of the southern California faults listed in Table 2. The faults of northern California are within the USGS-CALNET seismic network, which has been officially recording since 1969. The epicentral distribution of seismicity for events of $M \geq 3$ for the period 1969-92 is shown in Fig. 3a for a region encompassing the northern California faults listed in Table 2. The San Miguel-Vallecitos fault is the only fault zone considered in Baja California, Mexico. The RESNOR seismic network of northwestern Baja California has been in operation since 1976 (Vidal and Munguia, 1993). We show the polygon that encompasses northwestern Baja California in Fig. 3a. Seismicity in the vicinity of the Japanese faults has been recorded by the Japanese Meteorological Agency network since 1926 (Ichikawa, 1969; Mochizuki, Kobayashi and Kishio, 1978; Yokoyama, 1984). The epicentral distribution of $M \geq 3$ events in the vicinity of the Japanese faults listed in Table 2 is shown for the period 1926-92 in Fig. 3b. The Institute of Geological and Nuclear Sciences (formerly DSIR) has been operating a computerized seismic network in New Zealand since 1964 (Smith, 1976). The epicentral distribution of $M \geq 3$ events in the area of the New Zealand faults listed in Table 2 is shown in Fig. 3c for the period 1964-92. All the epicentral distributions represented in Fig. 3 are limited to events with depths <20 km. Slightly different methods are used in each network to estimate magnitude, but the various scales (local magnitude, M_L, in southern California and New Zealand, coda magnitude, Mc, in northern California and Baja California, and the Japanese Meteorological Agency magnitude, M_{JMA}, in Japan) generally correlate with moment magnitude (Given et al., 1987; Smith, 1976; Lee, Bennett and Meagher, 1972; Utsu, 1982; Hanks and Kanamori, 1979), which we use later in the paper to define the size of the largest earthquakes on all of the faults.

For each of the regions enclosed by polygons in Fig. 3a (northern and southern California, and Baja California), Fig. 3b (Japan) and Fig. 3c (New Zealand), the number of events per year are plotted as a function of magnitude in Fig. 4 (magnitude-frequency distributions). Also shown in Fig. 4 are histograms of the number of events per year for each region. The magnitude-frequency curves are approximately of linear slope over the range of highest magnitudes for each region, and show a decrease to smaller slopes at smaller magnitudes. For the purpose of this analysis we attribute the decrease in slope at smaller magnitudes to the magnitude detection threshold for each region. We note that value by a vertical dotted line in each plot of Fig. 4 and only consider seismicity of magnitude greater than the detection threshold in the ensuing analysis. Analysis of the distributions is therefore limited to $M \geq 3$ for the southern California region, $M \geq 2$ for the northern California region, $M \geq 3$ for the northwest Baja California area, $M \geq 4.5$ for central Japan, and $M \geq 4$ for central New Zealand (Fig. 4). We also limit our attention to the period 1944-92 in the case of the CIT-USGS data because magnitudes were only reported to the nearest 0.5 magnitude unit prior to that time. Each magnitude-frequency distribution is described by a set of lines in the form of eq.(1). The value of b is fit by the maximum likelihood method (Utsu, 1965; Aki, 1965), and is shown for each region in Fig. 4. The value of a is fit to satisfy the total number of events greater than the detection threshold magnitude obtained in Fig. 4. For each region, the three diagonal dotted lines represent the maximum-likelihood fit to the data and the 95% confidence limits for that fit, and thus define the regional b-value. The number N of events used in determining the b-value, the estimated b-value and 95% confidence limits,

and the instrumental seismic moment rate $\dot{M}_o$ *(instr)* is also listed in the top right corner of each plot. $\dot{M}_o$ *(instr)* is the sum of the seismic moments of all recorded events of magnitude greater than the detection threshold magnitude divided by the number of years of recording, where the seismic moment of each event is determined from the magnitude by use of the relationship Log Mo=1.5M+16.1 (Hanks and Kanamori, 1979).

To characterize the magnitude-frequency distribution for individual faults, we consider only seismicity recorded within polygons encompassing each of the faults in Table 2. The polygons for faults in California, Baja California, Japan and New Zealand are shown in Fig. 5. The polygons generally include seismicity within approximately 20 km of the respective faults, except in cases where neighboring active faults are closer than 20 km, in which case the width is reduced. The character of seismicity for each fault is depicted by the plots in Fig.s 6 and 7. Fig. 6 shows the discrete number of events per year versus magnitude and Fig. 7 shows a histogram of the number of events per year determined from the seismicity recorded in the respective polygons. The histograms serve to show any temporal variations in seismicity rates. The open circles in the magnitude-frequency plots for each fault (Fig. 6) represent the instrumental record of seismicity. The plots do not show events of magnitudes less than the detection threshold magnitudes for each region, except in the case of Japan where seismicity down to M4 is shown. The recorded seismicity at M4 is assumed on the basis of Fig. 4 to closely approximate actual seismicity in central Japan. Lines of the form of eq.(1) are fit to the instrumental record of seismicity (open circles) for each fault by use of the maximum-likelihood method. The maximum-likelihood fit to the instrumental record and 95% confidence limits are also shown as a set of three heavy dotted lines which, for clarity, are only plotted at magnitudes greater than 5. We have not attempted to fit lines of the form of eq.(1) to the Hope, Wairau, Wairarapa, Wellington and Japanese faults, because each of these areas record fewer than 10 events with magnitudes greater than the detection threshold magnitude. With the assumption that the magnitude-frequency distributions remain linear at magnitudes greater than those recorded during the instrumental recording period, the heavy dotted lines may be used to place bounds on the expected rate of occurrence of the largest expected earthquakes along the fault zones. Also plotted in the magnitude-frequency plots for each fault are a set of open and closed diamonds. The diamonds represent bounds on the size and recurrence rate of the maximum expected earthquake along each fault zone arising from interpretation of geological observations. Determination of the values is described in the following paragraphs.

Estimation of the maximum expected earthquake size along mapped faults commonly arises from measures of fault length. For the purposes of this analysis, we assume that each of the faults is capable of rupturing along the entire fault length during a single earthquake. The seismic moment that would be associated with rupture of the entire fault length can be estimated from empirical measurements of seismic moment versus fault length for instrumentally recorded earthquakes in interplate (Fig. 8a) and Japanese intraplate (Fig. 8b) environments. The interplate and Japanese intraplate data sets are taken from the compilations of Romanowicz (1992) and Wesnousky et al. (1983), respectively. Lines of the form $M_o^e = C_o L^d$ are fit to the data sets, where M_o^e is the expected seismic moment, L is earthquake rupture length, and C_o and d are empirically derived constants. The curve fits labeled "preferred", "minimum" and "maximum" provide us the empirical basis to estimate the preferred (M_o^epref), minimum (M_o^emin) and maximum (M_o^emax) bounds on the seismic moment for an earthquake rupturing the entire length of each fault listed in Table 2. The seismic moments (M_o^e) of earthquakes, assuming a complete rupture of each fault are converted to moment magnitude and listed for each fault in Table 2.

We may further estimate the recurrence interval T of maximum expected events along each fault zone in Table 2 by dividing the cumulative seismic moment release ΣM_o expected during the recurrence interval T by a geologically determined average seismic moment rate $\dot{M}_o^g$ for the fault

$$T=\Sigma M_o/\dot{M}_o^g=(M_o^e+\Sigma M_o^{sm})/\dot{M}_o^g \qquad (2)$$

where M_o^e is the seismic moment of the maximum expected event and ΣM_o^{sm} is the sum of seismic moment release of events with $M_o < M_o^e$ which will contribute to fault slip during the recurrence interval T. Eq. (2) can be rewritten as follows:

$$T=(M_o^e/\dot{M}_o^g)/(1-(\dot{M}_o^{sm}/\dot{M}_o^g)) \qquad (3)$$

whereby $\dot{M}_o^{sm}$ is approximated by the empirically determined instrumental moment release rate $\dot{M}_o$ *(instr)*, which is listed for each fault in the lower left of each plot in Fig. 6. Seismic moment *Mo* is defined to equal μLWU (Aki and Richards, 1980), where μ is the shear modulus (assumed to equal 3×10^{11} dyne/cm^2), L the fault length, W the fault width (approximated to 15 km for all faults), and U the coseismic slip. Substituting geologically determined fault slip rate $\dot{U}^g$ for coseismic slip U, we can define the rate of seismic moment release $\dot{M}_o^g=\mu LW\dot{U}^g$ (e.g. Brune, 1968), using the same values of μ and W as above. The fault maps we have used to estimate fault lengths L and a discussion of the geological data bearing on the slip rate $\dot{U}^g$ for each of the faults listed in Table 1 are provided in the Appendix. The minimum, maximum and preferred values of slip rate are further summarized in Table 1 along with values of fault length L. The data provide the basis to define the preferred $\dot{M}_o^g$ *(pref)*, maximum $\dot{M}_o^g$ *(max)*, and minimum $\dot{M}_o^g$ *(min)* values of seismic moment release rate for each fault. $\dot{M}_o^g$ *(min)* and $\dot{M}_o^g$ *(max)* are shown at the bottom of each plot in Fig. 6 ($\dot{M}_o$ *(geol)*). Recalling that minimum, maximum and preferred values of M_o^e may be determined from empirical relationships in Fig. 8, we use eq.(3) to place bounds on the recurrence interval T for the largest expected earthquakes along the fault zones. More specifically, the preferred estimate of return time is defined as

$$Tpref=(M_o^e(pref)/\dot{M}_o^g(pref))/(1-(\dot{M}_o^{sm}/\dot{M}_o^g(pref))) \qquad (4)$$

and maximum *(Tmax)* and minimum *(Tmin)* bounds on recurrence interval are calculated as

$$Tmin1=(M_o^e(min)/\dot{M}_o^g(max))/(1-(\dot{M}_o^{sm}/\dot{M}_o^g(max))) \qquad (5a)$$

$$Tmin2=(M_o^e(min)/\dot{M}_o^g(min))/(1-(\dot{M}_o^{sm}/\dot{M}_o^g(max))) \qquad (5b)$$

$$Tmax1=(M_o^e(max)/\dot{M}_o^g(min))/(1-(\dot{M}_o^{sm}/\dot{M}_o^g(min))) \qquad (5c)$$

$$Tmax2=(M_o^e(max)/\dot{M}_o^g(max))/(1-(\dot{M}_o^{sm}/\dot{M}_o^g(min))) \quad (5d)$$

The results of applying eqs.(4) and (5) to each of the fault zones are summarized in Table 2 and also depicted as small diamond symbols on the magnitude-frequency distribution plots provided for each of the faults in Fig. 6. In each case, the solid diamond represents the preferred estimate of maximum earthquake size derived from Fig. 8 and recurrence rate derived from eq.(4). The four open diamonds define the bounds placed by the maximum and minimum earthquake size (Fig. 8) and application of the four return time equations (eq.(5)). Finally, the set of light dotted lines are drawn to bound the geological estimates of recurrence rate from eqs.(4) and (5) (diamonds), with slopes equal to the b-value determined from analysis of the regional seismicity shown in Fig. 4.

DISCUSSION

In the application of magnitude-frequency observations to seismic hazard analysis, there are two end member cases that have commonly been assumed. The first arises when geological data are available to place constraints on the size and recurrence rate of the largest earthquakes on a fault, but no instrumental record of seismicity exists to place limits on the rate of small to moderate events. In this case a line of the form of eq.(1) is chosen to intersect the geologically determined value and, in turn, used to estimate the recurrence rate of lesser-sized but potentially damaging earthquakes (e.g. Wesnousky et al., 1983). The slope b of the line is often taken to equal the value determined from an analysis of seismicity over a much broader region. The slopes of the light dotted lines in Fig. 6 that intersect the preferred (solid diamonds) and bounding (open diamonds) estimates of recurrence rate arising from interpretation of geological data are equal to the maximum-likelihood and 95% confidence limits on b that were derived from analysis of seismicity recorded in the enclosing region (Figs. 3 and 4). It may be observed that the recurrence rate of lesser-sized events predicted by the b-value curves is generally greater than the actual number of events observed for each fault. We formalize the difference by calculating the ratio of the recurrence rate of M4 earthquakes predicted by extrapolation of the b-value curves to the actual rate of M4 earthquakes observed during the instrumental period of recording (open circles). The ratio should be near 1 if the magnitude-frequency distribution is described by the Gutenberg-Richter relationship (Fig. 1a). A ratio >1 indicates that the shape of the magnitude-frequency distribution is better described by the characteristic earthquake model (Fig. 1b). The ratio of predicted to observed recurrence rate of M4 earthquakes is plotted in Fig. 9 as a function of the cumulative strike-slip offset registered across each fault. The most striking aspect of Fig. 9 is that the ratio of preferred estimates is never less than 1. Indeed, in most cases extrapolation of the geological data predicts tens to hundreds of times more M4 events than are actually observed. In only three of the 19 cases do the error bars permit a ratio of 1. Thus, in nearly all cases, the magnitude-frequency distributions resulting from combining the instrumental and geological observations appear most consistent with the characteristic earthquake model.

The second end member arises for the situation where geological constraints are not available to place limits on the size and recurrence rates of the largest expected earthquakes along a particular fault. In this case the instrumental record of seismicity along the fault zone is described by eq.(1) and the resulting b-value curve extrapolated to larger magnitudes to estimate the recurrence rate for the largest expected earthquakes along a fault zone. In Fig. 6, we compare for each fault the recurrence rates of the largest earthquakes determined on geological grounds (diamonds) to the recurrence rate determined by extrapolating the maximum likelihood fits to the

instrumental data (open circles) to large magnitudes (heavy dotted lines). The ratio of the preferred geological estimate of recurrence rate (solid diamond) to the maximum-likelihood fit to the instrumental data at the same magnitude is plotted for the faults as a function of cumulative strike-slip offset in Fig. 10. Again, the ratio should be near 1 if the magnitude-frequency distribution is described by the Gutenberg-Richter relationship, and a ratio >1 indicates the magnitude-frequency distributions are better described by the characteristic earthquake model. All the ratios of the preferred estimates are greater than 1, and the error bars allow a ratio of 1 in only two out of 11 cases in Fig. 10. In most cases, the preferred geological estimate of recurrence rate is tens to hundreds of times greater than the recurrence rate predicted by extrapolating the maximum-likelihood fit to the instrumental data. The observations are consistent with nearly all of the magnitude-frequency distributions being described by the characteristic earthquake model (Fig. 1).

An important consideration is whether or not the magnitude-frequency distributions in Fig. 6 reflect the long term seismicity of the respective faults. Although the magnitude-frequency distributions we have constructed appear to be consistent with the characteristic earthquake model, it is possible that our observations are due to non-stationarity or clustering of seismicity, and that seismicity rates satisfy the Gutenberg-Richter relationship over an entire earthquake cycle. The instrumental records would therefore have sampled quiet periods of seismicity relative to long term rates for at least 80% of the faults in our data set. We can use a simple model to place bounds on the amount of clustering in rate of seismicity that would be necessary for all the faults to have long-term seismicity consistent with the Gutenberg-Richter relationship. Assume that fluctuations in seismicity rates along a fault are reflected by changes in productivity, while the b-value remains constant. Further note that, on average, the instrumental recording period is about 10% of the return time of the largest earthquakes on each fault, or in other words, 10% of the earthquake cycle (Fig. 11a), and that the average discrepancy between the actual number of M4 events recorded and the number of M4 events predicted by the geological data is about one order of magnitude (Fig. 11 b). For our analysis, assume that the average productivity over the entire earthquake cycle for any fault (in this case number of M4 events per year) is equal to 1, but the cycle is divided into periods of 'high' and 'low' rates of seismicity. We set the 'low' rates of seismicity equal to 0.1, consistent with our observations in Fig. 11b. The 'high' seismicity rates must therefore be >1, and would for example average 1.9 if they occupied 50% of the cycle. The model is schematically illustrated in Fig. 11c. With this model, we may use a Monte Carlo approach to answer the question "Given that seismicity is clustered, the cluster is randomly located in the earthquake cycle, and the instrumental period of recording is limited to 10% of the earthquake cycle (also randomly placed), what is the probability that the rate of seismicity sampled by the instrumental record is less than the long-term average?" The results are shown by a set of histograms (Fig. 12) for the cases where we have limited 'high' seismicity rates to 20%, 30% and 50% of the duration of the cycle, respectively. The histograms show the rates of seismicity predicted in 2000 simulations. Examination of the histograms indicates that 'high' seismicity rates must be limited to <20% of the earthquake cycle to yield results similar to our observations (Fig. 12a), that is, 18 out of the 22 faults in the data set showing rates of seismicity less than the predicted long-term average rates (Fig. 6). Similar results are obtained if we assume that the period of 'high' rates always occurs at the same position in the cycle. We also see in Fig. 12a that there should be a number of faults that show 'high' rates, or in other words seismicity rates that are considerably greater than the predicted recurrence rates of M4 in Fig. 6. 'High' rates are clearly observed only along the Yamasaki fault, and uncertainty estimates of predicted M4 recurrence rate might also allow for the possibility of 'high' rates on an additional three faults (Fig. 6 and Fig. 9). Hence, the possibility exists that the seismicity of the faults is described by the Gutenberg-Richter relationship over an entire earthquake cycle, but if so, it

appears that extreme clustering is required to argue that this is true. Alternatively, the magnitude-frequency distributions in Fig. 6 may reflect the long-term seismicity of the faults, in which case it is useful to examine the physical ramifications of such an interpretation.

Because geometrical complexities along fault traces appear to control the character of earthquake ruptures (e.g. Seagall and Pollard, 1980; Sibson, 1985), it is also reasonable to question whether the shape of the magnitude-frequency distribution along faults is also a function of fault trace complexity. To this end we further investigate the hypothesis that fault trace complexity is a decreasing function of cumulative slip (Wesnousky, 1988). A trend of decreasing complexity as a function of increasing cumulative slip is evident in Fig. 2, clearly consistent with the early hypothesis. The plot of M4 ratio versus cumulative slip (Fig. 9) therefore allows the possibility that the discrepancy between predicted and observed number of M4 events may be an increasing function of cumulative slip and decreasing fault trace complexity. The seismicity of faults may therefore initially be characterized by ratios of 1 or less, but with the process of smoothing eventually resulting in the development of a long, throughgoing fault trace, an increase in size of the largest earthquakes, and a decrease in the number of small earthquakes (ratio >1), the latter attributed to a smoothing of the stress field along the fault (e.g. Wesnousky, 1990; Ben Zion and Rice, 1993). We might then hypothesize that ongoing cumulative slip eventually causes actual faults to coalesce, and so the longest faults are products of the largest amounts of cumulative slip, and have the largest ratios. Additionally, the rate at which fault smoothing and seismicity changes occur might be influenced by the fault slip rate. We investigate these possibilities by plotting the M4 ratio (as used in Fig. 9) against fault length in Fig. 13 and slip rate in Fig. 14. The plots together show that the highest values of ratio tend to be associated with the longest and most rapidly slipping faults. The trend of increasing ratio with both fault length and slip rate (Fig. 13 and Fig. 14) would imply that the size of the largest earthquakes on a fault increase and the number of small events decrease as both individual fault strands and faults coalesce to form a long, smooth fault trace, and the rate at which the fault trace becomes longer and smoother depends on the slip rate on the fault. However, the argument that faults lengthen as a direct result of cumulative slip may not be strictly applicable to all strike-slip faults. The San Andreas fault, for instance has grown in length as a result of northward movement of a plate boundary triple junction, and not strictly by coalescence of a number of fault strands. Also, it is possible that transform faults that displace thin oceanic crust initiate with relatively simple traces, and so minimal step reduction would occur with ongoing cumulative slip. In general, the different tectonic environments represented in our data-set will influence the rates of fault smoothing and lengthening, and so contribute to the scatter evident in Figs. 2, 9, 10, 13 and 14.

Although our estimates of recurrence rate are based on geological observations, they are also model dependent (eqs.(4) and (5)). The use of total fault length in deriving maximum earthquake size may be inconsistent with observations in areas like California, where the largest historical earthquakes may arise from rupture of segments of the fault less than the total fault lengths. However, assumption of a smaller rupture length on a fault will only add more support to our interpretation of Fig. 6, that most of the faults show a characteristic earthquake distribution. Assumption of a lesser maximum fault rupture length predicts a smaller maximum earthquake M_o^e. But interpretation of the smaller value with eqs. (4) and (5) also predict that it should occur more frequently. The net result is then to generally increase the discrepancy between the geological estimates and the extrapolation of the instrumental record. One may also consider the possibility of ruptures extending beyond our defined fault lengths, and factor larger values of M_o^e into eqs. (4) and (5). The tendency will be to reduce the predicted recurrence rates of M_o^e, and therefore reduce the discrepancy between geological and extrapolated instrumental recurrence rates. However, the recurrence rates will only be reduced significantly in terms of our

interpretation of Fig. 6 if on average M_o^e is increased about 30 fold. It seems physically unrealistic to consider increasing M_o^e by this amount on those faults we have considered.

There may be some bias in our calculations because we assume that the majority of seismic moment is released during the repeated occurrence of earthquakes of the same size. The concern can be addressed by further assuming that seismicity satisfies the Gutenberg-Richter relationship up to the maximum expected event defined by assuming rupture of the entire fault length. Seismic moment is therefore also released by events close in size but < Mmax, and the recurrence rate of the events across the entire magnitude range can be calculated by using estimates of Mmax, b-value and slip rate for each fault. Following the approach of Wesnousky et al. (1983), and using the estimate of Mmax, slip rate, and b-value for each fault, we calculate and show in Fig. 15 the expected number of M4 earthquakes for each of the faults in the data set versus the actual observed number of events. On average, the predicted recurrence rates are about 10 times greater than the observed values. The discrepancy is consistent with the characteristic earthquake model. Hence, the principal observations and interpretations made from Figs. 6, 9 and 10 are apparently not significantly altered if a distribution of large earthquakes is allowed.

Our estimates of earthquake recurrence rates along the faults estimated from eqs. (4) and (5) may also be compared to estimates of earthquake size and recurrence that come directly from trenching studies, where the estimation of large surface rupturing events is determined directly from structural and stratigraphic analysis of offset sediments in the trench. Similarly, historical data define the sizes of large earthquakes for a number of the faults listed in Table 2. The results of trenching studies and historical observations are summarized in Table 3 and the Appendix, and plotted as open triangles in Fig. 6. For the majority of the faults, the estimates of earthquake size and recurrence rate resulting from paleoearthquake and historical data (triangles in Fig. 6) fall within or close to the uncertainties in our estimates based on fault length and eqs.(4) and (5) (diamonds). It is only along the Whittier-Elsinore, Calaveras-Concord-Green Valley-Bartlett Springs and San Jacinto faults that predicted recurrence rates and event sizes resulting from trenching and historical records do not fall within the bounds resulting from application of eqs. (4) and (5). The discrepancies likely reside in the trenching studies and historical observations reflecting the occurrence of events that rupture less than the entire length of the respective faults. Nonetheless, even in these cases, the discrepancies between the recurrence intervals predicted by trenching studies and historical observations (triangles) and those predicted from extrapolation of instrumental records are similar to the discrepancies found when using the fault model embodied in eqs.(4) and (5). Hence, whether we use the direct results of trenching studies and historical observations or estimates from eqs.(4) and (5), it is observed that the majority of faults display distributions consistent with the characteristic earthquake model.

The magnitude-frequency distributions for most of the faults in Table 2 are consistent with the characteristic earthquake model, despite the fact that many of the boxes shown in Fig. 5 encompass events that have not occurred directly on the faults, most notably the aftershocks of some major earthquakes. The distributions of moderate to large earthquakes appear as large peaks on the histograms of Fig. 7 for the San Jacinto, northern and southern San Andreas, Awatere, Yamasaki and Tanna faults. To examine the influence of aftershock activity on the magnitude-frequency distributions, we remove seismicity occurring up to one year after each of the main shocks, and plot the resulting recurrence rates (solid circles) and maximum-likelihood fits to the instrumental data (hachured lines) in Fig. 6. The removal of aftershocks clearly increases the discrepancy between predicted and observed recurrence rates of all events, and so strengthens the interpretation that the characteristic earthquake model best describes the seismicity of the faults. We do not attempt to alter our box widths to selectively exclude "background" seismicity that we observe in the crustal blocks adjacent to the faults, but in light

of the above, the effect of doing this would be to increase the discrepancy between predicted and observed recurrence rates.

CONCLUSIONS

Magnitude-frequency distributions from a data set of 22 strike-slip faults from around the world are generally consistent with the characteristic earthquake model, whereby geological estimates of the recurrence rate of the largest earthquakes are orders of magnitude more frequent than rates predicted from interpretation of earthquake statistics. It is possible that the magnitude-frequency distributions may simply be an artifact of a short instrumental recording period, and seismicity over an entire earthquake cycle is instead described by the Gutenberg-Richter relationship. However such an interpretation requires that seismicity along faults be limited or clustered in periods of time less than or equal to about 20% of the return period of the largest expected earthquakes on a fault. We suggest that the observed magnitude-frequency distributions do reflect the long-term character of seismicity along faults. The suggestion allows the possibility that the ratio of small to large earthquakes along a fault decreases with increasing cumulative slip. We observe that fault trace complexity is a decreasing function of cumulative slip, a smoothing process that would allow for longer rupture lengths and a more homogenous stress field along the fault, therefore increasing the size of the largest earthquakes and reducing the number of small earthquakes. Regardless of a physical basis for the characteristic earthquake model, the model is more appropriate than the Gutenberg-Richter relationship in describing the seismicity of strike-slip faults for seismic hazard analysis.

APPENDIX

We outline here the references and basis for assigning maximum, minimum and preferred slip rates to faults, and data bearing on the cumulative strike-slip offset registered across each fault listed in Tables 1, 2 and 3. Additionally, a strip map for each fault in Table 1 is provided (Fig. A) and annotated to show the number of steps $\geq$ 1 km width. The descriptions for individual faults given below follow the same sequence as that presented in Table 1.

Southern California

Right separation of at least 150 km has been accommodated along the present trace of the *San Andreas fault* since early Miocene (Crowell 1962; Grantz and Dickenson, 1968; Hill, 1981). The total length of the fault where exposed onshore is about 1000 km. The surface trace of the San Andreas fault is uninterrupted except for a 1 km releasing step at Parkfield. The southern 550 km length of the San Andreas fault strikes southeast between Parkfield and Bombay Beach. The summary of Petersen and Wesnousky (1994) places the slip rate of the fault at 16 to 43 mm/yr between Tejon Pass and Cajon Pass, 11 to 35 mm/yr south of Cajon Pass, and the preferred slip rate at Cajon Pass is 24 $\pm$ 4 mm/yr.

Cumulative left-lateral strike-slip offset across the *Garlock fault* is 64 km, as evidenced by the separation of a Mesozoic dike swarm (Smith, 1962). A 3-4 km wide step occurs along the fault at Fremont Valley. The summary by Petersen and Wesnousky (1994) places the slip rate of the Garlock fault at 4 to 9 mm/yr.

The *Newport-Inglewood fault* strikes northwest from Newport Beach to the Baldwin Hills and is expressed topographically by an aligned series of low hills that rise 120 m above the adjacent plains. The fault zone is a series of discontinuous north to northwest striking faults and

northwest to west trending folds (Barrows, 1974). Estimates of total dextral strike-slip offset across the fault zone range from 200 m near the Baldwin Hills to a maximum of 10 km near Huntington Beach (Barrows, 1974). The fault zone is about 60 km long where it exists onshore, and is broken by four prominent steps. Petersen and Wesnousky (1994) show the slip rate of the Newport-Inglewood fault to be 0.1 to 6 mm/yr, with the most tightly constrained estimate equal to 0.6 mm/yr.

The *Whittier-Elsinore fault zone* strikes northwest for about 240 km from near the US-Mexico border to north of Lake Elsinore. A review of all relevant work to date led Hull and Nicholson (1992) to suggest 10-15 km as the most reliable estimate of total dextral strike-slip offset across the fault. The 240 km length of the fault zone is interrupted by three steps. The summary of Petersen and Wesnousky (1994) places the slip rate of the Whittier-Elsinore fault at between 1.5 and 9.3 mm/yr, with preferred value of 5 mm/yr.

The *San Jacinto fault zone* strikes southeastward from the southern San Andreas fault for a distance of about 230 km. The summary of Petersen and Wesnousky (1994) reports 24 km cumulative right-lateral strike-slip offset across the San Jacinto fault, and Rockwell et al. (1990) estimate a slip rate of 7 to 19 mm/yr, with preferred value of 12 mm/yr. North of the Imperial fault, the San Jacinto fault is interrupted by five steps greater than 1 km width, dividing the fault into the Claremont, Casa Loma-Clark, Coyote Creek, Borrego Mountain, Superstition Mountain and Superstition Hill segments.

Mojave Desert

Estimates of slip rates on the Mojave faults are thus far primarily limited to determination from offset rocks of pre-Quaternary age. For that reason we limit our attention to observations of cumulative strike-slip offset and fault trace complexity.

Mesozoic intrusive, and Tertiary volcanic rocks record dextral strike-slip offset of 8.2 km across the *Calico-Mesquite fault* (Dokka, 1983). Three, and possibly four steps 1 km or more in width are mapped along the 125 km long, northwest-striking fault.

Right-lateral strike-slip offset of Tertiary volcanic and sedimentary rocks of 6.4-14.4 km has occurred across the *Pisgah fault* in 2 to 20 m.y. (Dokka, 1983). Two steps occur along the 64 km long fault.

The *Camp Rock fault* has produced 1.6 to 4 km dextral strike-slip offset of Tertiary volcanic and Mesozoic intrusive rocks during the late Cenozoic (Dokka, 1983). One, and possibly three steps are mapped along the fault, and the southern half of the Camp Rock fault ruptured during the June 28, 1992, magnitude 7.5 Landers earthquake (e.g. Petersen and Wesnousky, 1994).

The *Helendale fault* is the western-most of northwest striking faults in the Mojave Desert. 3 km dextral strike-slip offset has occurred across the fault during late Cenozoic times (Dokka, 1983). Three steps are mapped along the fault.

Strike-slip offset of 1.5 to 3 km has occurred across the *Lenwood fault* in the late Cenozoic (Dokka, 1983). The fault has one, and possibly up to two poorly defined steps.

Northern Baja California, Mexico

The *San Miguel-Vallecitos fault* strikes northwest across northern Baja California (Gastil, Phillips and Allison, 1975; Harvey, 1985) for about 160 km. Maximum post Cretaceous strike-slip offset across the fault is 500 m (Harvey, 1985) to 600 m (Hirabayashi et al. 1994). Long term slip rates of 0.1-0.5 mm/yr have been determined for the fault (Hirabayashi, Rockwell, Wesnousky, Stirling and Suarez-Vidal, 1995). Four, and possibly six steps are mapped along the length of the fault.

Northern California

The 460 km long northern section of *San Andreas fault* of the fault between Cape Mendocino and San Juan Bautista has slip rate estimates that range from 7 to 32 mm/yr. The minimum is based on a displaced channel in the San Francisco peninsula area (Prentice, Niemi and Hall, 1993), and the latter based on unpublished geodetic analyses (Working Group on California Earthquake Probabilities, 1990). The fault trace is not interrupted by any steps.

The northern section of the *Calaveras-Concord-Green Valley-Bartlett Springs fault zone* lies to the north of the junction of the Hayward and Calaveras faults, and is about 220 km long. Kintzer, Brooks and Cummings (1977) report that a middle Miocene shoreline exposed near Calaveras Reservoir may be offset in a right-lateral sense for a distance of 24 km across the Calaveras fault. The fault zone is broken by five and possibly seven steps of greater than 1 km width. A minimum slip rate of 3 mm/yr for the fault zone occurs on the Concord fault (Galehouse, 1991), and a 25 mm/yr maximum slip rate is based on subtracting the minimum slip rates of the northern San Andreas and Hayward faults from the geodetic strain rate across the San Andreas, Hayward and Calaveras faults (38$\pm$3 mm/yr; Matsu'ura, Jackson and Cheng, 1986). An 8 mm/yr preferred slip rate is calculated by assuming that the 17 mm/yr southern Calaveras slip rate (Savage, et al., 1979) is partitioned between the Hayward and Calaveras faults to the north of the junction of the two faults.

The *Hayward-Rogers Creek-Maacama fault zone* strikes northwest for about 250 km from near the junction with the Calaveras fault. Slip rates of 2.1 mm/yr have been determined for the Rogers Creek fault from offset buried channel deposits (Budding, Schwartz and Oppenheimer, 1991), and 9 mm/yr for the Hayward fault (Lienkaemper, Borchardt and Lisowski, 1991). No estimates of the total strike-slip offset are available for the Hayward-Rogers Creek-Maacama fault zone. Two steps are mapped on the fault zone at the intersection of the Rogers Creek and Maacama faults, and one step may exist beneath San Pablo Bay.

Japan

Three, to possibly five steps occur along the 215 km of the *Median Tectonic Line* that crosses Shikoku Island. Minimum right-lateral strike-slip offset across the fault is about 5 km (Okada, 1980), and slip rates are in the range 7-8 mm/yr, with 7 mm/yr being the preferred value (Okada, 1980; Research Group for Active Faults of Japan, 1992).

Paleozoic rocks have undergone left-lateral separation of 3-5 km across the *Neodani fault.* Slip rates of 1-2 mm/yr, sinistral, have been estimated for the fault, with 2 mm/yr being the preferred value (Okada and Ikeda, 1991; Research Group for Active Faults of Japan, 1992). Two, and possibly three steps occur along the fault.

Left-lateral separations of 7 to 10 km have been recorded by Quaternary land forms offset across the *Atera fault* (Research Group for Active Faults of Japan, 1992). Slip rates of 3-5.2 mm/yr have been estimated for the fault, with 5.2 mm/yr being the preferred value (Okada and Ikeda, 1991; Research Group for Active Faults of Japan, 1992). The fault is broken by one, and possibly two steps.

Right-lateral separation across the *Atotsugawa fault* is about 3 km, based on offset of a major river system (Research Group for Active Faults of Japan, 1992). Estimates of slip rates are in the range 1-5 mm/yr (Okada and Ikeda, 1991). The fault is broken by two, and possibly three steps at least 1 km wide.

Left-lateral separation of 0.5-1m.y. volcanic rocks of 1 km has occurred across the *Tanna fault.* Slip rates of 1-2 mm/yr have been estimated for the fault on the basis of this left separation, with 2 mm/yr being the preferred value (Okada and Ikeda, 1991; Research Group for Active Faults of Japan, 1992). The fault is broken by two, and possibly three steps of 1 km width or more.

Late Quaternary slip rates of 0.3-0.8 mm/yr are reported for the *Yamasaki fault*, based on offset of 150,000 year old stream channels (Research Group for Active Faults of Japan, 1992). Two poorly defined steps occur along the fault. No unambiguous estimates of the total cumulative strike-slip offset are available for the Yamasaki fault.

New Zealand

The *Alpine fault* strikes northeast along the western side of the South Island for about 520 km, and forms the boundary of the Australian plate to the west and the Pacific plate to the east. The present relative plate motion is obliquely convergent, but longer term plate motion has been dominantly strike-slip. 480 km dextral separation of Mesozoic and Paleozoic rocks has occurred across the Alpine fault in the Cenozoic (Wellman, 1953). Late Quaternary dextral slip rates are 25-45 mm/yr, and uplift rates of 17 mm/yr occur to the east of the fault (Hull and Berryman 1986; Berryman and Beanland, 1988).

The 100 km long *Wairau fault* is the northeastern extension of the Alpine fault in the Marlborough area. The fault has a dextral slip rate of 3.8-6 mm/yr, based on a faulted late Quaternary terrace sequence (Berryman and Beanland, 1988). The slip rate is much slower than the present Alpine fault slip rate, as late Quaternary relative plate motion is distributed across several faults in the Marlborough area. Total right-lateral strike-slip offset across the Wairau fault amounts to 430-480 km. The maximum value of offset is simply the total offset of Mesozoic and Paleozoic rocks across the Alpine and Wairau faults reported by Wellman (1953), and the minimum value is based on the assumption that the total offsets registered across the other Marlborough faults (see Awatere, Clarence and Hope fault descriptions below) accommodate about 50 km of the total Alpine fault offset in the north. Our value of complexity in **Table 1** is based on the nil to one steps that occur along the 75 km of fault length between Tophouse and Renwick, as the fault is not mapped across the young sediments immediately northeast of Renwick.

The *Awatere fault* is situated to the southeast of the Wairau fault. Slip rates of 5-10 mm/yr, right-lateral, have been estimated for the fault, based on offset late Quaternary terraces (Knuepfer, 1992). Total right separation of greywackes across the fault has been estimated at 19 km (Lensen, 1960).

The *Clarence fault* is situated approximately 50 km southeast of the Awatere fault, and is approximately 180 km in length. Cumulative dextral strike-slip offset of 15 km has been estimated across the fault, based on offset of the Mesozoic Esk Head Subterrane, and the fault has a late Quaternary dextral slip rate of 4-8 mm/yr (Browne, 1992).

The *Hope fault* is the most southeastern of major dextral strike-slip faults in the Marlborough fault system (e.g. Cowan, 1990). It extends about 220 km from the Alpine fault in Westland to the eastern coast. Total strike-slip offset across the fault has been estimated at 19 km (Freund, 1971). The fault is interrupted by one, and possibly three steps along the total length, with bends in the fault trace in the Hanmer Basin area. Slip rates of 11-25 mm/yr have been calculated for the fault, based on offset moraines and terraces (Cowan, 1990; 1991; Cowan and McGlone, 1991; Van Dissen and Yeats, 1991).

The *Wairarapa fault* strikes northeast from near the southern tip of the North Island. Progressive offset of terraces indicate dextral slip rates of 8-12.3 mm/yr, with 8 mm/yr as the preferred value (Wellman, 1972; Berryman and Beanland, 1988). Uplifted Holocene shorelines indicate vertical slip rates of about 4 mm/yr, and a major range front to the west of the fault indicates long term uplift. Three, and possibly six steps occur along the fault, but no estimates are available as to the amount of total dextral slip across the fault.

The *Wellington fault* strikes northeast from the coast near Wellington city (Officers of the New Zealand Geological Survey, 1983). Latest Quaternary slip rates are estimated to be 5-7.6 mm/yr, right-lateral, with 7.1 mm/yr as the preferred value (Berryman and Beanland, 1988; Van Dissen et al., 1992). One and possibly two steps occur along the fault, and cumulative dextral strike-slip offset of 10-12 km has been measured across the fault, based on offset of the Esk Head melange (Colin Mazengarb pers comm.).

China

The *Altun fault* strikes northeast for about 1600 km across western China. 65-75 km of left-lateral strike-slip offset of Mesozoic and Paleozoic rocks is recorded across the fault (Institute of Geology, 1991, page 156), and two to possibly seven steps greater than 1 km wide have been mapped.

To the east of the Altun fault, two to four steps occur along the 280 km long *Haiyuan fault.* 12-14.5 km sinistral strike-slip offset has occurred across the fault (Institute of Geology 1990, page 102).

Turkey

The *North Anatolian fault* strikes east across Turkey for a distance of about 980 km. A review of Barka and Gulen (1988) indicates that displacement initiated along the North Anatolian fault in the late Miocene to early Pliocene and ranges between 25 and 45 km. 12 steps at least 1 km wide occur along the fault.

REFERENCES

Aki, K., 1965. Maximum likelihood estimates of b in the formula logN=a-bM and its confidence limits, *Bulletin of the Earthquake Research Institute*, **43,** 237-239.

Aki, K., and Richards, P.G., 1980. *Quantitative Seismology: Theory and Methods*, W.H. Freeman, San Francisco, California: 1-932.

Anderson, J. G., Rockwell, T. and Agnew, D., 1989. A study of seismic hazard of San Diego, *Earthquake Spectra* , **5(2),** 299-333

Awata, Y. Mizuno, K., Tsukuda, E. and Yamazaki, H., 1986. The recurrence interval of faulting on the Atera fault and the age of its last activity, *Program and abstracts, Japan Association of Quaternary Research* , **16,** 132-133.

Barka, A.A. and Kadinsky-Cade, K., 1988. Strike-slip fault geometry in Turkey and its influence on earthquake activity, *Tectonics* **7(3),** 663-684.

Barka, A. A., and Gulen, L., 1988. New constraints on age and total offset of the north Anatolian fault zone: Implications for tectonics of the eastern Mediterranean region, In *Special Publication of the Middle East Technological University,* 1987. Meloh Tokay Geology Symposium, Ankara, Turkey.

Barrows, A. G., 1974. A review of the geology and earthquake history of the Newport-Inglewood structural zone, southern California, *Special Report, California Division of Mines and Geology,* **114,** 115 pp.

Bent, A.L., Helmberger, D.V., Stead, R.J. and Ho-Liu, P., 1989. Waveform modeling of the November 1987 Superstition Hills earthquakes, *Bulletin of the Seismological Society of America* , **79,** 500-513.

Ben-Zion, Y. and Rice, J.R., 1993. Earthquake failure sequences along a cellular fault zone in a 3D elastic solid containing asperity and nonasperity regions, *Journal of Geophysical Research* , **98,** 14109-14131.

Berryman, K.R., 1990. Late Quaternary movement on the Wellington Fault in the Upper Hutt area, New Zealand, *New Zealand Journal of Geology and Geophysics,* **33(2),** 257-270.

Berryman, K.R and Beanland, S., 1988. The rate of tectonic movement in New Zealand from geological evidence, *Transactions of the Institute of Professional Engineers of New Zealand* ,**15,** 25-35.

Brake, J.F. and Rockwell, T.K., 1987. Magnitude of slip from historical and prehistorical earthquakes on the Elsinore fault, Glen Ivy marsh, southern California, *Geological Society of America Abstracts with Programs* ,**19.**

Brown, R.D., 1970. Map showing recently active breaks along the San Andreas and related faults between the northern Gabilan Range and Cholame Valley, California, *U.S.G.S. Miscellaneous Geologic Investigations Map*, v. **I-575.**

Brown, R.D. and Wolfe, E.W., 1972. Map showing recently active breaks along the San Andreas fault between Point Delgada and Bolinas Bay, California, *U.S.G.S. Miscellaneous Geologic Investigations Map.* **I-692.**

Browne, G.H., 1992. The northeastern portion of the Clarence fault: tectonic implications for the late Neogene evolution of Marlborough, New Zealand, *New Zealand Journal of Geology and Geophysics,***35(2),** 437-446.

Brune, J.N., 1968. Seismic moment, seismicity and rate of slip along major fault zones, *Journal of Geophysical Research* ,**73(2),** 777-784.

Budding, K.E. Schwartz, D.P. and Oppenheimer, D.H., 1991. Slip rate, earthquake recurrence, and seismogenic potential of the Rogers Creek fault zone, northern California: initial results, *Geophysical Research Letters,* **18,** 447-450.

Burdick, L. and Mellman, G.R., 1976. Inversion of body waves from the Borrego Mountain earthquake to source mechanism, *Bulletin of the Seismological Society of America.* **66,** 1485-1499.

California Division of Mines and Geology, 1992. Preliminary fault activity map of California, *DMG open file report* , **92-03.**

Clark, M.M., 1972. Surface rupture along the Coyote Creek fault, the Borrego Mountain earthquake of April 9. 1968, *U.S. Geological Survey Professional Paper, 787,* 55-86.

Clark, M.M., Grantz, A., Rubin, M., 1972. Holocene activity of the Coyote Creek fault as recorded in sediments of Lake Cahuilla. The Borrego Mountain Earthquake of April 9, 1968, *USGS Professional Paper* , **787.** 1-55-86.

Clark, M. M., 1973. Map showing recently active breaks along the Garlock and associated faults, California, *U.S.G.S. Misc. Geol. Invest. Map* ,**74.**

Clark, M.M., 1984. Map showing recently active breaks along the San Andreas fault and associated faults between Salton Sea and Whitewater River - Mission Creek, California, *U.S.G.S Misc.Field Invest. Map,* **I 1483.**

Cowan, H.A., 1990. Late Quaternary displacements on the Hope fault at Glynn Wye, North Canterbury, *New Zealand Journal of Geology and Geophysics* ,**33(2),** 285-294.

Cowan, H.A., 1991. The North Canterbury earthquake of September 1, 1888, *Journal of the Royal Society of New Zealand,* **21(1),** 1-12.

Cowan, H.A. and McGlone, M.S., 1991. Late Holocene displacements and characteristic earthquakes on the Hope River segment of the Hope Fault, New Zealand, *Journal of the Royal Society of New Zealand,* **21(4),** 373-384.

Crowell, J. C., 1962. Displacement along the San Andreas fault, California, *Geological Society of America Special Paper* ,**7,** 61.

Darby, D.J. and Beanland, S., 1992. Possible source models for the 1855 Wairarapa earthquake, New Zealand. *Journal of Geophysical Research 97(B9)*: 12375-12390

Dokka, R. K., 1983. Displacements on late Cenozoic strike-slip faults of the central Mojave Desert, California, *Geology* ,**11,** 305-308.

Freund, R., 1971. The Hope fault, a strike-slip fault in New Zealand, *New Zealand Geological Survey Bulletin* , **86,** 1-49 p.

Galehouse, J.S., 1991. Creep rates on the Bay Area faults during the past decade (abstracts), *Seismological Research Letters,* **62,** 12.

Gastil, R.G., Phillips, R.P., Allison, E.C., 1975. Reconnaissance geologic map of the State of Baja California, Mexico, *Geological Society of America Memoir,* **140**.

Given, D., Hutton, L., Jones, L.M., 1987. The Southern California Network Bulletin, July - December, 1986.

Grantz, A., and Dickenson, W.R. (ed) 1968. Indicated cumulative offsets along the San Andreas fault in California Coast Ranges, *Proceedings of Conference on Geologic problems of the San Andreas fault system,* Stanford University Publication **XI**, 117-120.

Gutenberg, B., and Richter, C.F. 1944. Frequency of earthquakes in California, *Bulletin of the seismological society of America,* **34,** 185-188.

Hanks, T.C., and Kanamori, H. 1979. A moment magnitude scale, *Journal of Geophysical Research* , **84,** 2348-2350.

Harvey, T. W., 1985. *Geology of the San Miguel fault zone, northern Baja California. Mexico.* PhD thesis, San Diego State University, 330 pp.

Herd, D.G. and Helley, E.J., 1977. Faults with Late Quaternary displacement, Northern San Francisco Bay region, California, 1:125000. *U.S.G.S. Miscellaneous Field Studies Map* **MF818**.

Herd, D. G., 1979. Neotectonic framework of central California and its implications to microzonation of the San Francisco Bay region, *US. Geol. Surv. Circ.,* **807,** 3-12.

Herd, D.G., 1988. Map of active traces of Hayward - Macaama and Calaveras - Rogers Creek - Green Valley fault zones at 1:250000 scale (unpublished map).

Hill, R.I., 1981. Geology of Garner Valley and Vicinity, in Geology of the San Jacinto Mountains, *Field Trip Guide 9*, edited by A.R.Brown and R.W. Ruff, South Coast Geological Society, Irvine, California, 90-99.

Hirayabashi, K.C., Rockwell, T.K. and Wesnousky, S.G., 1993. Clustering of seismic activity on the San Miguel fault, Baja California, Mexico, *Abstracts of the 1993 AGU Fall meeting,* 575

Hirayabashi, K.C., Rockwell, T.K., Wesnousky, S.G., Stirling, M.W., and Suarez-Vidal, F., 1995. A neotectonic study of the San Miguel-Vallecitos fault, Baja California, Mexico, *Bulletin of the Seismological Society of America,* (in press)

Hope, R.A., 1969. Map showing recently active breaks along the San Andreas and related faults between Cajon Pass and Salton Sea, *U.S.G.S. Open file report,* **69-130**.

Hudnut, K.W. and Sieh, K.E., 1989. Behavior of the Superstition Hills fault during the past 330 years, *Bulletin of the Seismological Society of America* , **79,** 304-329.

Hull, A.G. and Berryman, K.R., 1986. Holocene tectonism in the region of the Alpine fault at Lake McKerrow, Fiordland, New Zealand, *Royal Society of New Zealand Bulletin,* **24,** 317-331.

Hull, A. G., and Nicholson, C., 1992. Seismotectonics of the Northern Elsinore fault zone, Southern California, *Bulletin of the Seismological Society of America,* **82,** 800-818.

Ichikawa, M., 1969. Epicenter determination capability of the seismological network of Japan Meteorological Agency (in Japanese), *Journal of Meteorological Research,* **21,** 297-308.

Institute of Geological and Nuclear Sciences Ltd, 1994. Unpublished active fault database.

Institute of Geology, 1990. *The Haiyuan Active Fault Zone.* (in Chinese) Special Issue. Beijing, China.

Institute of Geology, 1991. *The Altun Fault Zone.* (in Chinese) Special Issue. Beijing, China.
Ishikawa, Y., 1987. Change of JMA hypocenter data and some problems (in Japanese), *Quarterly Journal of Seismology.* **51,** 47-56.
Ishimoto, M., and Iida, K., 1939. Observations sur les seisms enregistre par le microseismograph construite derniermente (I), *Bulletin of the Earthquake Research Institute at the University of Tokyo.* **17,** 443-478.
Johnston, M.R., 1990. Geology of the St Arnaud District, Southeast Nelson (Sheet N29), *New Zealand Geological Survey Bulletin* , **99.**
Jones, C.H. and Wesnousky, S.G., 1990. Variations in strength and slip rate along the San Andreas fault system, *Science.* **256,** 83-86
Kintzer, F. C., Brooks,J.C., and Cummings, J.C., 1977. An offset Miocene shoreline: implications for Calaveras fault movement, *Geol. Soc. Am. Abstracts with programs*, **9,** 65.
Knuepfer, P.L.K., 1992. Temporal variations in latest Quaternary slip across the Australian-Pacific plate boundary, northeastern South Island, New Zealand, *Tectonics* , **11(3),** 449-464.
Lawson, A.C., 1908. The San Andreas rift as a geomorphic feature. In: Report of the State Earthquake Investigation Committee Vol 1, *The California Earthquake of April 18 1906,* 25-115.
Lee, W.H.K., Bennett, R.E., and Meagher, K.L., 1972. A method of estimating magnitude of locel earthquakes from signal duration, *USGS Open File Report* , **28.**
Lensen, G.J., 1960. A 12 mile lateral drag along the Awatere fault, *Abstract for the 9th Scieince Congress, Royal Society of New Zealand,* **47**
Lensen, G.J., 1976. Sheets N28D, O28C and N29B- Hillersden; sheets O28BD, P28A and P28C-Renwick. *Late Quaternary tectonic map of New Zealand 1:50,000.* Two maps and notes, Department of Scientific and Industrial Research, Wellington, New Zealand, 20pp.
Lensen, G.J., 1978. Historic tectonic earth deformation, in Suggate, R.P., Stevens, G.R., and Te Punga, M.T. (editors), *The Geology of New Zealand,* Government Printer, Wellington, New Zealand, 33-39.
Lienkaemper, J.J., Borchardt, G., and Lisowski, M., 1991. Historic creep rate and potential for seismic slip along the Hayward fault, California, *Journal of Geophysical Research* , **96,** 18261-18283.
Lindvall, S.C., Rockwell, T.K. and Hudnut, K.W., 1989. Slip distribution of prehistorical earthquakes on the Superstition Hills fault, San Jacinto fault zone, southern California, based on offset geomorphic features, *Abstracts with Programs, geological Society of America* , **21,**107.
Magistrale, H., Jones, L. and Kanamori, H., 1989. The Superstition Hills, California earthquakes of 24 November 1987, *Bulletin of the Seismologica Society of America* **79,** 239-251.
Matsu'ura, M., Jackson, D.D. and Cheng, A., 1986. Dislocation model for aseismic crustal deformation at Hollister, California, *Journal of Geophysical Research,* **91,** 12661-12674.
Matti, J.C., Morton, D.M., Cox, B.F., 1985. Distribution and geologic relations of fault systems in the vicinity of the Central Transverse ranges, southern California. *U.S.G.S. Open file report,* 85-365.
Mochizuki, E., Kobayashi, E., and Kishio, M., 1978. Hypocenter determination ability of JMA seismological observation system during 1965-1974 (in Japanese), *Quarterly Journal of Seismology,* **42,** 23-30.
Morton, D. M., Miller, F.K. and Smith, C.C., 1980. Photo-reconnaissance maps showing young-looking fault features in the southern Mojave Desert, California, *U.S.G.S. Miscelleneous Field Studies Map,* MF-1051.

Officers of the New Zealand Geological Survey, 1983. Late Quaternary tectonic map of New Zealand 1:2,000,000. 2nd ed. *New Zealand Geological Survey Miscellaneous Series Map* **12**. Department of Scientific and Industrial Research,Wellington, New Zealand.

Okada, A., 1980. Quaternary faulting along the Median Tectonic Line of Southwest Japan, In Ichikawa, K. (editor), *The Median Tectonic Line of Southwest Japan, Memoirs of the Geological Society of Japan,* **18,** 79-108.

Okada, A., and Ikeda, Y., 1991. Active faults and neotectonics in Japan, *The Quaternary research* , **30(2),** 161-174.

Petersen, M.D. and Wesnousky, S.G., 1994. fault slip rates and earthquake histories for active faults in southern California, *Bulletin of the Seismological Society of America*, **84(5),** 1608-1649.

Pinault, C.T. and Rockwell, T.K., 1984. Rates and sense of Holocene faulting on the southern Elsinore fault: Further constraints on the distribution of dextral shear between the Pacific and North American plates, *Geological Society of America Abstracts with Programs, 16,* 624.

Prentice, C.S., Niemi, T.M. and Hall, T.M., 1993. Quaternary tectonics of the northern San Andreas fault, San Francisco Peninsula, Point Reyes, and Point Arena, California. *USGS fieldtrip guide- S.F. Peninsula Transect.*

Radbrush-Hall, D.H., 1974. Map showing recently active breaks along the Hayward Fault zone and the southern part of the Calaveras fault zone, California, *U.S.G.S. Miscellaneous Investigation Series Map* **,I-813**.

Research Group for Active faults of Japan, 1992. *Map of active faults in Japan with an explanatory text.* University of Tokyo Press.

Rockwell, T.K., Lamar, D.L., McElwain, R.S., and Millman, D.E., 1985. Late Holocene recurrent faulting on the Glen Ivy north strand of the Elsinore fault, southern California, *Geological Society of America Abstracts with Programs* **,17,** 404

Rockwell, T.K., McElwain, R.S., Millman, D.E., and Lamar, D.L., 1986. Recurrent late Holocene faulting on the Glen Ivy north strand of the Elsinore fault at Glen Ivy marsh. *Guidebook and Volume on Neotectonics and Faulting in southern California. Cordilleran section. Geological Society of America* **167,**1275.

Rockwell, T.K., Loughman, C., and Merifield, P., 1990. Late Quaternary rate of slip along the San Jacinto fault zone near Anza, southern California. *Journal of Geophysical Research* **95,** 8593-8605.

Romanowicz, B., 1992. Strike-slip earthquakes on quasi-vertical transcurrent faults: Inference from general scaling relations, *Geophysical Research Letters* , **2(2),** 56-59.

Ross, D.C., 1969. Map showing recently active breaks along the San Andreas fault between Tejon Pass and Cajon Pass, southern California, *U.S.G.S. Miscellaneous field investigation map,* **I-553**.

Savage, J.C., Prescott, W.H., Lisowski, M. and King, N., 1979. Geodetic measurements of deformation near Hollister, California, 1971-1978, *Journal of Geophysical Research,* **84,** 7599-7615.

Schwartz, D.P., and Coppersmith, K.J., 1984. Fault behavior and characteristic earthquakes: Examples from the Wasatch and San Andreas fault zones, *Journal of geophysical research,* **89,** 5681-5698.

Seagall, P. and Pollard, D.D., 1980. Mechanics of discontinuous faults, *Journal of Geophysical Research,* **85(B8),** 4337-4350.

Sharp, R. V., 1975. En echelon fault patterns of the San Jacinto fault zone, Southern California, *Bull. Calif. Div. Mines Geol,* **196,** 187-194.

Sharp, R.V., 1981. Variable rates of late Quaternary strike-slip on the San Jacinto fault zone, southern California, *Journal of Geophysical Research,* **86,** 1754-1762.

Sibson, R.H., 1985. Stopping of earthquake ruptures at dilatational fault jogs, *Nature.* **316(6025),** 248-251.

Sieh, K.E., 1978. Slip along the San Andreas fault associated with the great 1857 earthquake, *Bulletin of the Seismological Society of America,* **68,** 1421-1448.

Sieh, K.E. and Jahns, R.H., 1984. Holocene activity of the San Andreas fault at Wallace Creek, California, *Geological Society of America Bulletin,* **95,** 883-896.

Smith, G. I., 1962. Large lateral displacement on the Garlock fault, California, as measured from offset dike swarm, *Bull. Am. Assoc. Petrol. Geol.,* **46,** 85-104.

Smith, W.D., 1976. A computer file of New Zealand earthquakes, *New Zealand Journal of Geology and Geophysics,* **19,** 393-394

Thatcher, W., 1975. Strain accumulation and release mechanism of the 1906 San Francisco earthquake, *Journal of Geophysical Research,* **80,** 4862-4872.

Toppozada, T.R., Real, C.R., Parke, D.L., 1981. Preparation of isoseismal maps and summaries of reported effects for pre-1900 California earthquakes, *California Division of Mines and Geology Open File Report* , **81-11.***SAC.* 182 pp.

Utsu, T., 1965. A method for determining the value of b in a formula log n = a - bM showing the magnitude-frequency relation for earthquakes (in Japanese), *Geophysics Bulletin. Hokkaido University.* **13,** 99-103.

Utsu, T., 1982. Relationships between earthquake magnitude scales, *Bulletin of the Earthquake Research Institute, University of Tokyo,* **57,** 465-497.

Van Dissen, R.J., Berryman, K.R., Pettinga, J.R., Hill, N.L., 1992. Paleoseismicity of the Wellington-Hutt Valley segment of the Wellington Fault, North Island, New Zealand, *New Zealand Journal of Geology and Geophysics,* **35(2),** 165-176.

Van Dissen, R.J. and Yeats, R.S., 1991. Hope fault, Jordan thrust, and uplift of the Seaward Kaikoura Range, New Zealand, *Geology,* **19,** 393-396.

Vedder, J.B., and Wallace, R.E., 1970. Map showing recently active breaks along the San Andreas and related faults between Cholame Valley and Tejon Pass, California, *U.S.G.S. Miscellaneous geological investigations map* **I-574.**

Weber, F. H. J. 1977. Seismic hazards related to geologic factors, Elsinore and Chino fault zones, northwestern Riverside county, California, *Calif. Div. Mines and Geology Open file report* , 77, 96 p.

Vidal, A. and Munguia, L., 1993. Ten years of functioning of the seismic network of northwestern Mexico (in Spanish), *Ciencia y Desarrollo,* **18(108),** 77-85.

Wellman, H.W., 1953. Jurassic-Recent data for the study of Recent and late Pleistocene faults in the South Island of New Zealand, *New Zealand Journal of Science and Technology, **B34,*** 270-288.

Wellman, H.W., 1972. Rate of horizontal fault displacement in New Zealand. *Nature* **237,** 275-277.

Wesnousky, S.G., 1986. Earthquakes, Quaternary faults and seismic hazard in California, *Journal of Geophysical Research* ,**91,**12587-12631.

Wesnousky, S.G., 1988. Seismological and structural evolution of strike-slip faults, *Nature,* **335,** 340-343.

Wesnousky, S.G., 1990. Seismicity as a function of cumulative geologic offset: Some observations from southern California, *Bulletin of the Seismological Society of America,* **80(5),** 1374-1381.

Wesnousky, S.G., 1994. The Gutenberg-Richter or Characteristic Earthquake Distribution, which is it?, *Bulletin of the Seismological Society of America* **84(6),**1940-1959.

Wesnousky, S.G., 1995. The Gutenberg-Richter or Characteristic Earthquake Distribution, which is it?, **Reply** *Bulletin of the Seismological Society of America* (submitted August 1995).

Wesnousky, S.G., Scholz, C.H., Shimazaki, K., and Matsuda, T., 1983. Earthquake frequency distributions and the mechanics of faulting, *Journal of Geophysical Research.* **88(B11),** 9331-9340.

Williams, P.L., 1991. Evidence of late Holocene ruptures, southern Hayward fault, California [abstract], *Seismological Research Letters* **62,** 14.

Working Group on California Earthquake Probabilities 1990. Probabilities of large earthquakes occurring in California on the San Andreas fault, *US Geological Survey Open File Report*, **88-398,** 62.

Yang, J.S., 1991. The Kakapo fault - a major active dextral fault in the central North Canterbury-Buller regions of New Zealand, *New Zealand Journal of Geology and Geophysics,* **34(2),**137-143.

Yokoyama, H., 1984. Epicenter determination ability of the recent JMA network:1979-1983 (in Japanese), *Quarterly Journal of Seismology,* **49,** 53-65.

Youngs, R.R. and Coppersmith, K.J., 1985. Implications of fault slip rates and earthquake recurrence models to probabilistic seismic hazard estimates. *Bulletin of the Seismological Society of America.* **75(4),** 939-964.

TABLES

TABLE 1: GEOLOGICAL DATA

ID & FAULT (km)	LENGTH (km)	STRIKE SLIP OFFSET (mm/yr)	SLIP RATE	NO OF STEPS (steps/km)	COMPLEXITY
Southern California					
1 San Andreas (total length)	1000	≥150	7-43 RL	1	.001
Bitterwater - Salton Sea 550		≥150	11-43(24)RL	1	.0018
2 Garlock	240	64	4-9 LL	1	.0042
3 Newport-Inglewood	60	0.2-10	0.1-6(0.6) RL	4	.066
4 Whittier-Elsinore	240	10-15	1.5-9.3(5) RL	3	.0125
5 San Jacinto	230	24	7-19(12)RL	5	.022
Mojave Desert					
6 Calico-Mesquite	125	8.2		3-4	.024-.032
7 Pisgah	64	6.4-14.4		2	.031
8 Camp rock	73-93	1.6-4		1-3	.011-.041
9 Helendale	58-80	3		3	.038-.052
10 Lenwood	75	1.5-3		1-2	.013-.014
Baja California					
11 San Miguel-Vallecitos	160	0.5	0.1-0.5 RL	4-6	.025-.038
Northern California					
12 San Andreas (Mendocino-San Juan Bautista)	460	≥150	7-32 RL	0	0
13 Calaveras-Concord-Green Valley-Bartlett Sp	220	24	3-25(8) RL	5-7	.023-.032
14 Hayward-Rogers Creek-Maacama	250	-	2.1-9(9) RL	2-3	.008-.012
Japan					
15 MTL (Shikoku Island)	215	5	7-8(7) RL	3-5	.014-.023
16 Neodani	100	3-5	1-2(2) LL	2-3	.02-.03
17 Atera	60	7-10	3-5.2(5.2) LL	1-2	.017-.033
18 Atotsugawa	60	3	1-5 RL	2-3	.03-.05
19 Tanna	30	1	1-2(2) LL	2-3	.067-.1
20 Yamasaki	80	-	0.3-0.8 LL	0-2	0-.025
New Zealand					
21 Alpine (onland extent; OS)	520	480	25-45 RL	-	-
22 Wairau	100	430-480	3.8-6 RL	0-1	0-.013
23 Awatere	170	19	5-10 RL	-	-
24 Clarence	180	15	4-8 RL	-	-
25 Hope	220	19	11-25 RL	1-3	.0045-.014
26 Wairarapa (OS)	180	-	8-12.3(8) RL	3-6	.033-.167
27 Wellington	200	10-12	5-7.6(7.1) RL	1-2	.005-.01
China					
28 Altun	1600	65-75		2-7	.00125-.00375
29 Haiyuan	280	12-14.5		2-4	.00714-.0143
Turkey					
30 N. Anatolian	980	25-45		12	.012

Table 1: Geological data. Note that LL= left-lateral strike-slip offset, RL= right-lateral strike-slip offset RL = right-lateral slip, LL = left-lateral slip, OS = fault with oblique slip motion. Slip rates are shown for the faults that form the data set in Table 2, and published preferred slip rates are given in parentheses; see Appendix. The minimum step number represents the number of clearly defined steps, and the maximum number represents the total of clearly defined and possible steps. Fault length, cumulative offset and slip rate data sources are as follows: **(1)** Crowell (1962); Grantz and Dickenson (1968); Hill (1981); Petersen and Wesnousky (1994); **(2)** Smith (1962); Petersen and Wesnousky (1994); **(3)** Barrows (1974); Petersen and Wesnousky (1994); **(4)** Hull and Nicholson (1992); Petersen and Wesnousky (1994); **(5)** Rockwell et al. (1990); Petersen and Wesnousky (1994); **(6-10)** Dokka (1983); **(11)** Gastil et al. (1975); Harvey (1985); Hirayabashi et al. (1993); **(12)** Prentice et al. (1993); Working Group on California Earthquake Probabilities (1990); **(13)** Kintzer et al. (1977); Matsu'ura et al. (1986); Galehouse (1991); **(14)** Budding et al. (1991); Lienkaemper et al. (1991); **(15)** Okada (1980); Research Group for Active Faults of Japan (1992); **(16-19)** Okada and Ikeda (1991); Research Group for Active Faults of Japan (1992); **(20)** Research Group for Active Faults of Japan (1992); **(21)** Wellman (1953); Hull and Berryman (1986); Berryman and Beanland (1988); **(22)** Wellman (1953); Berryman and Beanland (1988); **(23)** Lensen (1960); Knuepfer (1992); **(24)** Browne (1992); **(25)** Freund (1971); Cowan (1990, 1991); Cowan and McGlone (1991); Van Dissen and Yeats (1991); **(26)** Wellman (1972); Berryman and Beanland (1988); **(27)** Berryman and Beanland (1988); Van Dissen et al. (1992); Institute of Geological and Nuclear Sciences (1994); **(28)** Institute of Geology (1991); **(29)** Institute of Geology (1990); **(30)** Barka and Gulen (1988).

TABLE 2: MAXIMUM MAGNITUDES & RETURN TIMES

ID & FAULT	MAXIMUM MAGNITUDE*			RETURN TIME (yrs)**				
	pref	min	max	pref	Tmin1	Tmin2	Tmax1	Tmax2
	(M_o^e pref)	(M_o^e min)	(M_o^e max)					
Southern California								
1 San Andreas (Bitterwater-Salton Sea)	7.9	7.7	8.1	146	39	154	799	204
2 Garlock	7.5	7.3	7.7	393	131	294	1184	526
3 Newport-Inglewood	7.0	6.8	7.2	2941	139	8348	52353	873
4 Whittier-Elsinore	7.5	7.3	7.7	468	126	781	3171	511
5 San Jacinto:	7.6	7.3	7.7	663	169	253	1678	1119
Baja California								
11 San Miguel-Vallecitos	7.4	7.2	7.6	11835	3023	7557	45280	18112
Northern California								
12 San Andreas	7.8	7.6	8.0	154	46	209	928	203
Mendocino - San Juan Bautista)								
13 Calaveras-Concord-Green V-Bartlett Sp	7.5	7.4	7.7	318	61	506	1715	206
14 Hayward-Rogers Ck-Maacama	7.6	7.4	7.8	281	151	646	2734	638
Japan								
15 MTL	7.9	7.5	8.3	1188	285	326	4753	4159
16 Neodani	7.5	7.1	7.9	2149	667	1334	18428	9214
17 Atera	7.2	6.8	7.6	573	164	285	3494	2015
18 Atotsugawa	7.2	6.8	7.6	1195	171	855	10607	2121
19 Tanna	6.8	6.5	7.2	900	270	540	8944	4472
20 Yamasaki	7.5	7.1	7.9	22016	3036	8097	559440	209790
New Zealand								
21 Alpine	7.8	7.6	8.1	79	33	60	310	172
22 Wairau	7.2	6.9	7.4	405	116	183	1011	640
23 Awatere	7.4	6.6	7.7	340	12	24	1184	592
24 Clarence	7.4	7.2	7.6	309	123	247	928	464
25 Hope	7.5	7.4	7.7	140	60	137	459	202
26 Wairarapa	7.4	7.2	7.6	231	80	123	463	301
27 Wellington	7.5	7.2	7.6	313	124	189	778	512

Table 2: Maximum magnitudes and return times calculated from the geological data in Table 1, assuming rupture of the entire lengths of the faults listed. Calculations are limited to those major faults that fall within the CIT-USGS (southern California), USGS -CALNET (northern California), RESNOR (northwest Baja California), Japanese Meteorological Agency (central Japan) and Institute of Geological and Nuclear Sciences (New Zealand).
* Magnitudes are calculated by use of the equation $logMo = 16.1 + 1.5M$
** Return times T are calculated from equations 4 and 5a-d in the text.

Negative values for T result from $\dot{M}_o^{sm} > \dot{M}_o^{g}$, the case for the extreme low bounds on $\dot{M}_o^{g}$ for the northern San Andreas and Tanna faults. $\dot{M}_o^{sm}$ is therefore based on records from which the mainshock of the Loma Prieta earthquake is removed in the case of the northern San Andreas, and the 1930 mainshock removed in the case of the Tanna fault. *Tmax1* and *Tmax2* should therefore be viewed as underestimates of *Tmax* for the northern San Andreas and Tanna faults.

TABLE 3: MAXIMUM MAGNITUDES AND RETURN TIMES ESTIMATED FROM PALEOSEISMIC STUDIES AND HISTORICAL OBSERVATIONS

ID&FAULT	LOCATION	MAGNITUDE	RETURN TIME
Southern California			
1. Southern San Andreas	Parkfield-Cajon Pass	7.8	350 yrs
4. Whittier-Elsinore	Corona-Lake Elsinore	6.2	175yrs
	Coyote Mtn	6.5-7	800 yrs
5. San Jacinto	Coyote Creek fault	6.5	70yrs
	Superstition Hills fault	6.6	225yrs
11. San Miguel-Vallecitos	Las Cuevitas-Jamu	6.8	2830 yrs
Northern California			
12. Northern San Andreas	Mendocino-San Juan Bautista	7.7	300 yrs
13. Calaveras-Concord-Green Valley-Bartlett Sp	northern Calaveras fault	6.1	150yrs
14. Hayward-Rogers Ck	Hayward fault	6.8	325yrs
-Maacama	Rogers Ck fault	7	464 yrs
Japan			
15. Median Tectonic Line	Shikoku Island	8	1000 yrs
16. Neodani	Central Japan	8	10000 yrs
17. Atera	Central Japan	7.8	1700 yrs
18. Atotsugawa	Central Japan	7	1700 yrs
19. Tanna	North Izu	7.3	850 yrs
20. Yamasaki	West central Japan	7-7.4	2550 yrs
New Zealand			
21. Alpine	south Westland	7.4-8	426 yrs
23. Awatere	Awatere valley	7.1	855 yrs
25. Hope	Hope River	7.3	148 yrs
26. Wairarapa	southern Wairarapa	8	1400 yrs
27. Wellington	Wellington-Hutt Valley	7.1-7.8	600 yrs

Table 3: Magnitude and average return time estimates for the largest earthquakes arising from paleoseismic studies and historical observations for the faults listed in Table 2. Data sources are as follows: **(1)** Sieh (1978); Sieh and Jahns (1984); **(4)** Pinault and Rockwell (1984); Rockwell et al., (1985, 1986); Brake and Rockwell (1987); **(5)** Sharp (1981); Clark, (1972); Clark et al. (1972); Burdick and Millman (1976); Bent et al. (1989); Hudnut and Sieh (1989); Magistrale et al., (1989); Lindvall et al., (1989); Rockwell et al. (1990); **(11)** Hirayabashi et al. (1993); **(12)** Lawson et al. (1908); Thatcher (1975); Sieh (1978); **(13)** Wesnousky (1986); **(14)** Toppozada et al. (1981); Budding et al. (1991); Williams (1991) **(15,16)** Okada and Ikeda (1991); **(17)** Awata et al. (1986); Okada and Ikeda (1991); **(18-20)** Okada and Ikeda (1991); **(21)** Hull and Berryman (1986); **(22)** Lensen (1976); Johnston (1990); **(23)** 66m lateral offset of 9,410±1570 yr terraces (Knuepfer, 1992), and 6m single event displacement of 1848, magnitude 7.1 Marlborough earthquake (Lensen, 1978) indicate 11 earthquakes in 9410 yrs = average return time of 855 years; **(25)** Cowan and McGlone (1991); **(26)** Wellman (1972); Darby and Beanland (1992); **(27)** Berryman (1990); Van Dissen et al. (1992).

FIGURE CAPTIONS

Figure. 1: Schematic illustration of the discrete and cumulative forms of the magnitude - frequency distributions for the faults described by the (a) Gutenberg-Richter relationship and (b) characteristic earthquake model of fault behavior during the repeat time of one maximum magnitude (M^{max}) event along a fault. The discrete number of events of a given magnitude per year is represented by n, and N is the cumulative number of events greater than or equal to a given magnitude. For the characteristic earthquake model, the largest earthquake during the repeat time of a maximum magnitude event is defined to equal the size of the largest aftershock (M^a) and the size distribution of aftershocks is assumed to satisfy the Gutenberg-Richter model.

Figure 2: Graph of fault trace complexity versus cumulative strike-slip offset for faults listed in Table 1. The identification numbers for the faults (Table 1) are also shown. Error bars reflect uncertainties in the definition of fault steps and in the amount of cumulative strike-slip offset.

Figure 3: Instrumental seismicity for $M \geq 3$ and depth ≤ 20 km plotted on map of major faults for (a) California and northern Baja California over the time periods 1932-92 (southern California and Baja California) and 1969-92 (northern California) respectively, (b) central Japan over the time period 1926-92, and (c) central New Zealand over the time period 1964-92. The boxes on each map represent the search areas used to extract data from the respective seismicity catalogs. We show the box used to extract seismicity from the RESNOR network of Baja California, but as the diagram is for illustrative purposes only, we have simplified the plotting procedure by showing seismicity from the CIT-USGS catalog over the area.

Figure 4: (left) Discrete number of events per year versus magnitude for the southern California, northern Baja California, northern California, central Japan and central New Zealand regions, showing the b-value and 95% confidence limits, detection threshold magnitude, number of events greater than the detection threshold magnitude, and instrumental seismic moment release rate in each case. (right) histograms of number of earthquakes versus time for each region.

Figure 5: Boxes used to define the seismicity of (a) California and Baja California faults, (b) central Japan faults and (c) central New Zealand faults. Faults are numbered according to identification numbers in Tables 1 and 2.

Figure 6: Discrete number of events per year versus magnitude for the faults listed in Table 2. Faults are numbered according to identification numbers in Tables 1 and 2. Open circles represent the instrumental data; preferred and bounding estimates of the size and recurrence rate of maximum earthquakes derived from fault length and eqs. (4) and (5) (Table 2) are shown as solid and open diamonds, respectively; open triangles represent the size and recurrence rate of large earthquakes determined from paleoearthquake studies (Table 3); heavy dotted lines represent the maximum-likelihood fit to the instrumental data (b-value curves); and light dotted lines bounding the diamonds on each plot have slopes equivalent to the b-value of the region that the fault is located within. The number of events greater than the detection threshold magnitude, the b-value fit to the instrumental data, the instrumental moment rate $\dot{M}_o$ *(instr)* and number of years of instrumental records represented by the open circles are shown for both the fault (left side) and the enclosing region (top right). The geologically derived moment rate $\dot{M}_o$ *(geol)* is also shown at the base of the plots.

Figure 7: Histograms of the number of earthquakes versus time for the faults listed in Table 2, shown alongside the equivalent magnitude-frequency distribution in Fig. 6. Faults are numbered according to identification numbers in Tables 1 and 2.

Figure 8: Seismic moment versus rupture length for (a) the global data set of major strike-slip faults listed in Romanowicz (1992), and (b) large intraplate earthquakes in Japan (Wesnousky et al., 1983). See the text for further explanation.

Figure 9: Ratio of the predicted recurrence rate of M4 earthquakes using the regional b-value to the observed recurrence rate of M4 earthquakes from the instrumental data versus cumulative strike-slip offset for the faults listed in Table 2. The identification numbers for the faults corresponding to Table 2 are also shown. We show only 19 of the 22 faults listed in Table 2, because cumulative strike-slip displacement measurement are absent for three of the faults. The vertical error bars on each point reflect the maximum and minimum ratio of predicted recurrence rate to observed recurrence rate, while the horizontal error bars represent the uncertainties in the amount of cumulative strike-slip offset.

Figure 10: Ratio of the recurrence rate of maximum-size earthquakes from geological data to the corresponding recurrence rate predicted by extrapolation of the maximum-likelihood fit to the instrumental data versus cumulative strike-slip offset for faults listed in Table 2, and the magnitude-frequency distributions in Fig. 6. The identification numbers for the faults corresponding to Table 2 are also shown. We are unable to represent 11 of the 22 faults listed in Table 2, owing either to the absence of cumulative strike-slip displacement measurements, or because it was not possible to fit b-value curves to the very small instrumental data sets for the Japanese faults and several New Zealand faults. The vertical error bars on each point reflect the maximum and minimum ratio of the bounding geological estimates (open diamonds in Fig. 6) to the 95% confidence limits on the extrapolated b-value curves (upper and lower heavy dotted lines), and the horizontal error bars reflect the uncertainties in the amount of cumulative strike-slip offset.

Figure 11: (a) Histogram of the ratio of instrumental recording time to the return time of the largest earthquakes for the faults listed in Table 2 (b) Histogram of the log of the preferred frequency ratio (predicted/observed recurrence rate of M4 earthquakes, or middle light dotted line in Fig. 6) for the faults listed in Table 2. The preferred ratios and uncertainty estimates (min and max ratios) are generally in the range 10 to 100 (log ratio=1 to 2) (c) A simple model of an earthquake cycle, whereby seismicity is consistent with the Gutenberg-Richter relationship over the entire cycle, but the cycle is characterized by periods of "low" and "high" seismicity rates (clustering). The model shows clustering into 20% of the earthquake cycle, and an instrumental recording period that is 10% of the cycle.

Figure 12: Histograms of predicted productivity during an instrumental recording period (average recording period from Fig. 11a), whereby productivity <1 represents "low" seismicity rates, productivity=1 represents average seismicity rates (consistent with the Gutenberg-Richter relationship), and productivity >1 represents "high" seismicity rates. See the text for further explanation.

Figure 13: Ratio of the predicted recurrence rate of M4 earthquakes using the regional b-value to the observed recurrence rate of M4 earthquakes from the instrumental data versus fault length for the faults listed in Table 2. The identification numbers for the faults corresponding to Table 2 are also shown. The vertical error bars reflect the maximum and minimum ratio (as in Fig. 9). The Yamasaki fault is the only fault that shows a preferred

value of ratio of less than 1, unable to be represented in the earlier plots due to the absence of an estimate of cumulative strike-slip offset (Table 1).

Figure 14: Ratio of the predicted recurrence rate of M4 earthquakes using the regional b-value to the observed recurrence rate of M4 earthquakes from the instrumental data versus slip rate for the faults listed in Table 2. The identification numbers for the faults corresponding to Table 2 are also shown. The vertical error bars reflect the maximum and minimum ratio (as in Fig. 9), and horizontal error bars represent uncertainties in the fault slip rates.

Figure 15: Recurrence rates of M4 earthquakes predicted by using estimates of slip rate (Table 1) and Mmax (Table 2), and by assuming that seismicity is distributed in accord with the Gutenberg-Richter relationship for all magnitudes up to Mmax (Wesnousky et al., 1983), versus the observed recurrence rate of M4 earthquakes from the instrumental data. The identification numbers for the faults corresponding to Table 2 are shown. We also show that the predicted and observed recurrence rates for the entire 1000 km length of the San Andreas fault, and for the 200 km combined length of the Newport-Inglewood-Rose Canyon faults (open symbols) are similar to those of the much shorter northern San Andreas, southern San Andreas, and Newport-Inglewood faults (1,12 and 3).

Figure A: Strip maps of faults listed in Table 1 and described in the Appendix. The numbering sequence on the maps and below corresponds to the identification numbers in Table 1. The reference and scale of source maps used to construct strip maps are (1&12) Hope (1969); Ross (1969); Brown (1970); Vedder and Wallace (1970); Brown and Wolfe (1972); Herd and Helley (1977); Clarke (1984); Matti *et al* (1985), 1:24,000-1:250,000; (2) Clark (1973), 1:24,000; (3) Barrows 1974, 1:125,000; (4) Anderson *et al.* 1989, California Division of Mines and Geology, 1992, 1:750,000-1:3,500,000; (5) Sharp 1975, 1:24,000; (6-10) Morton *et al.* (1980), 1:24,000; (11) Gastil *et al.* (1975); Harvey (1985), 1:30,000; (13&14) Radbrush-Hall (1974); Herd and Helley (1977); Herd (1979, 1988); California Division of Mines and Geology, 1992, 1:24,000-1:750,000; (15-20) Okada and Ikeda (1991); Research Group for Active Faults of Japan (1992), 1:25,000-1:200,000; (22) Lensen (1976); Johnston (1990), 1:50,000; (25) Freund (1971); Cowan (1990, 1991); Yang (1991), 1:250-1:63,360; (26&27) Institute of Geological and Nuclear Sciences (1994), 1:250,000; (28) Institute of Geology (1991), 1:200,000; (29) Institute of Geology (1990), 1:50,000; (30) Barka and Kadinsky-Cade (1988), 1:1,350,000-1:2,100,000. Strike-slip faults are shown as solid dark lines, and thrust faults show teeth on the up thrown side. Cumulative strike-slip offsets, in km, are labeled on each map (ss). Note that in the cases of the southern section of the San Andreas fault, Garlock, Newport-Inglewood, Whittier-Elsinore and San Jacinto faults we have used summary strip maps from Petersen and Wesnousky (1994), but have listed the original references and map scales above.

BIBLIOGRAPHY OF PUBLICATIONS RESULTING FROM THIS WORK.

Professional Papers:

Stirling, M. W., S. G. Wesnousky, and K. Shimazaki (1996), Fault Trace Complexity, Cumulative Slip, and the Shape of the MAgnitude-frequency Distribution for Strike-slip faults: a global survey, Geophsical Journal International, 124, 833-868.

Wesnousky, S. G. (1996), Reply to Yan Kagan's Comment on "The Gutenberg-Richter Earthquake Distribution, Which is it?", Bulletin of the Seismological Society of America, v. 86, 286-291)

Anderson, J. G., Wesnousky, S. G., and M. W. Stirling, (1996) Earthquake Size as a Function of Fault Slip Rate, Bulletin of the Seismological Society of America, Bulletinof the Seismological Society of America, 86, 683-691.

Abstracts:

1994 AGU Annual Fall Meeting, San Francisco, CA
Stirling, M., S. G. Wesnousky, and K. Shimazaki, Fault Trace Complexity, Cumulative Slip and the Shape of the Magnitude-Frequency Distribution fort Strike-Slip Faults: A Global Survey, EOS supplement, Nov 1, 1994, p. 437.

1995 SSA Annual Meeting, El Paso, TX
Anderson, J. G., S. G. Wesnousky, M.W. Stirling, M.P. Sleeman, and T. Kumamoto, Regressions for Magnitude of Earthquakes incorporating fault slip rate as an independent parameter.

1995 AGU Annual Fall Meeting, San Francisco, CA (INVITED)
Stirling, M. W. and S. G. Wesnousky, Shape of the Magnitude-Frequency Distribution for Strike-Slip Faults: a Global Survey, EOS supplement, November 7, 1995, p. F389

A. Gutenburg - Richter Relationship

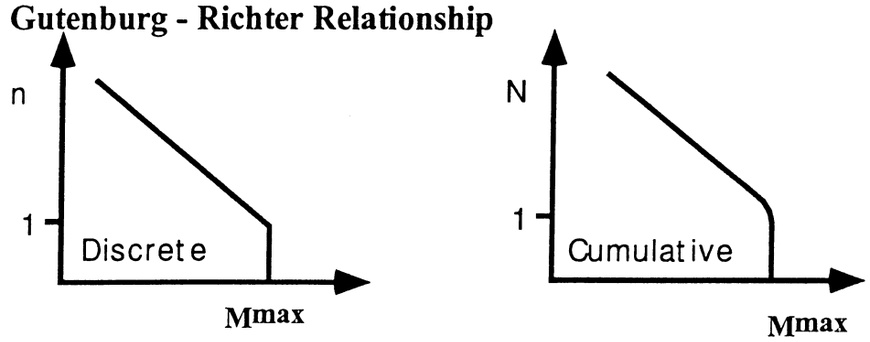

B. Characteristic Earthquake Model

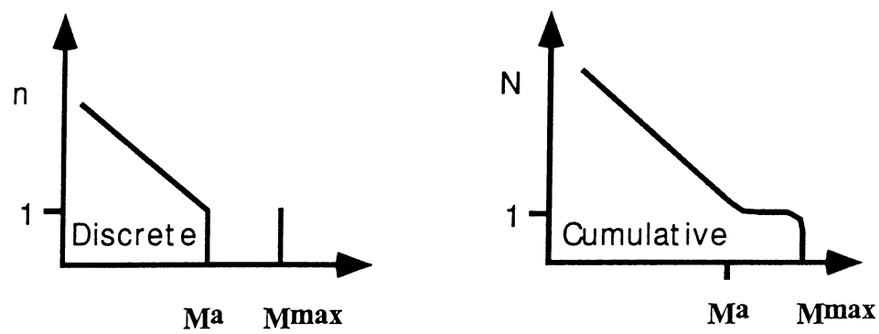

FIGURE 1

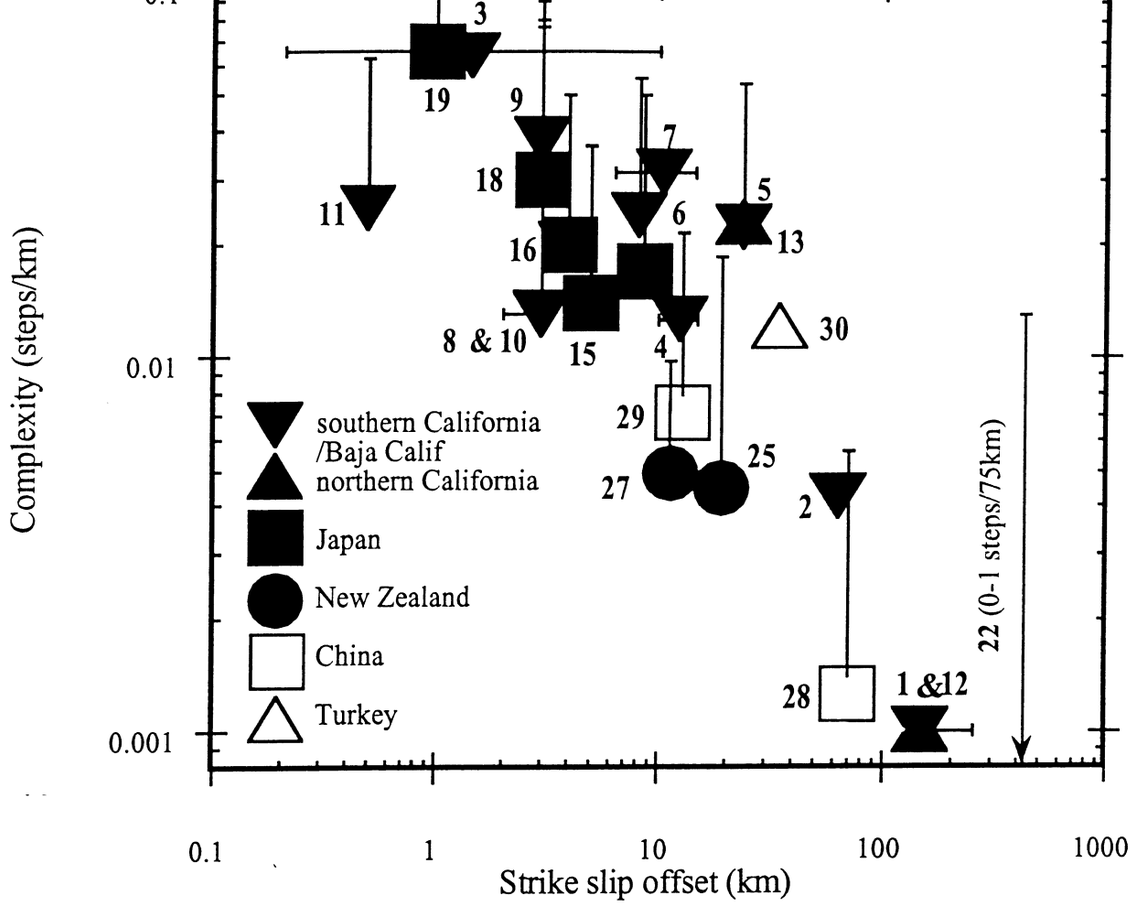
Complexity (steps/km)
0.01
0.001
0.1
1
10
100
1000
Strike slip offset (km)
southern California
/Baja Calif
northern California
Japan
New Zealand
China
Turkey
3
19
9
7
18
11
5
6
13
16
8 & 10
15
4
30
29
25
27
2
22 (0-1 steps/75km)
28
1 &12

FIGURE 2

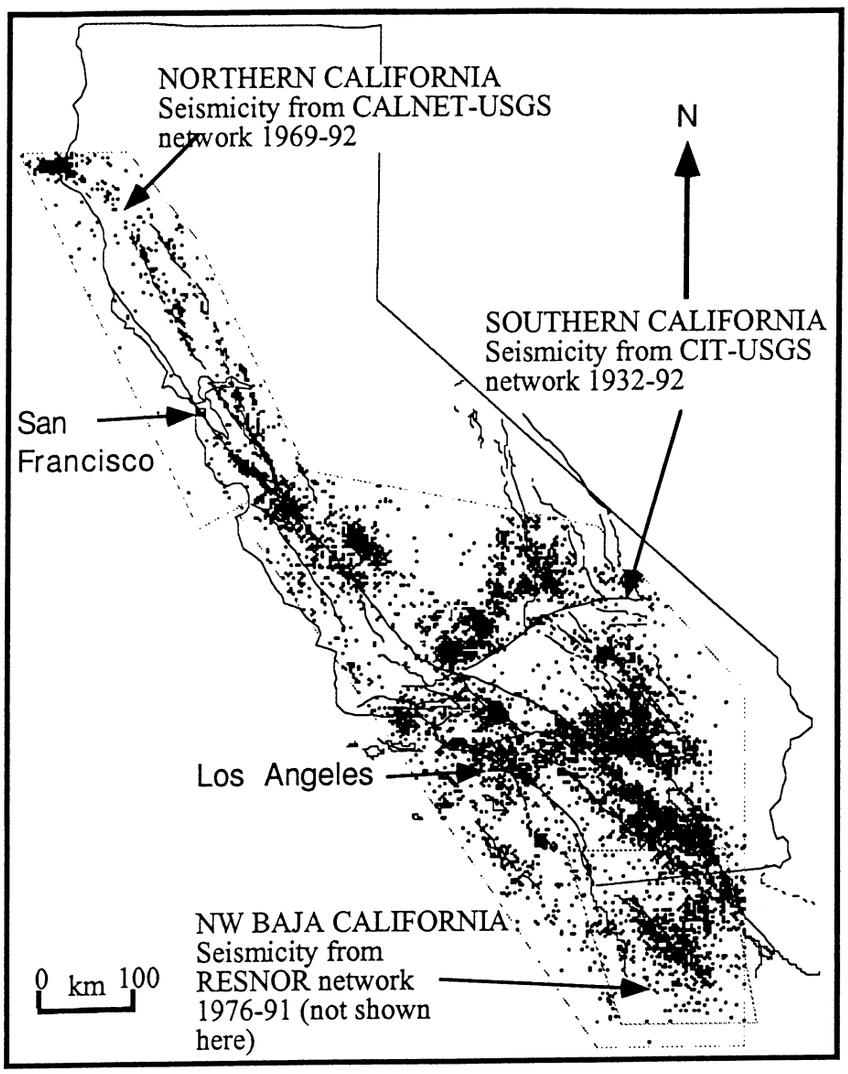
NORTHERN CALIFORNIA
Seismicity from CALNET-USGS
network 1969-92
N
SOUTHERN CALIFORNIA
Seismicity from CIT-USGS
network 1932-92
San
Francisco
Los Angeles
NW BAJA CALIFORNIA
Seismicity from
RESNOR network
1976-91 (not shown
here)
0 km 100

FIGURE 3A

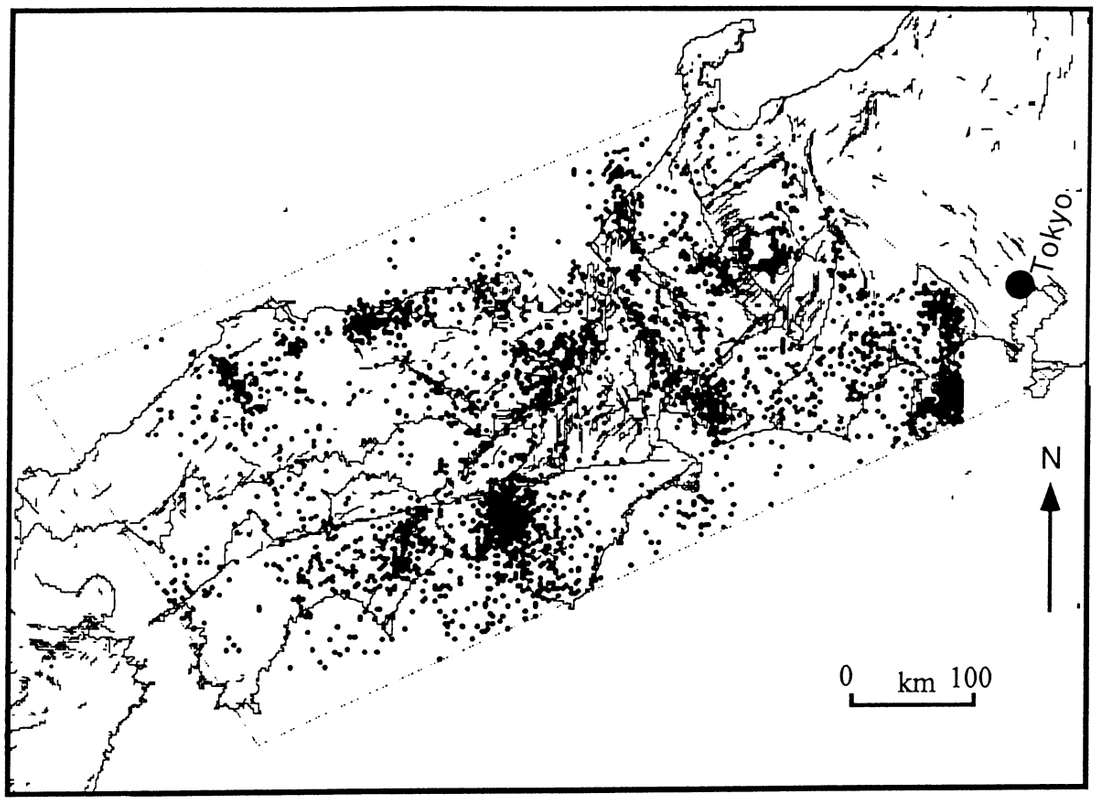

FIGURE 3B

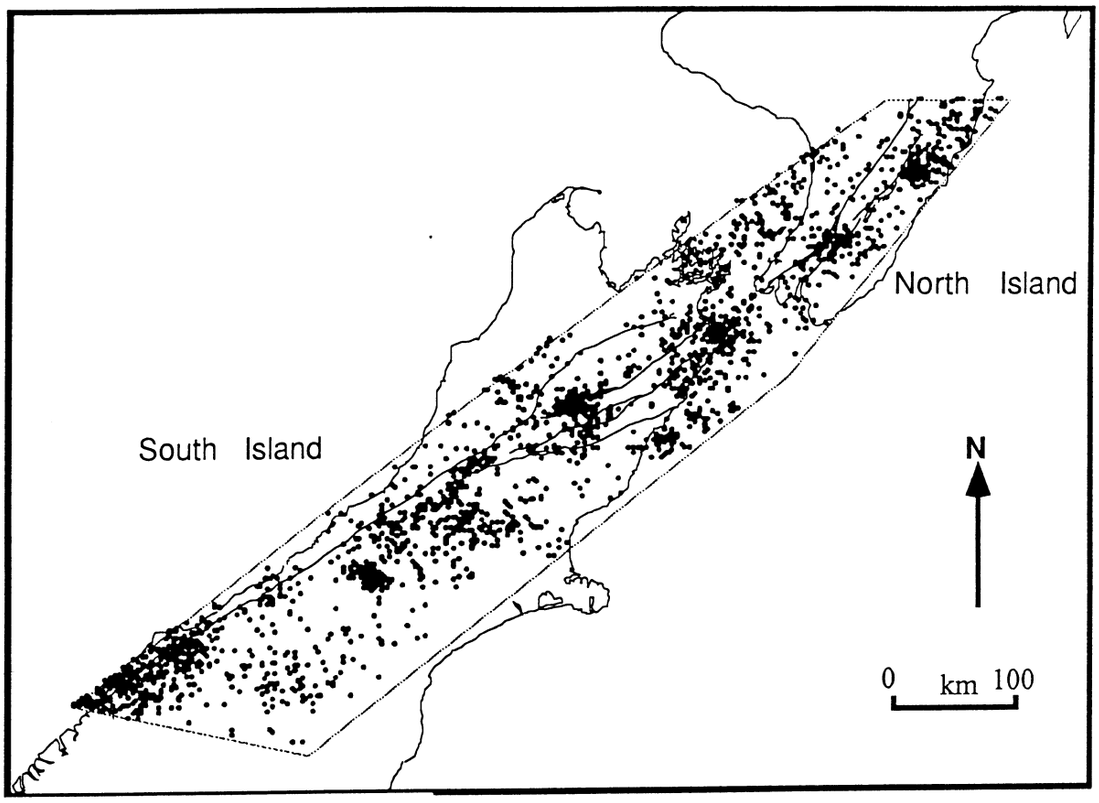

FIGURE 3C

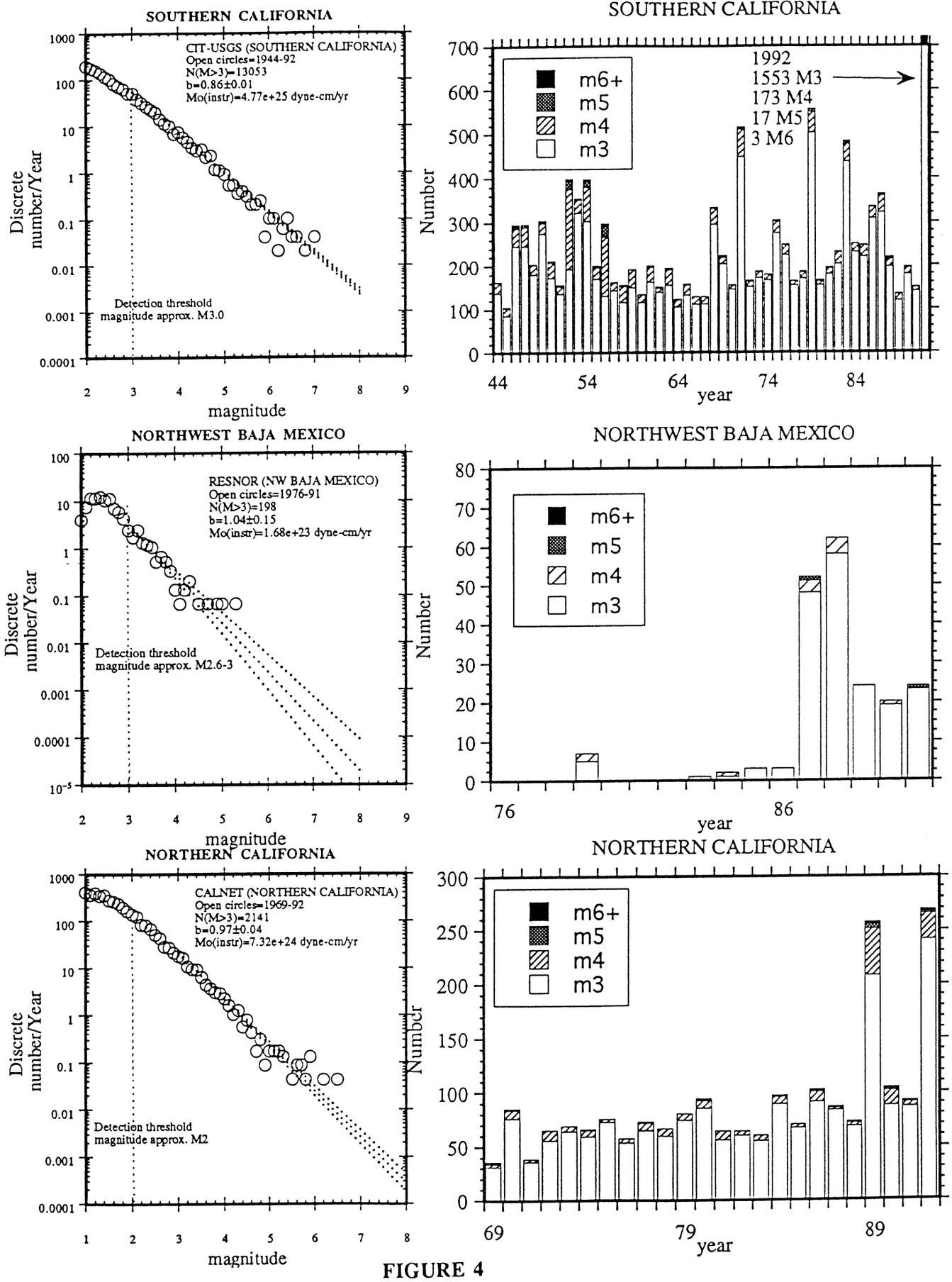
SOUTHERN CALIFORNIA
CIT-USGS (SOUTHERN CALIFORNIA)
Open circles=1944-92
N(M>3)=13053
b=0.86±0.01
Mo(instr)=4.77e+25 dyne-cm/yr
Detection threshold
magnitude approx. M3.0
Discrete number/Year
magnitude
SOUTHERN CALIFORNIA
m6+
m5
m4
m3
1992
1553 M3
173 M4
17 M5
3 M6
Number
year
NORTHWEST BAJA MEXICO
RESNOR (NW BAJA MEXICO)
Open circles=1976-91
N(M>3)=198
b=1.04±0.15
Mo(instr)=1.68e+23 dyne-cm/yr
Detection threshold
magnitude approx. M2.6-3
Discrete number/Year
magnitude
NORTHWEST BAJA MEXICO
m6+
m5
m4
m3
Number
year
NORTHERN CALIFORNIA
CALNET (NORTHERN CALIFORNIA)
Open circles=1969-92
N(M>3)=2141
b=0.97±0.04
Mo(instr)=7.32e+24 dyne-cm/yr
Detection threshold
magnitude approx. M2
Discrete number/Year
magnitude
NORTHERN CALIFORNIA
m6+
m5
m4
m3
Number
year

FIGURE 4

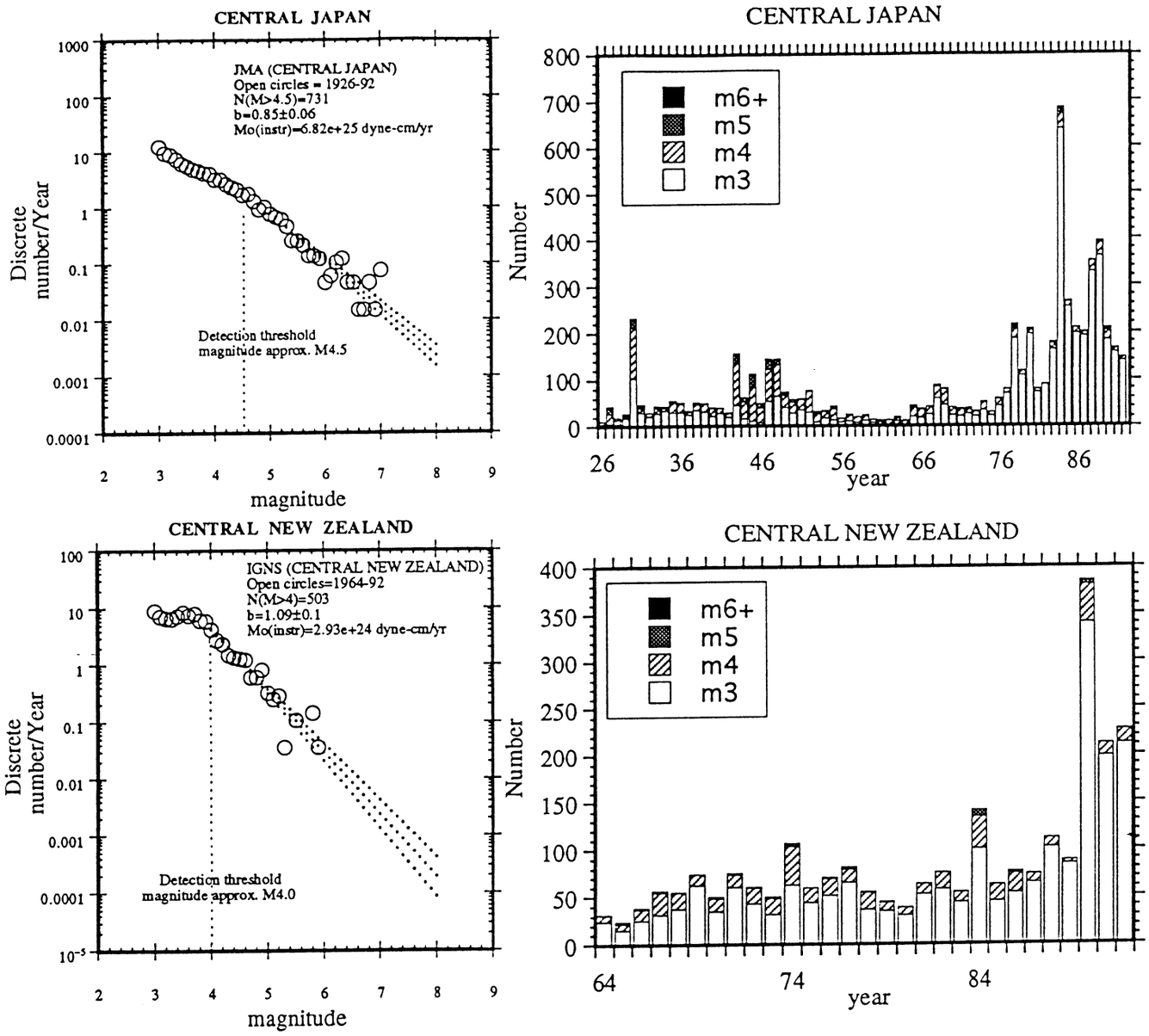

FIGURE 4 (CONT)

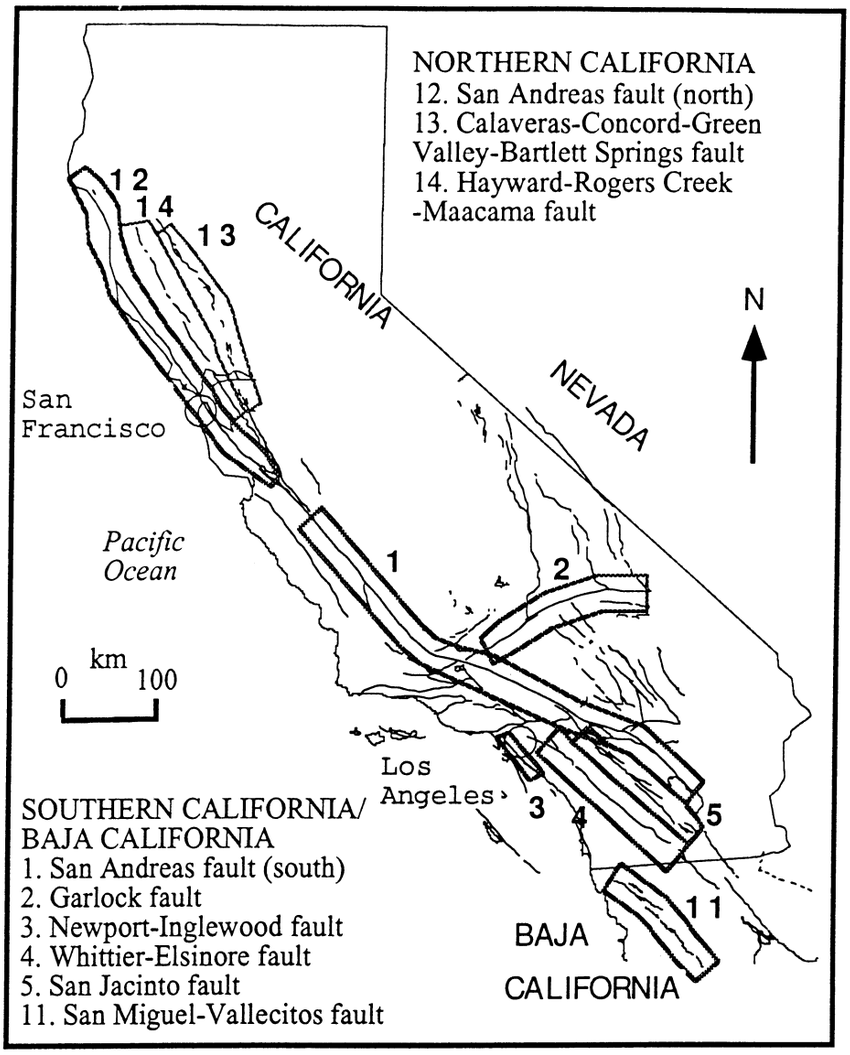
NORTHERN CALIFORNIA
12. San Andreas fault (north)
13. Calaveras-Concord-Green Valley-Bartlett Springs fault
14. Hayward-Rogers Creek -Maacama fault
12
14
13
CALIFORNIA
NEVADA
N
San Francisco
Pacific Ocean
1
2
km
0
100
Los Angeles
3
4
5
11
BAJA CALIFORNIA
SOUTHERN CALIFORNIA/ BAJA CALIFORNIA
1. San Andreas fault (south)
2. Garlock fault
3. Newport-Inglewood fault
4. Whittier-Elsinore fault
5. San Jacinto fault
11. San Miguel-Vallecitos fault

FIGURE 5A

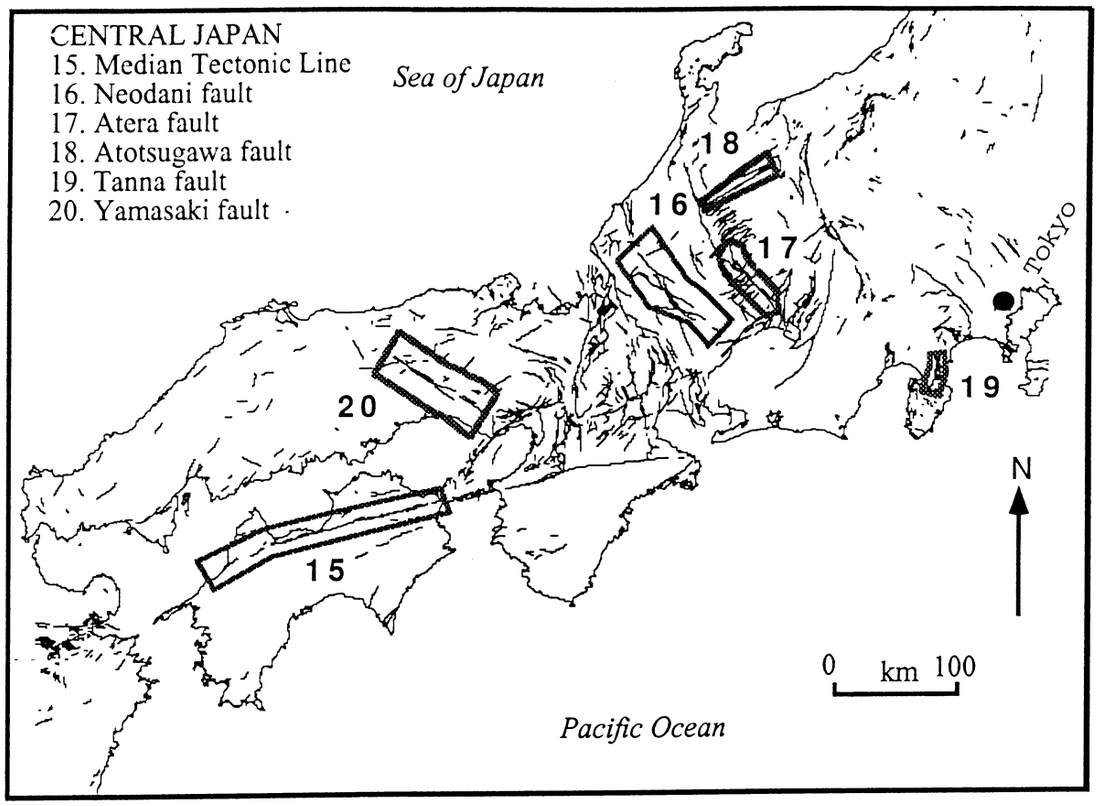
CENTRAL JAPAN
15. Median Tectonic Line
16. Neodani fault
17. Atera fault
18. Atotsugawa fault
19. Tanna fault
20. Yamasaki fault
Sea of Japan
18
16
17
Tokyo
19
20
15
N
0 km 100
Pacific Ocean

FIGURE 5B

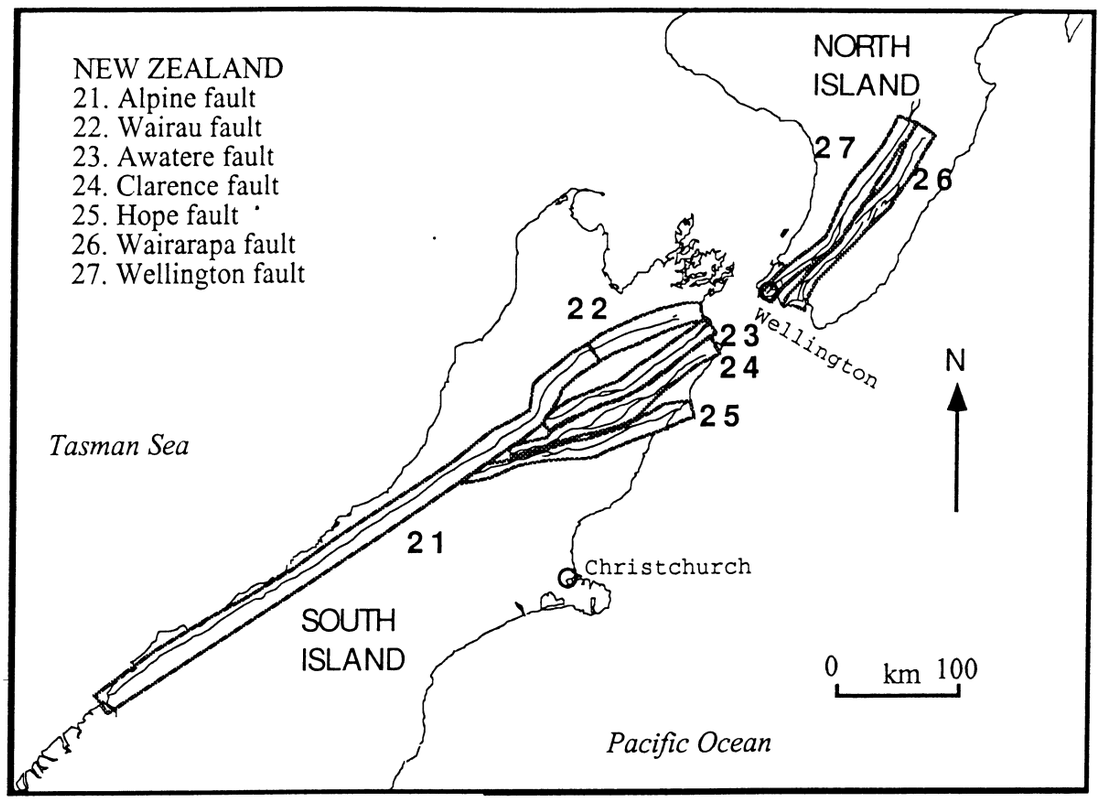
NEW ZEALAND
21. Alpine fault
22. Wairau fault
23. Awatere fault
24. Clarence fault
25. Hope fault
26. Wairarapa fault
27. Wellington fault
NORTH ISLAND
27
26
22
23
24
25
Wellington
N
Tasman Sea
21
Christchurch
SOUTH ISLAND
0 km 100
Pacific Ocean

FIGURE 5C

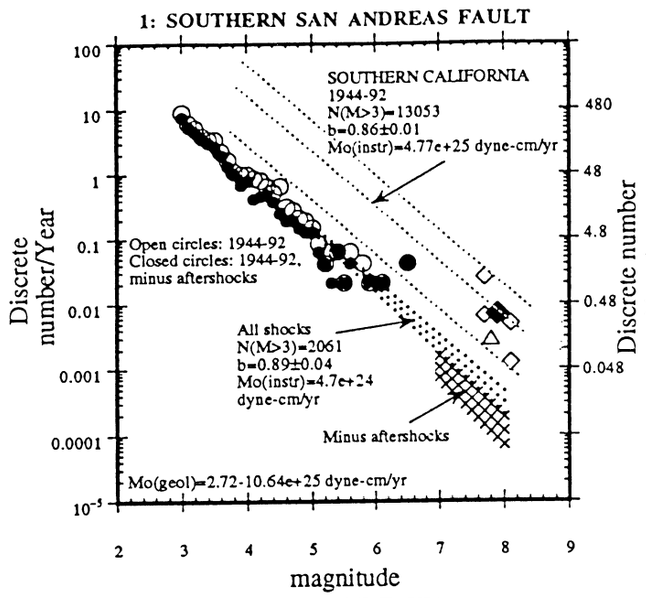

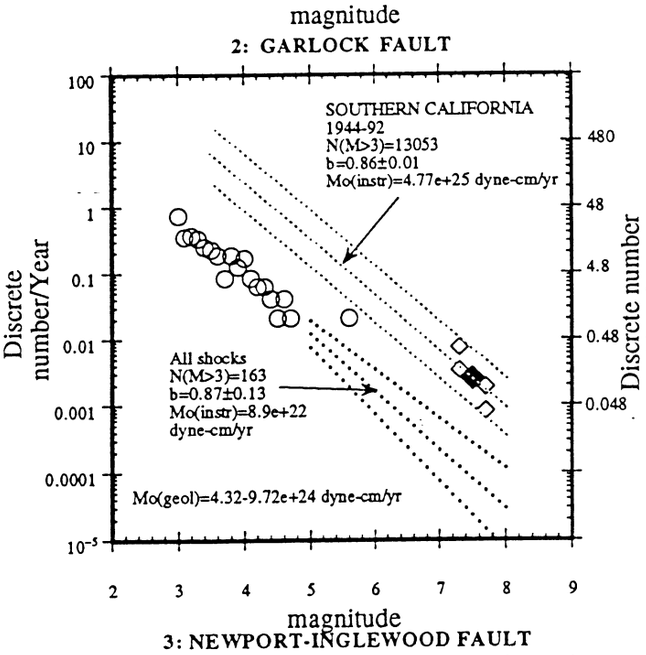

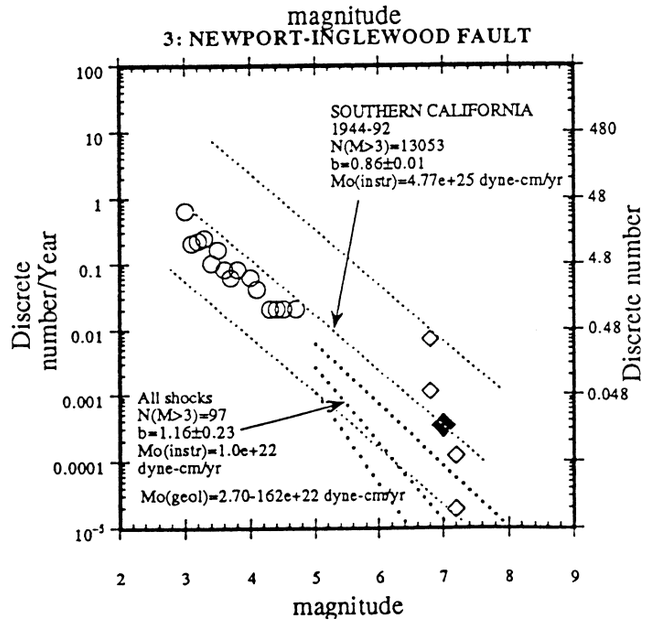

FIGURE 6

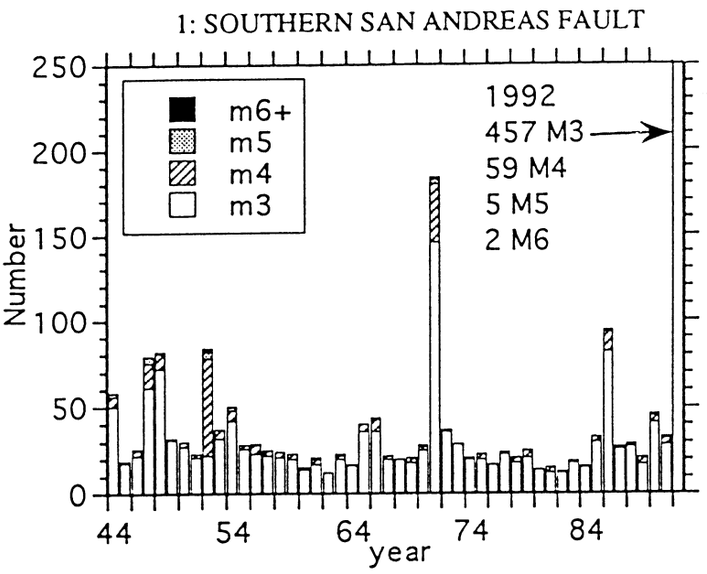

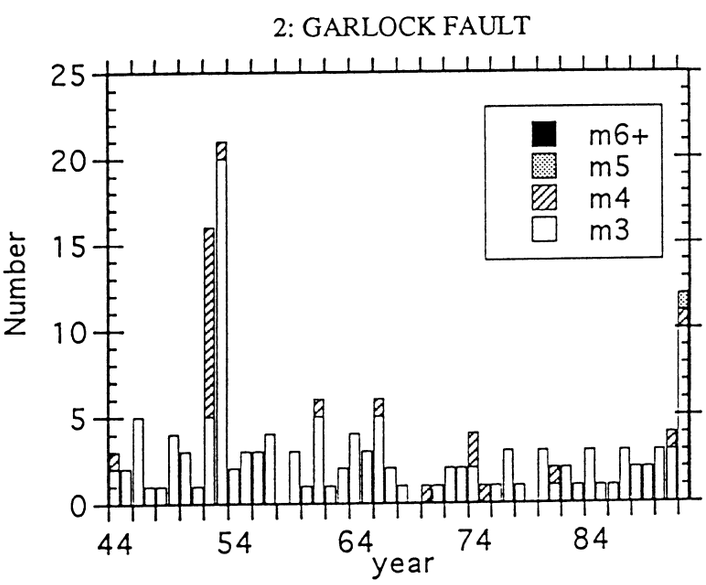

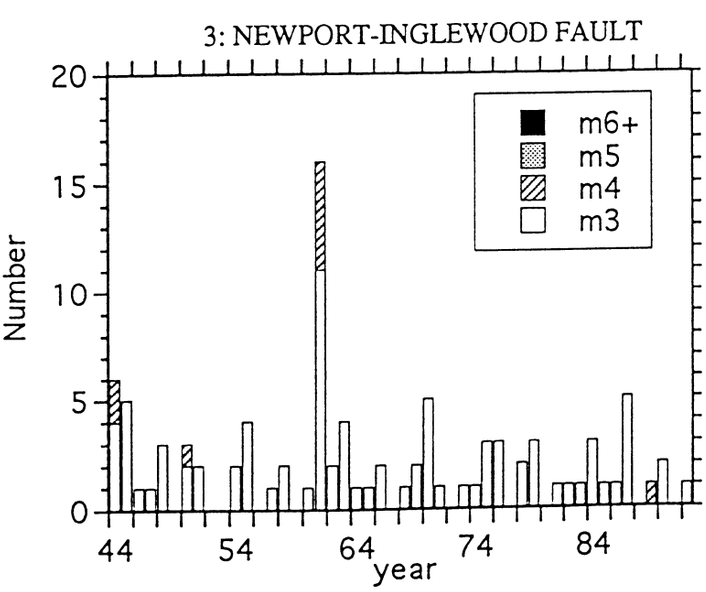

FIGURE 7

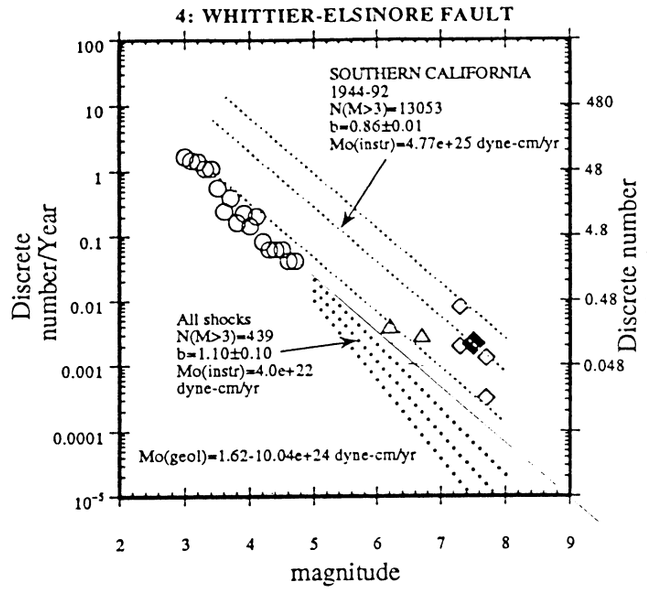

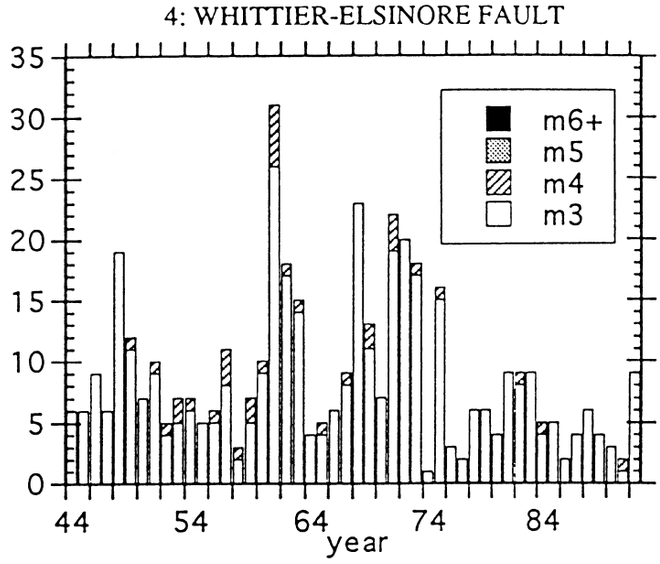

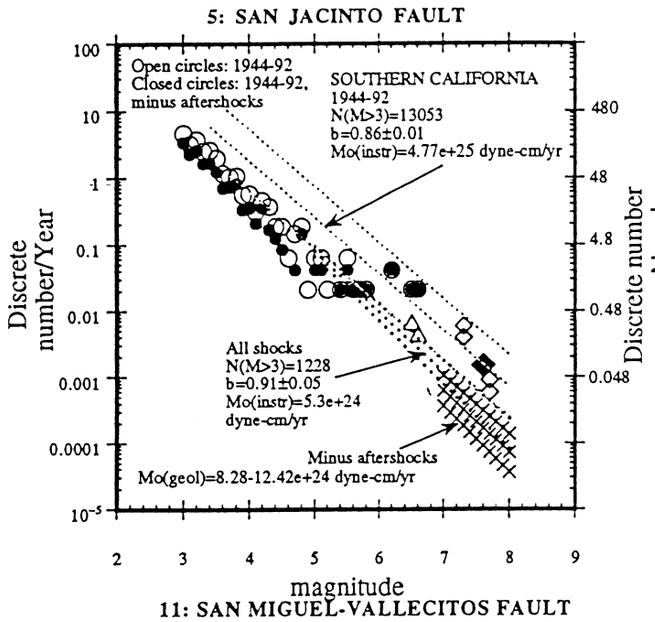

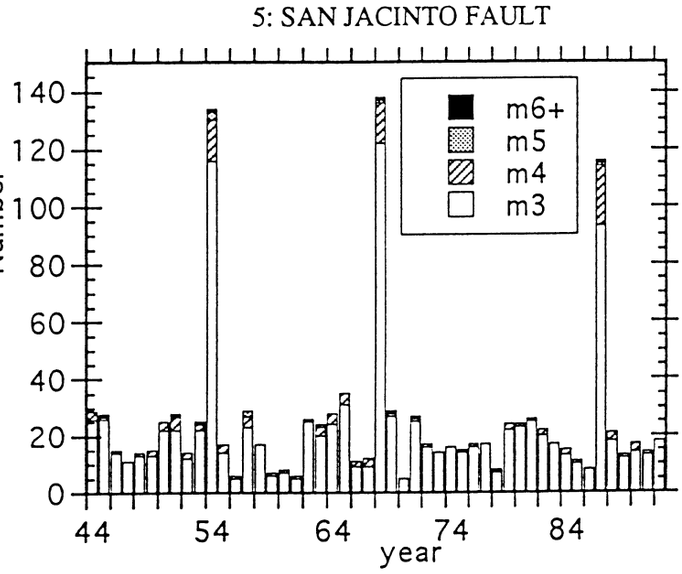

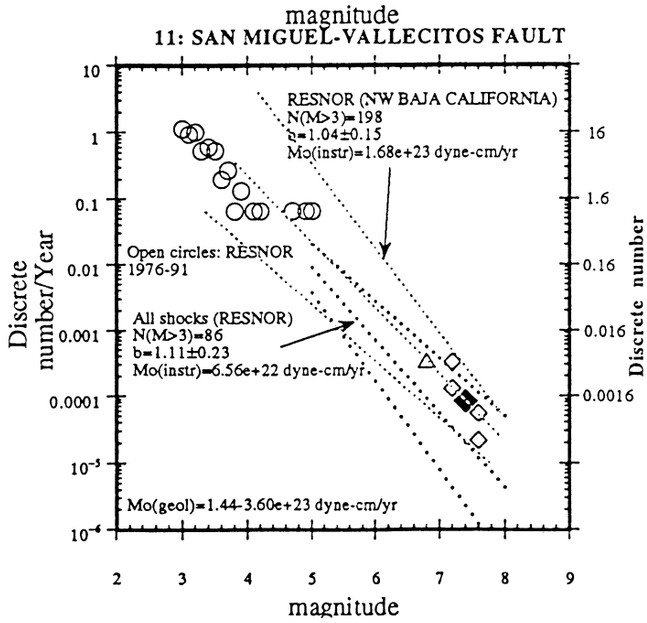

FIGURE 6 (CONT)

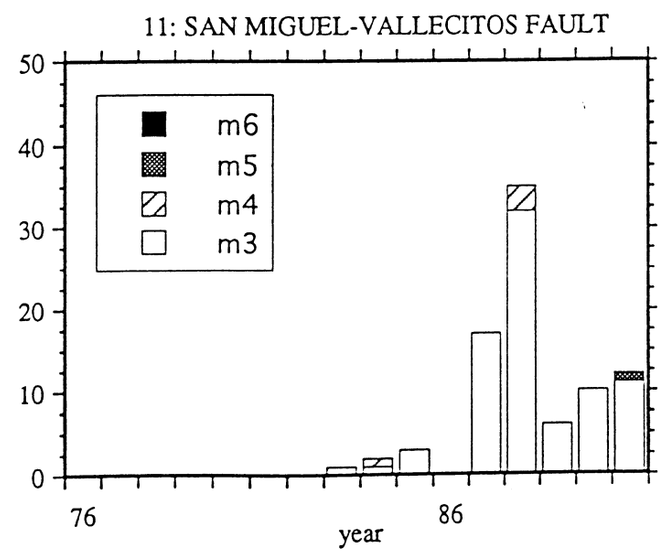

FIGURE 7 (CONT)

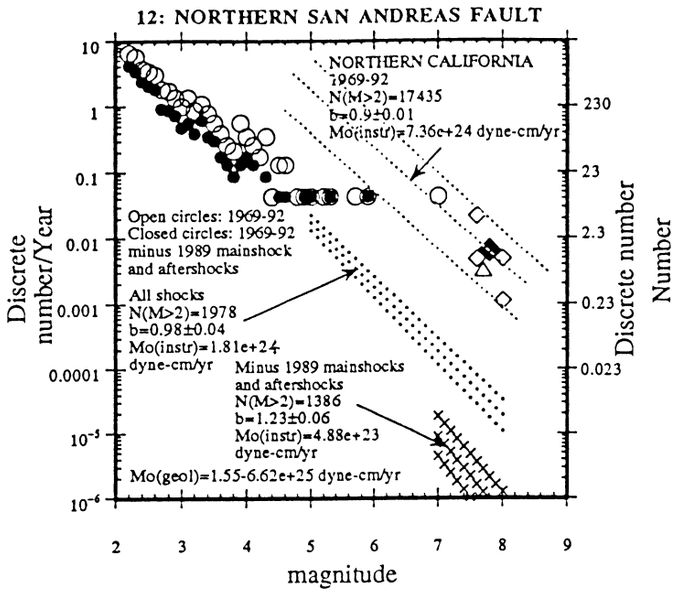

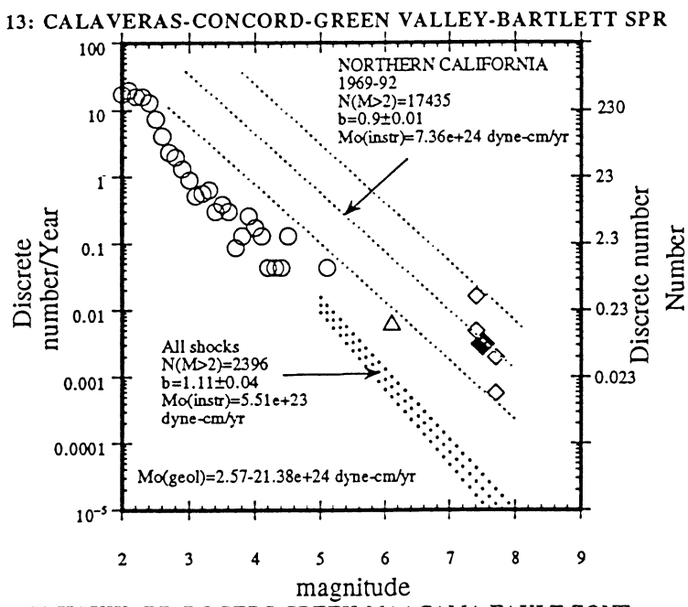

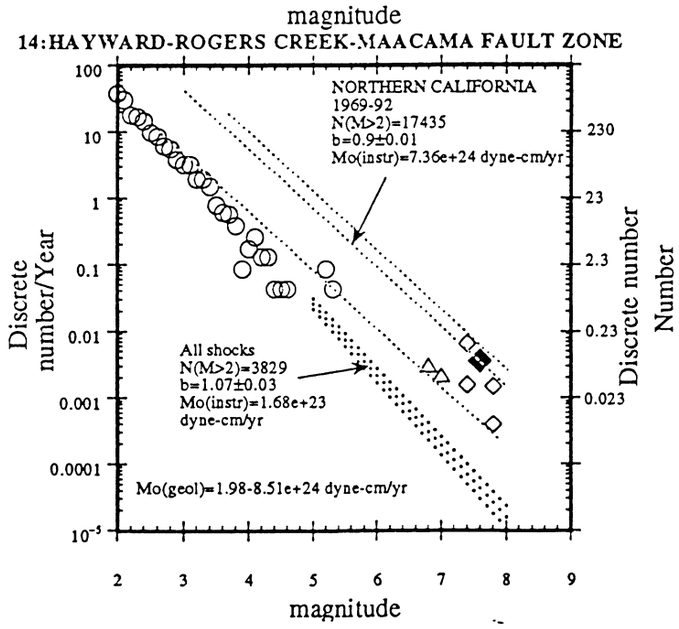

FIGURE 6 (CONT)

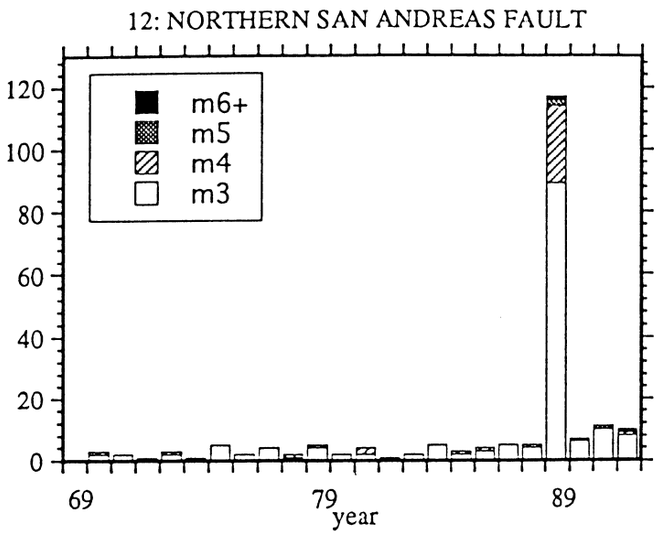

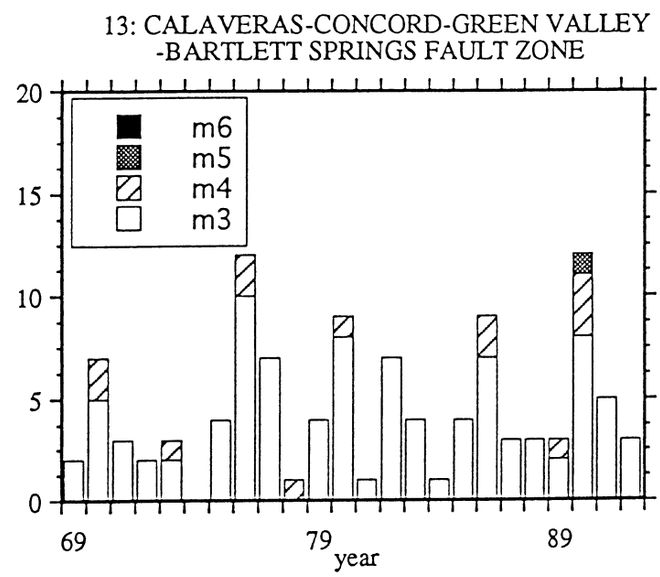

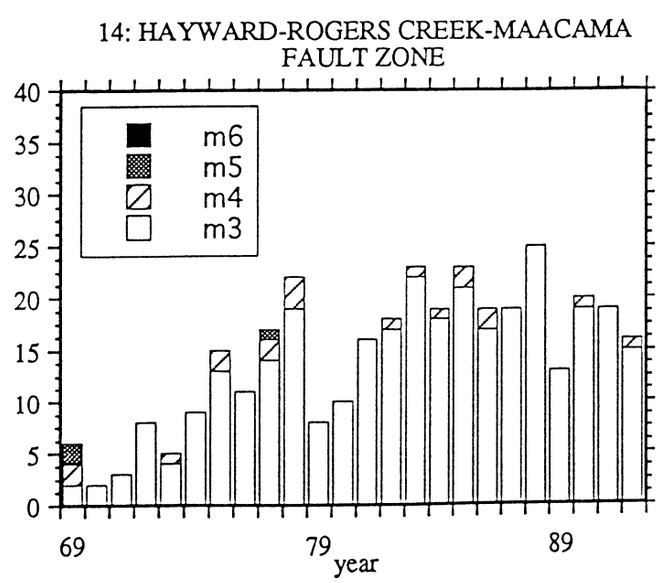

FIGURE 7 (CONT)

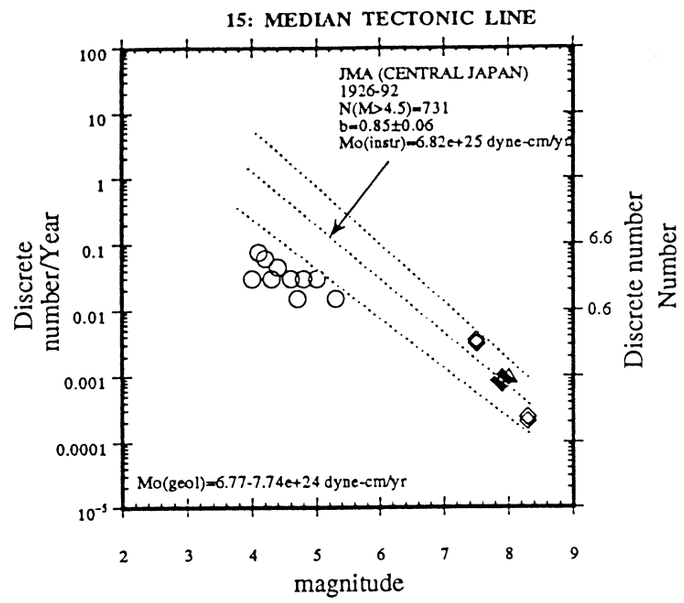

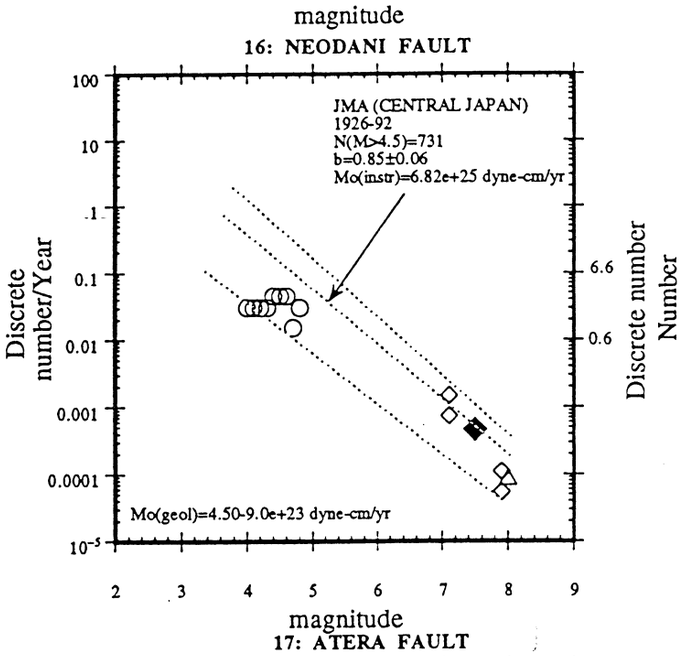

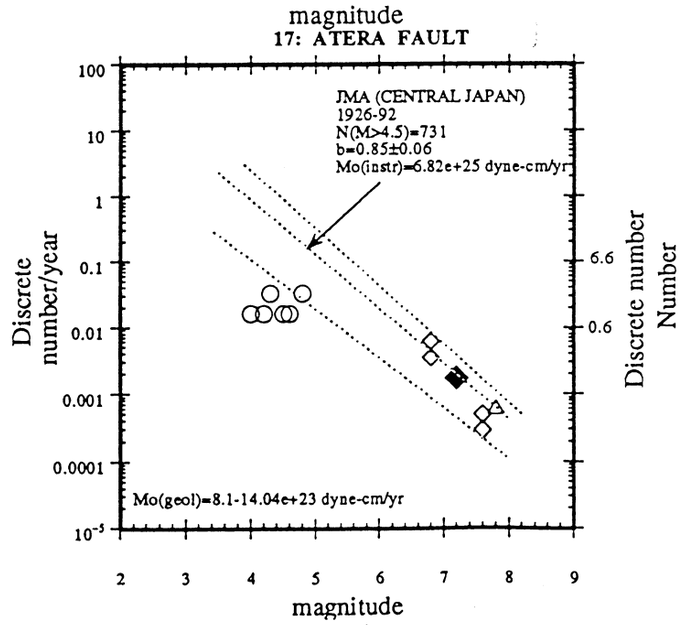

FIGURE 6 (CONT)

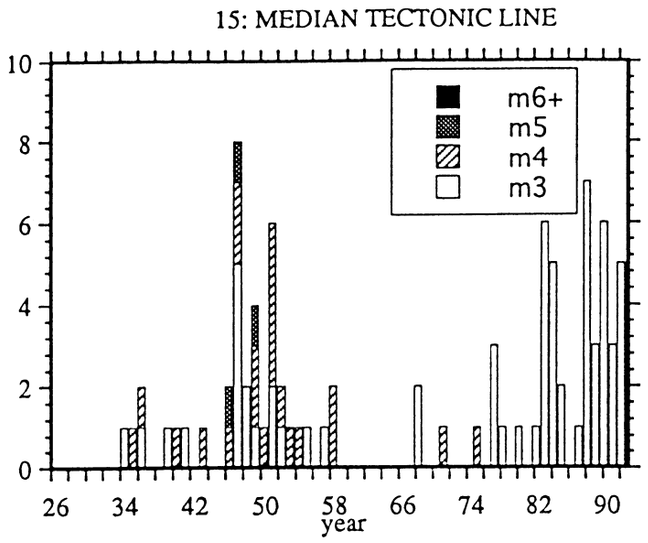

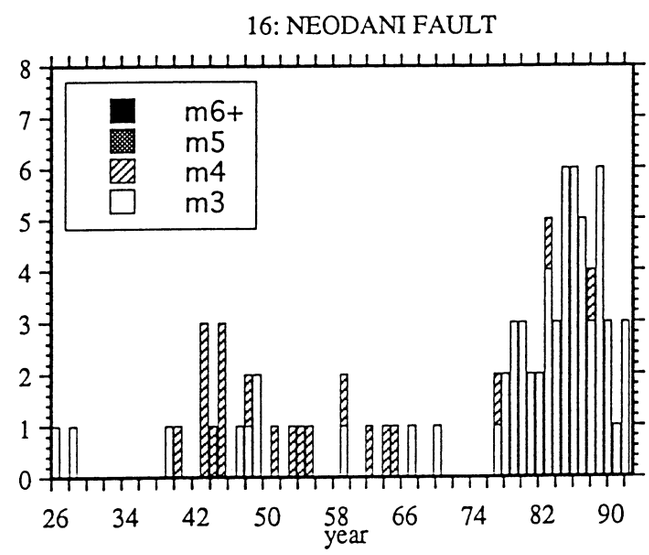

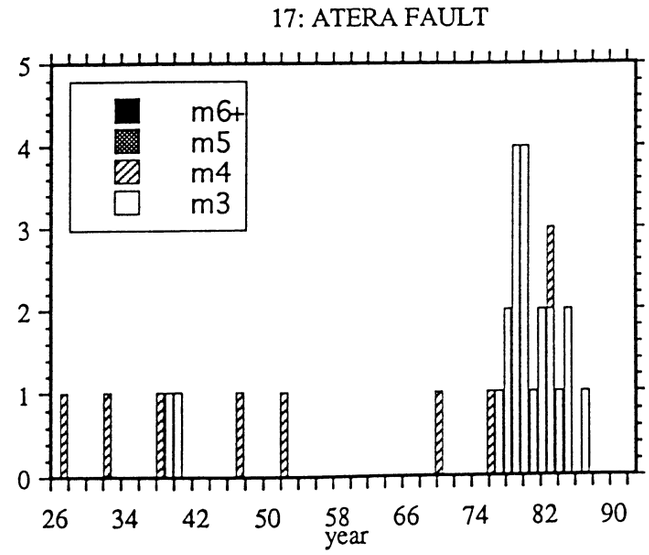

FIGURE 7 (CONT)

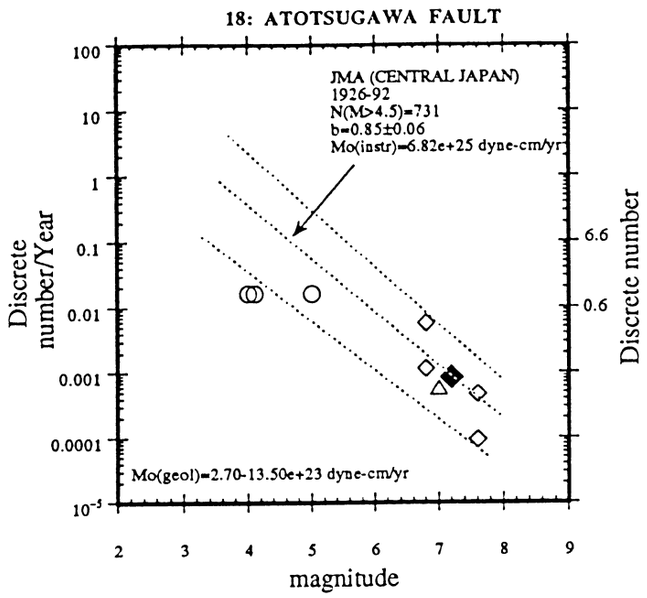

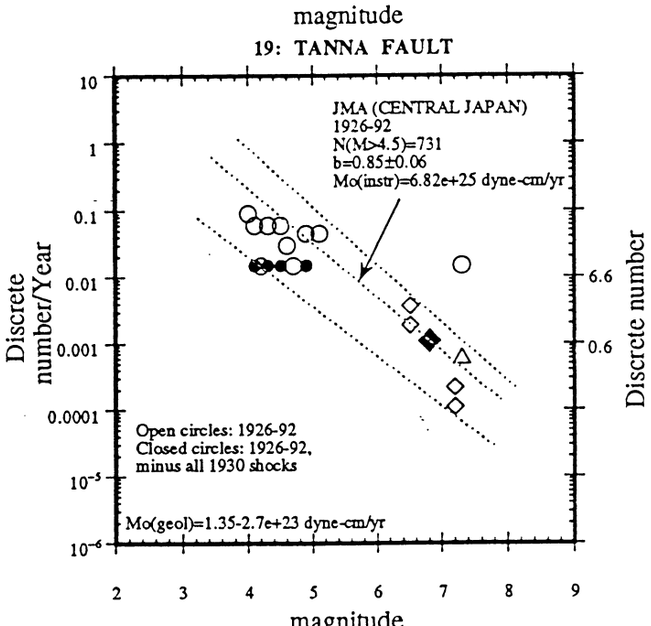

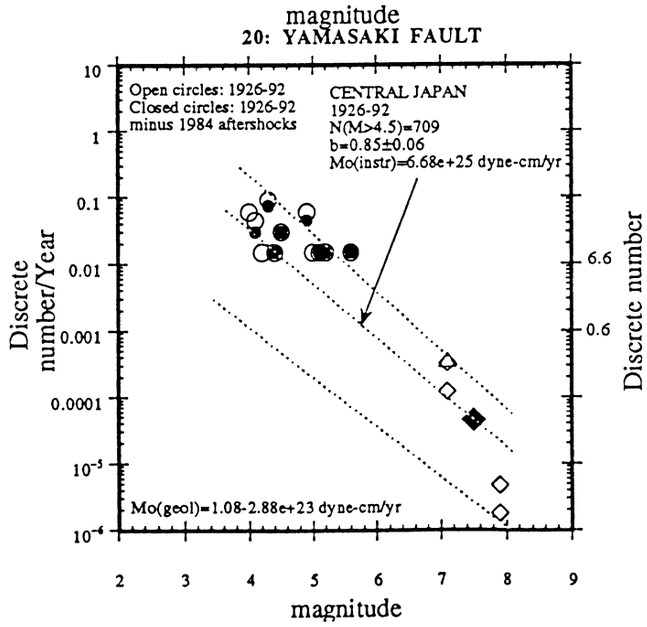

FIGURE 6 (CONT)

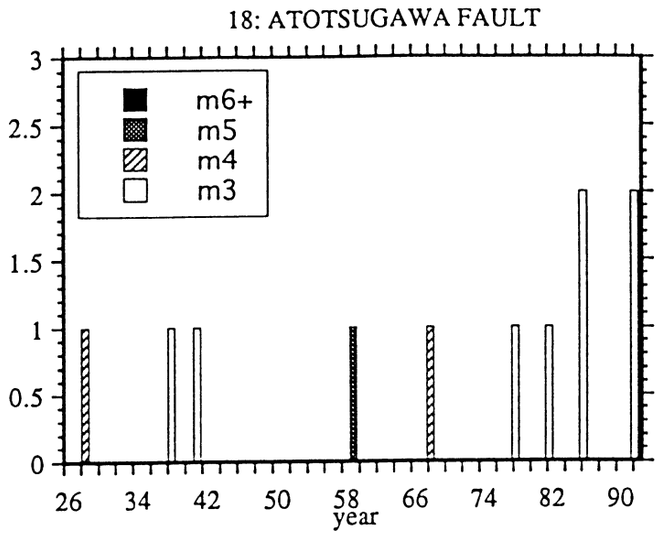

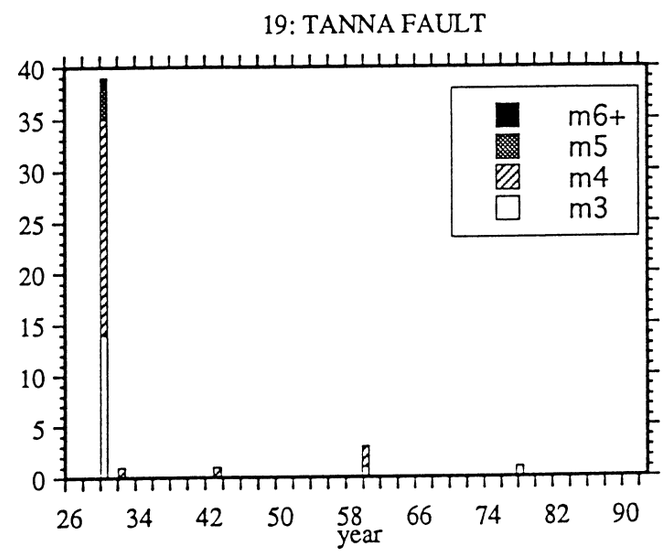

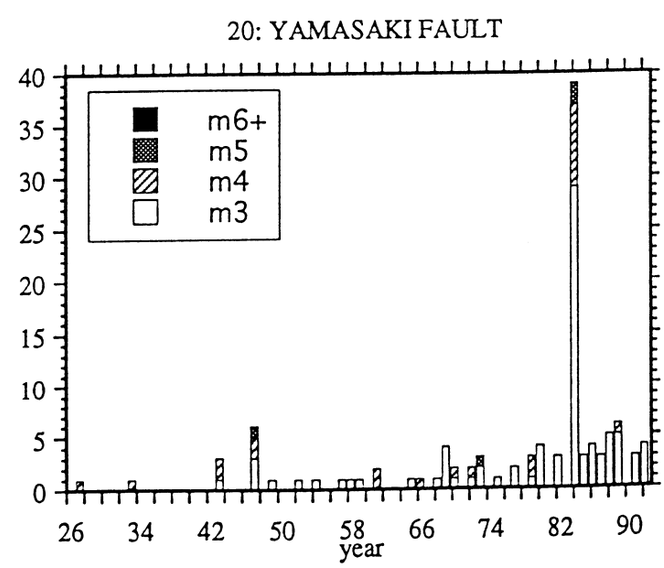

FIGURE 7 (CONT)

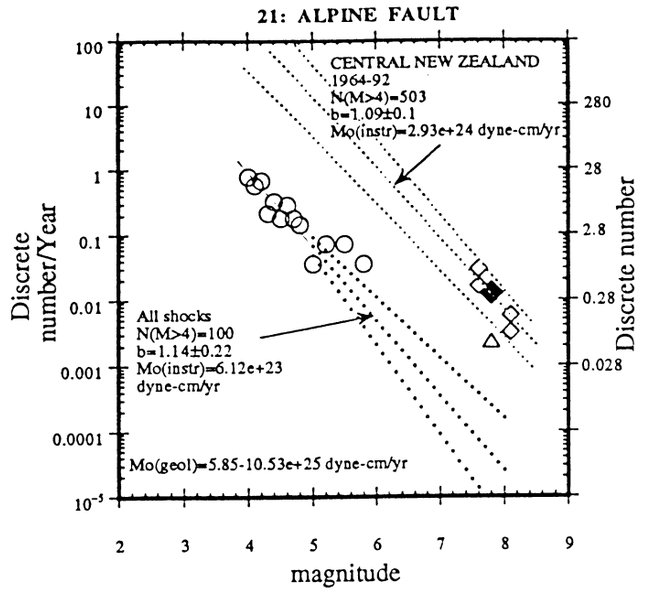

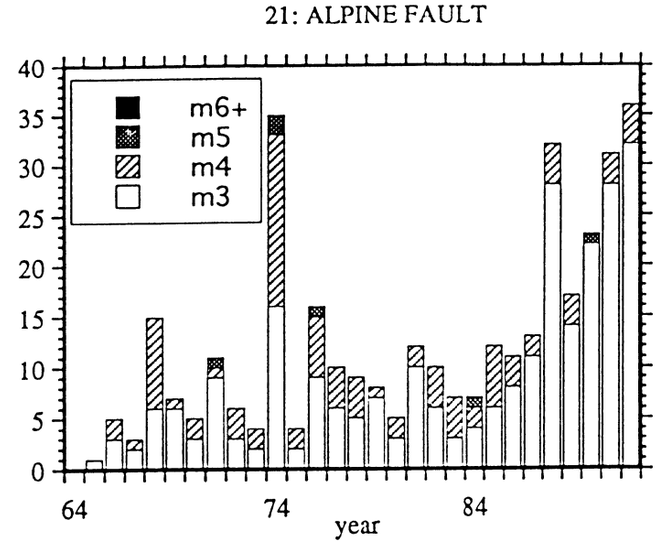

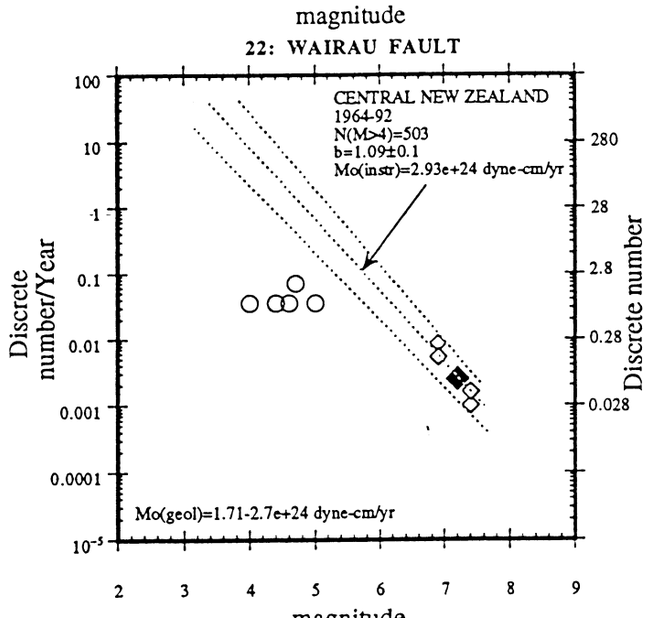

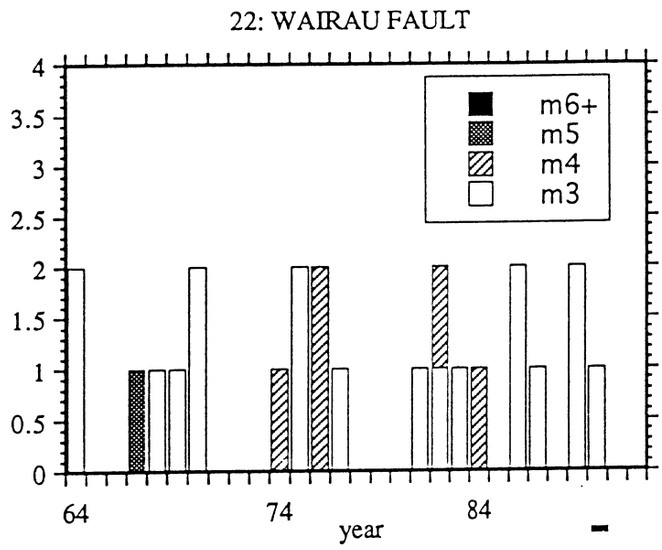

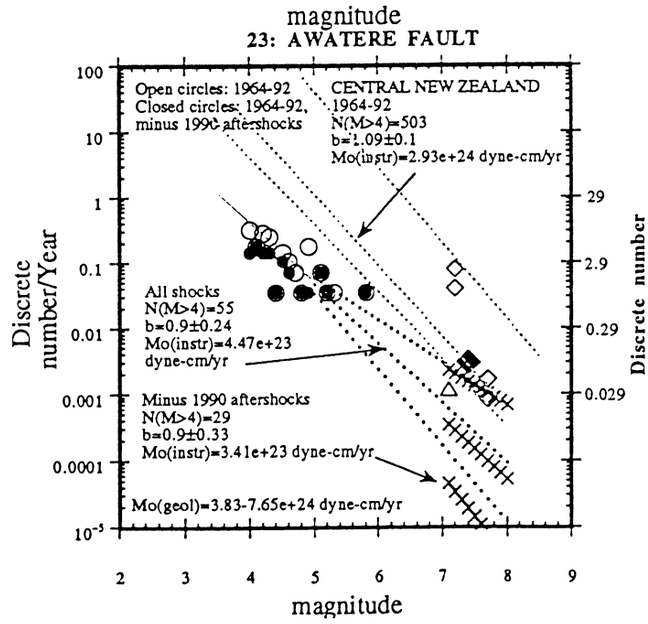

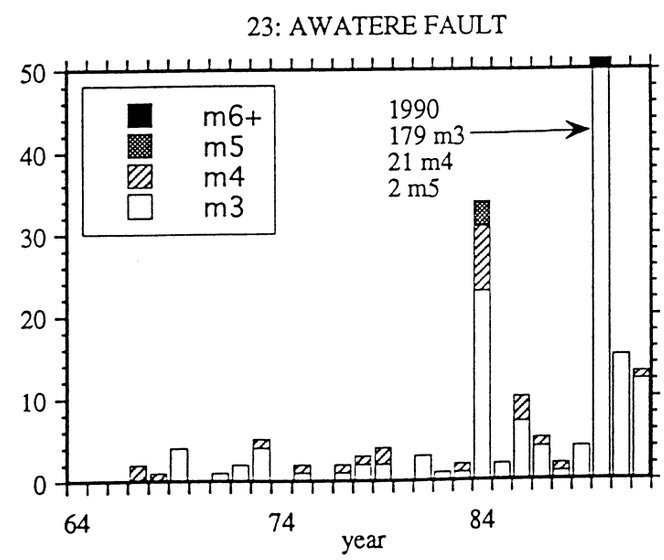

FIGURE 6 (CONT)

FIGURE 7 (CONT)

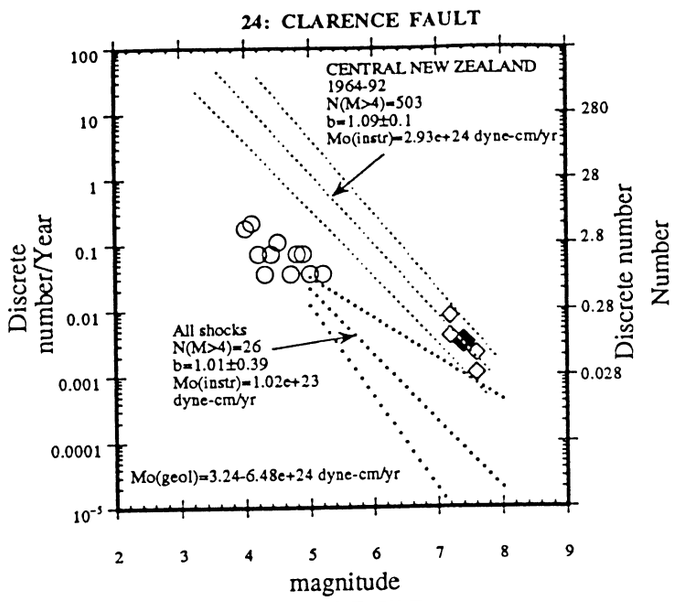

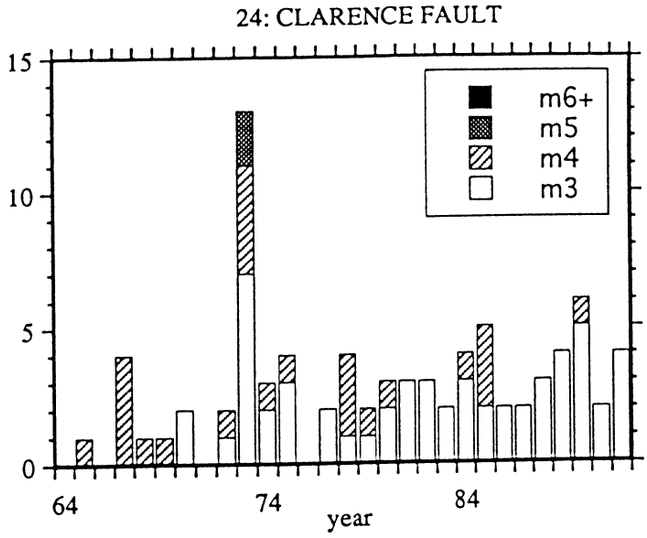

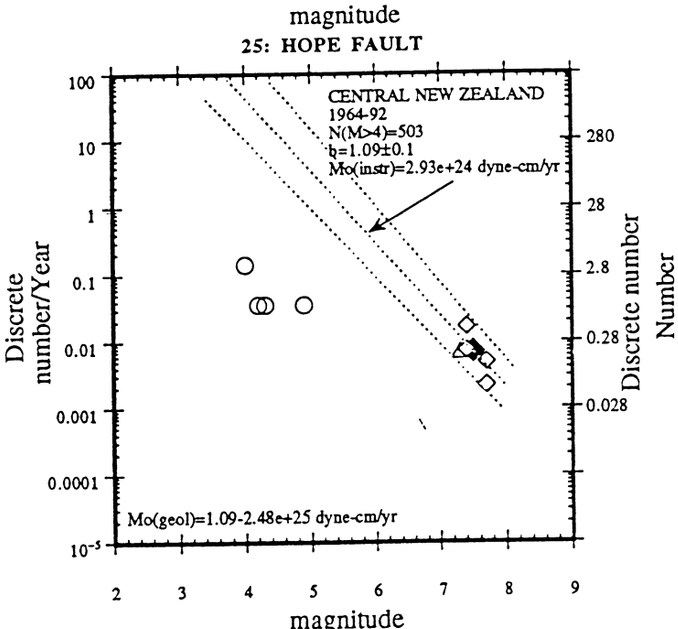

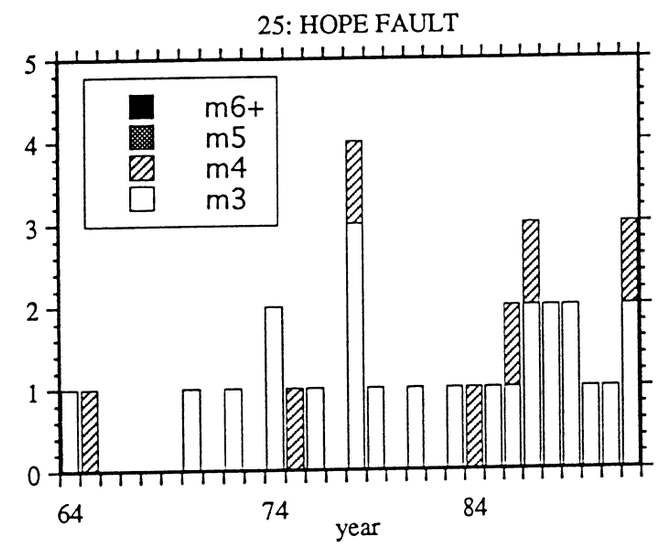

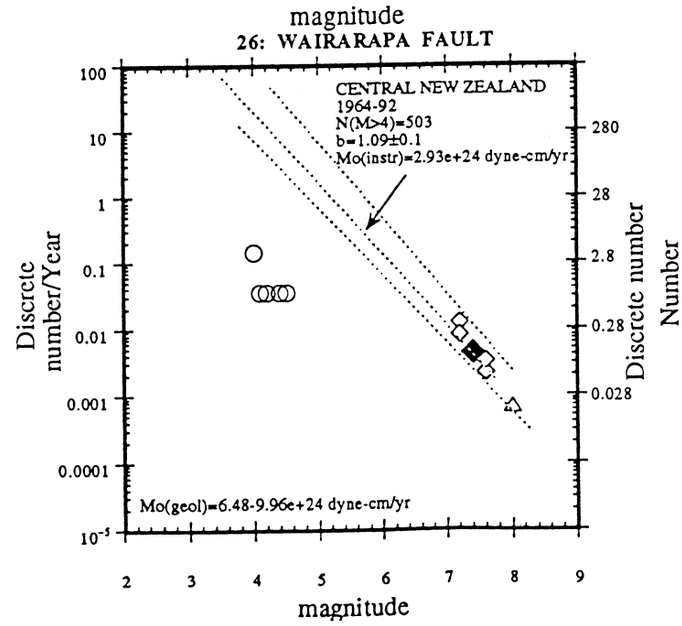

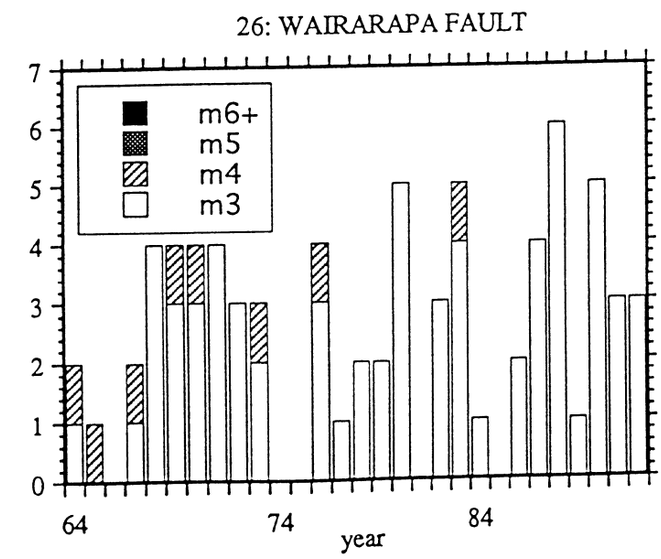

FIGURE 6 (CONT)

FIGURE 7 (CONT)

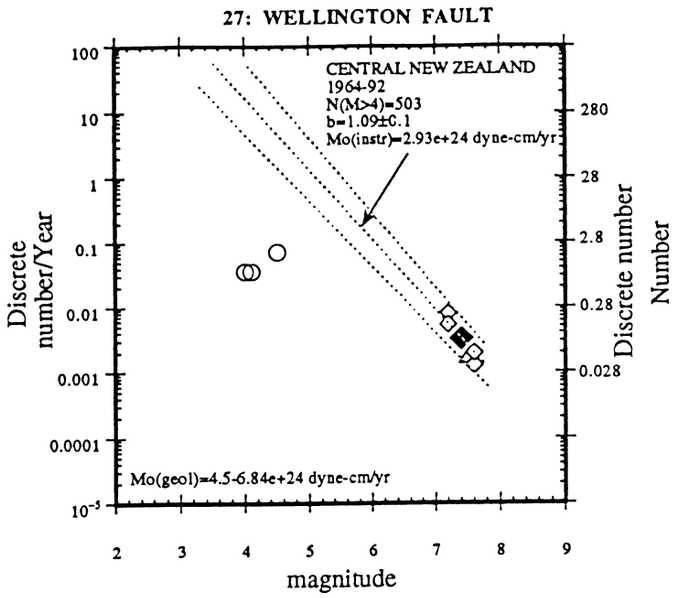

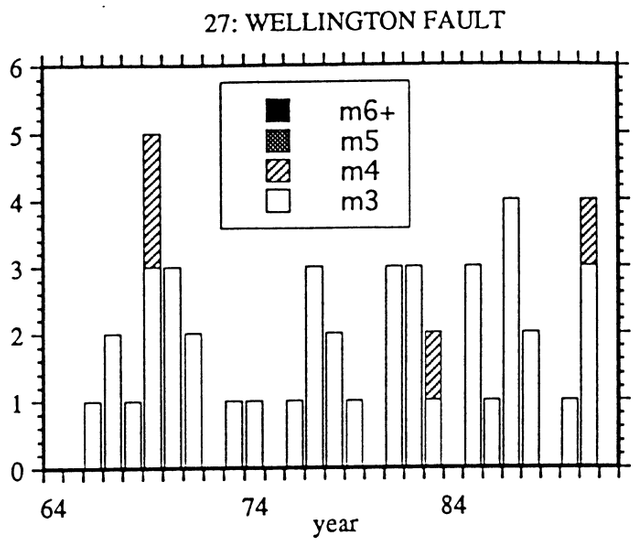

FIGURE 6 (CONT)

FIGURE 7 (CONT)

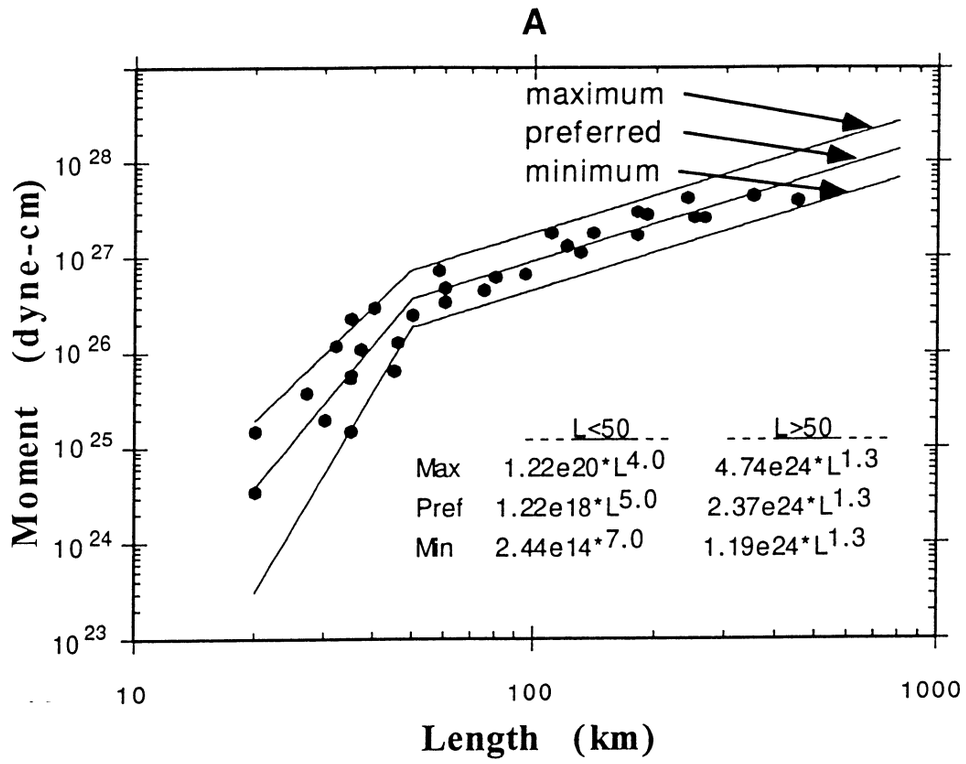
A
maximum
preferred
minimum
Moment (dyne-cm)
10 28
10 27
10 26
10 25
10 24
10 23
L<50
L>50
Max 1.22e20*L4.0 4.74e24*L1.3
Pref 1.22e18*L5.0 2.37e24*L1.3
Min 2.44e14*7.0 1.19e24*L1.3
10
100
1000
Length (km)

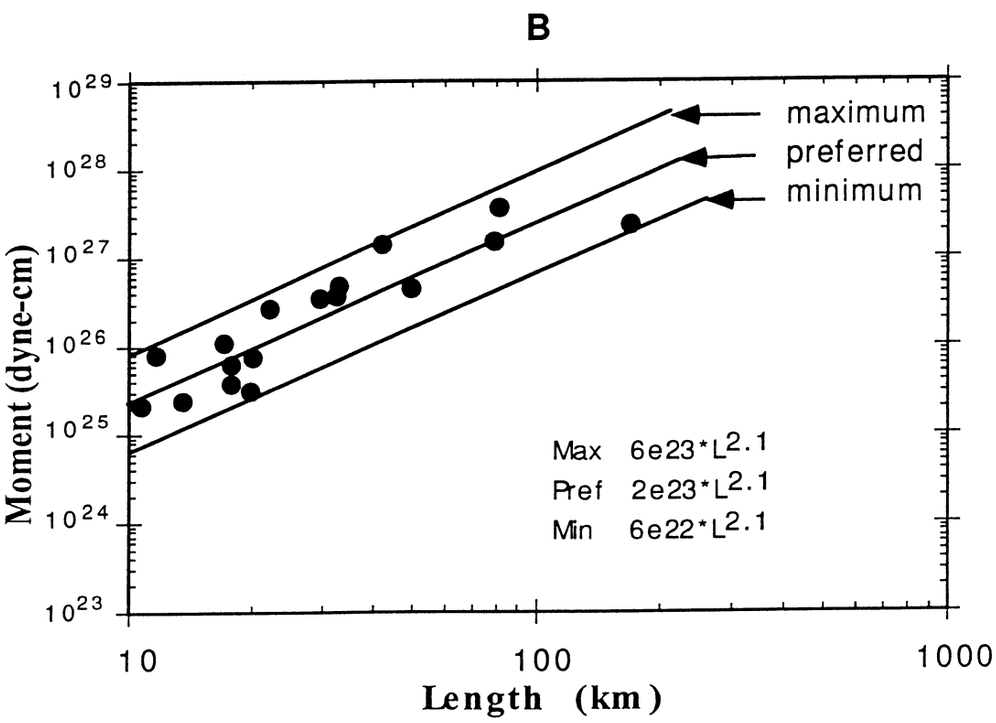
B
maximum
preferred
minimum
Moment (dyne-cm)
10 29
10 28
10 27
10 26
10 25
10 24
10 23
Max 6e23*L2.1
Pref 2e23*L2.1
Min 6e22*L2.1
10
100
1000
Length (km)

FIGURE 8

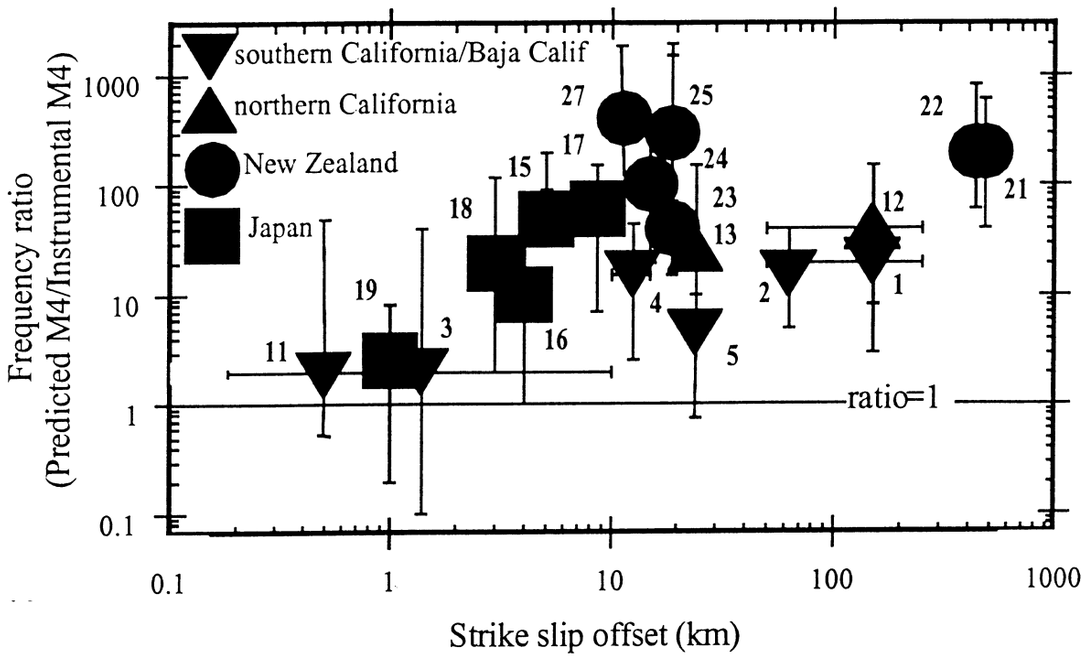
southern California/Baja Calif
northern California
New Zealand
Japan
Frequency ratio
(Predicted M4/Instrumental M4)
1000
100
10
1
0.1
0.1
1
10
100
1000
Strike slip offset (km)
ratio=1
11
19
3
18
15
17
27
25
24
23
13
4
16
5
2
12
1
22
21

FIGURE 9

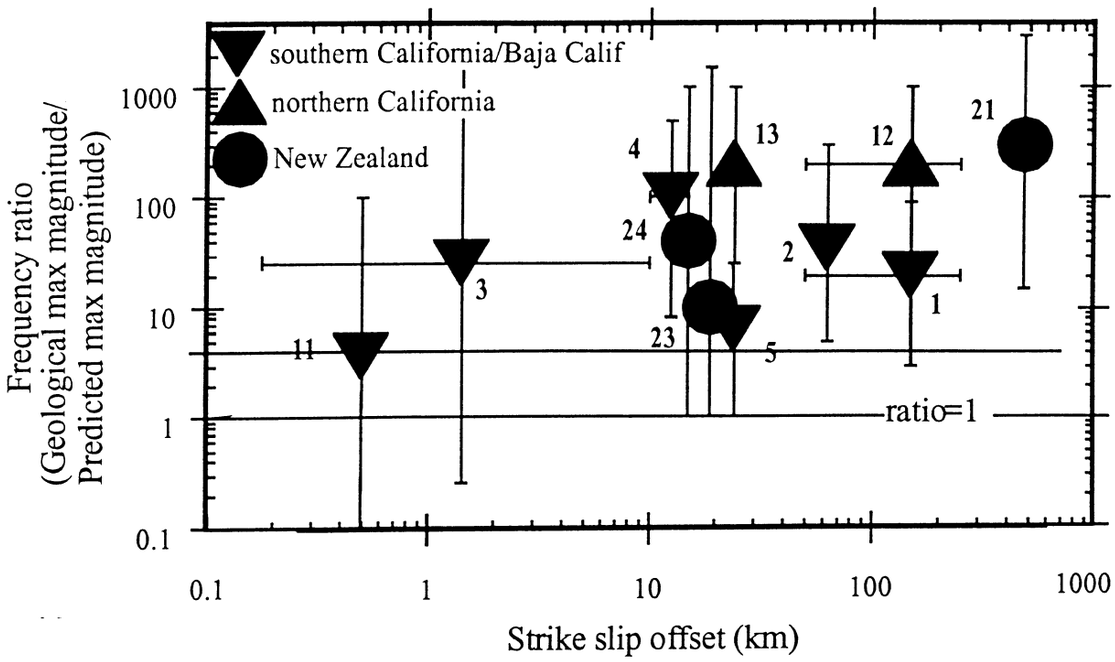
southern California/Baja Calif
northern California
New Zealand
Frequency ratio
(Geological max magnitude/
Predicted max magnitude)
1000
100
10
1
0.1
0.1
1
10
100
1000
Strike slip offset (km)
ratio=1
11
3
4
13
24
23
5
2
12
1
21

FIGURE 10

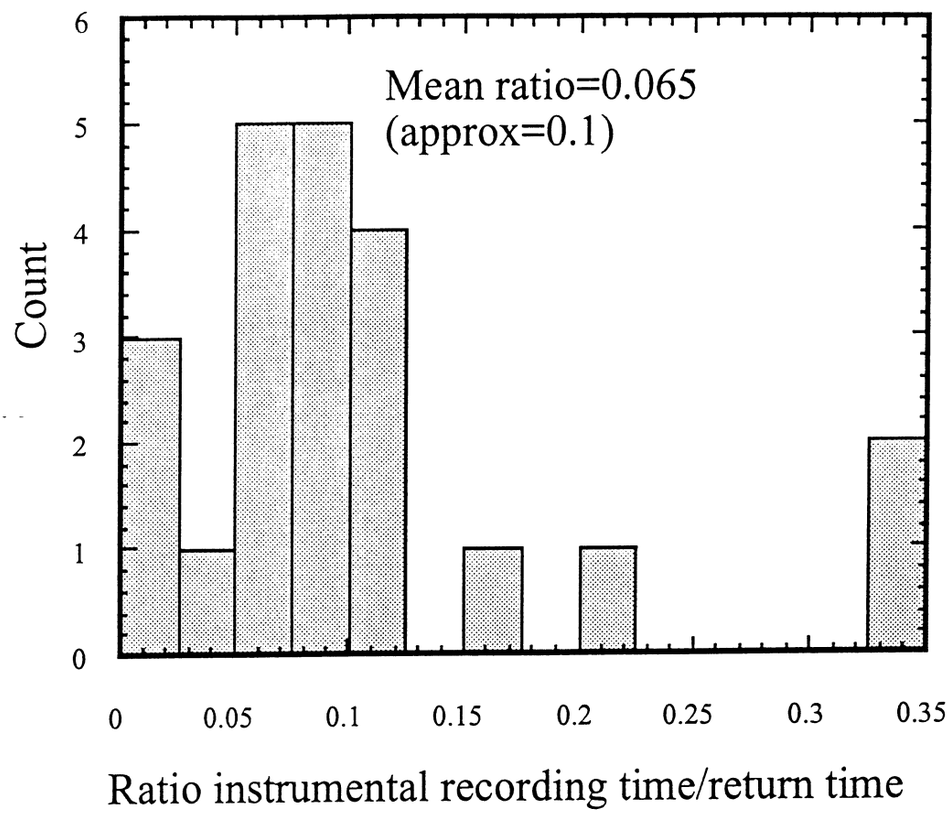
Mean ratio=0.065
(approx=0.1)
Count
0
1
2
3
4
5
6
0
0.05
0.1
0.15
0.2
0.25
0.3
0.35
Ratio instrumental recording time/return time

FIGURE 11A

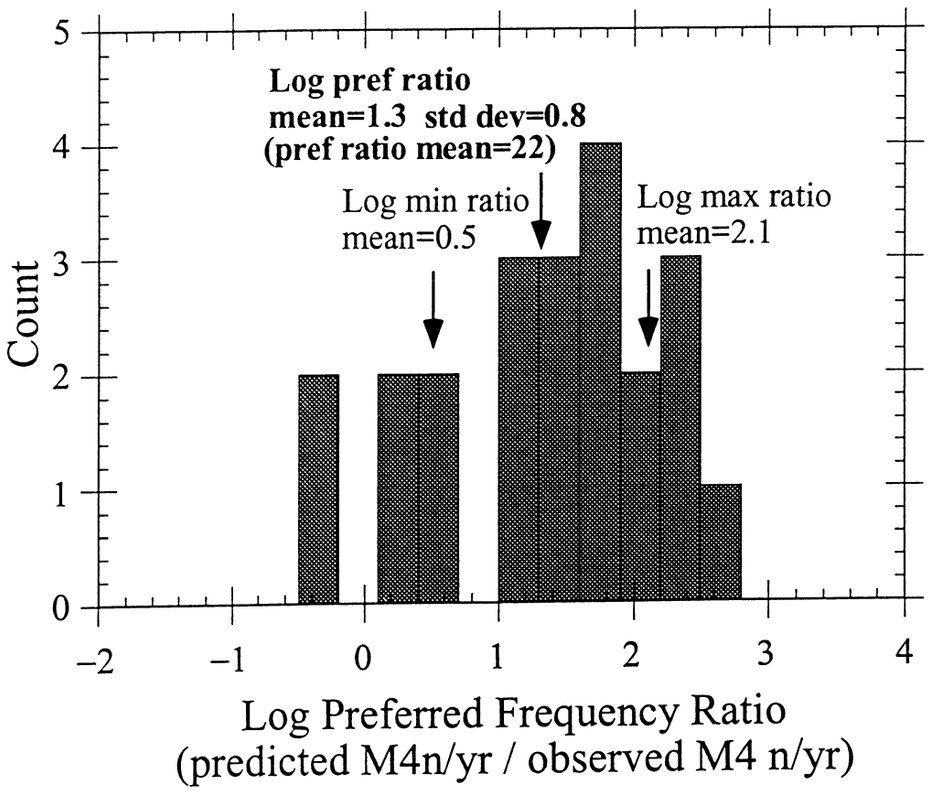
Log pref ratio
mean=1.3 std dev=0.8
(pref ratio mean=22)
Log min ratio
mean=0.5
Log max ratio
mean=2.1
Count
0
1
2
3
4
5
−2
−1
0
1
2
3
4
Log Preferred Frequency Ratio
(predicted M4n/yr / observed M4 n/yr)

FIGURE 11B

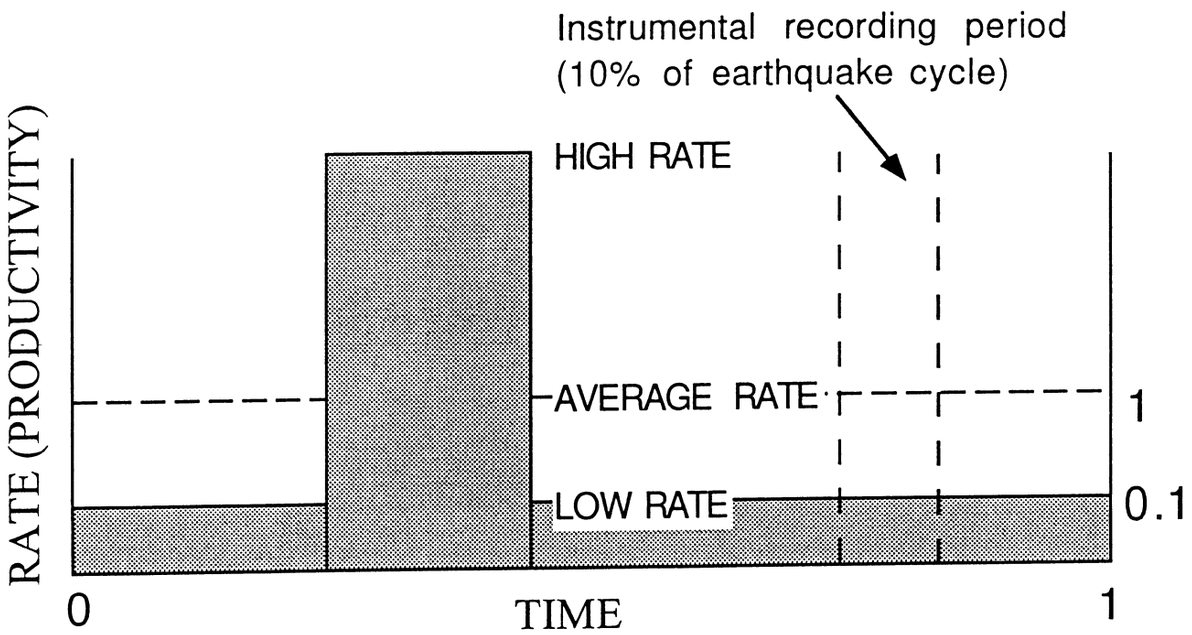
Instrumental recording period
(10% of earthquake cycle)
HIGH RATE
AVERAGE RATE
LOW RATE
RATE (PRODUCTIVITY)
1
0.1
0
TIME
1

FIGURE 11C

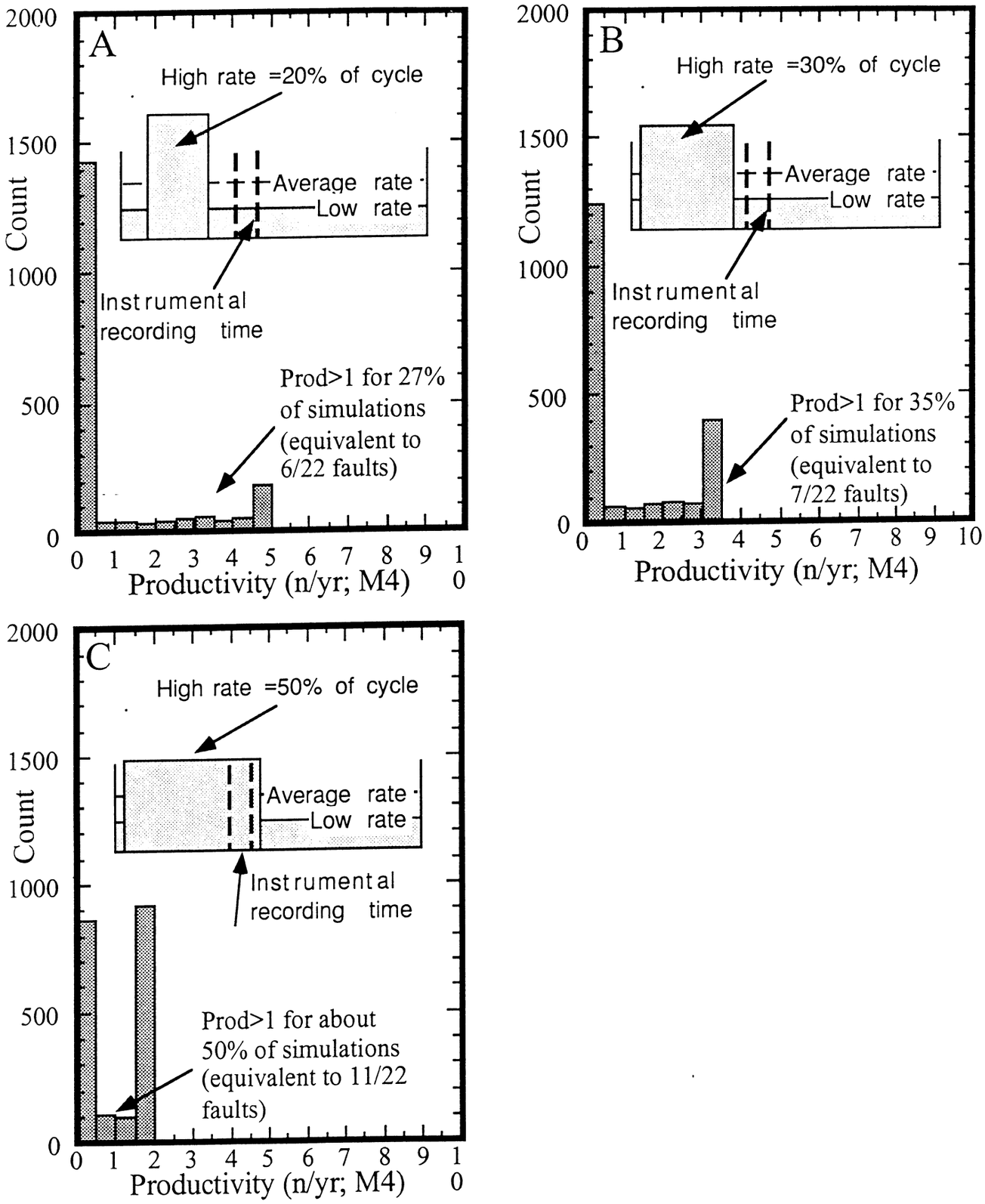
A
High rate =20% of cycle
Average rate
Low rate
Instrumental recording time
Prod>1 for 27% of simulations (equivalent to 6/22 faults)
Count
Productivity (n/yr; M4)
B
High rate =30% of cycle
Average rate
Low rate
Instrumental recording time
Prod>1 for 35% of simulations (equivalent to 7/22 faults)
Count
Productivity (n/yr; M4)
C
High rate =50% of cycle
Average rate
Low rate
Instrumental recording time
Prod>1 for about 50% of simulations (equivalent to 11/22 faults)
Count
Productivity (n/yr; M4)

FIGURE 12

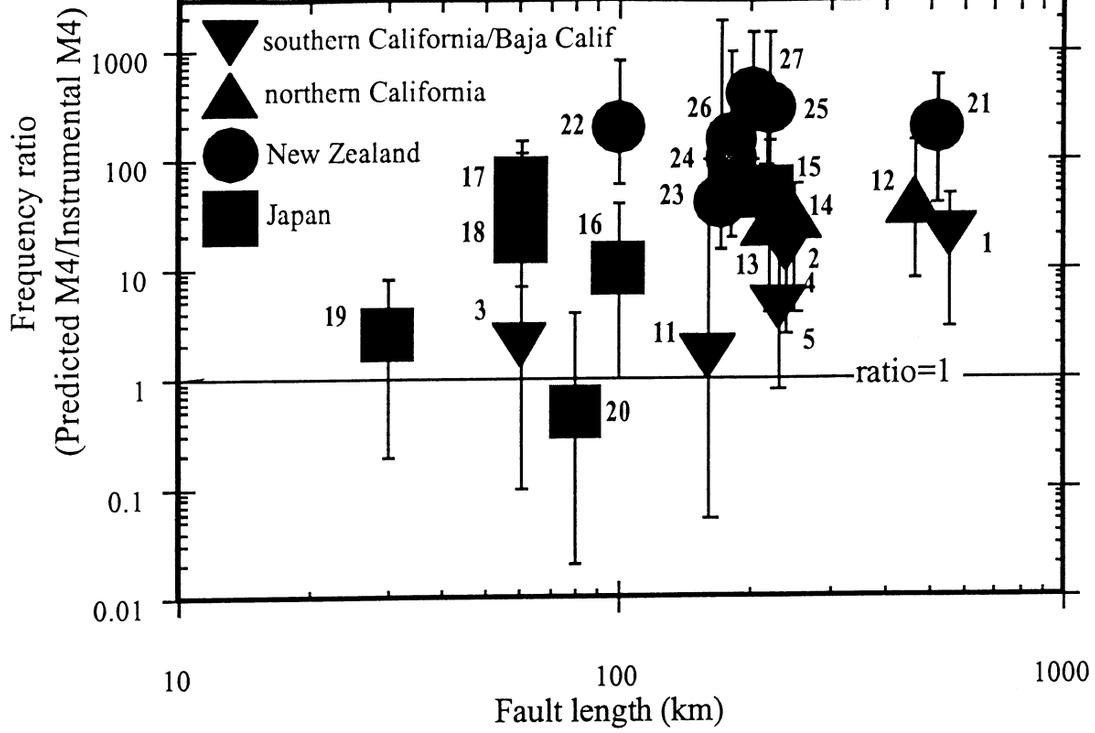
southern California/Baja Calif
northern California
New Zealand
Japan
Frequency ratio
(Predicted M4/Instrumental M4)
1000
100
10
1
0.1
0.01
ratio=1
10
100
1000
Fault length (km)
1
2
3
4
5
11
12
13
14
15
16
17
18
19
20
21
22
23
24
25
26
27

FIGURE 13

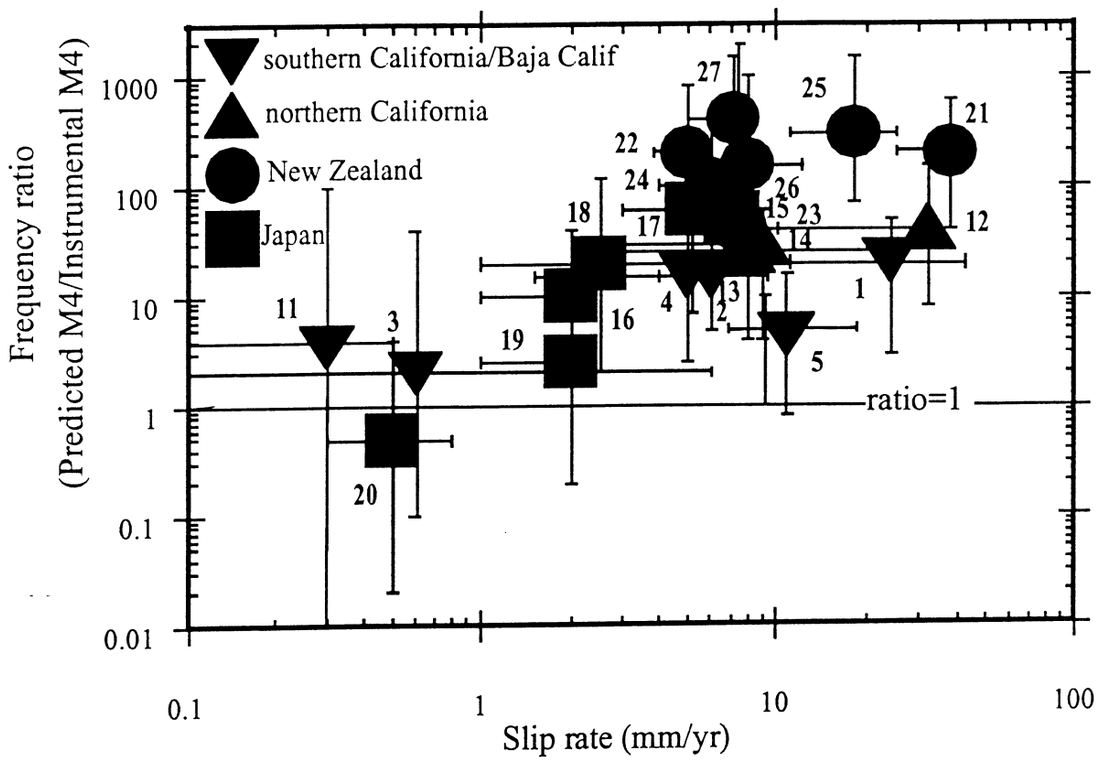
southern California/Baja Calif
northern California
New Zealand
Japan
Frequency ratio
(Predicted M4/Instrumental M4)
1000
100
10
1
0.1
0.01
0.1
1
10
100
Slip rate (mm/yr)
ratio=1
1
2
3
4
5
11
12
14
15
16
17
18
19
20
21
22
23
24
25
26
27

FIGURE 14

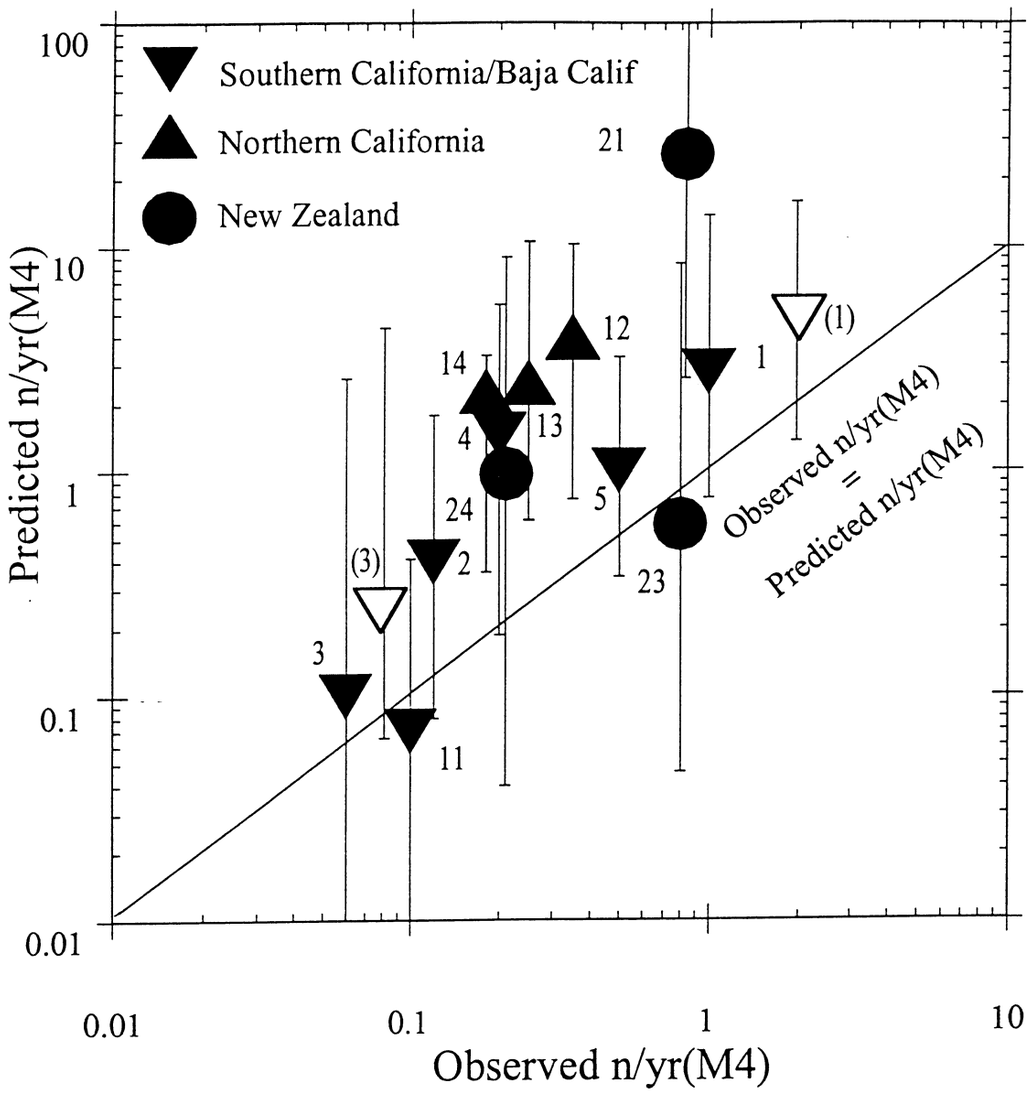
Southern California/Baja Calif
Northern California
New Zealand
Observed n/yr(M4)
=
Predicted n/yr(M4)
Predicted n/yr(M4)
Observed n/yr(M4)
100
10
1
0.1
0.01
0.01
0.1
1
10
21
1
(1)
12
14
13
4
5
24
2
(3)
23
3
11

FIGURE 15

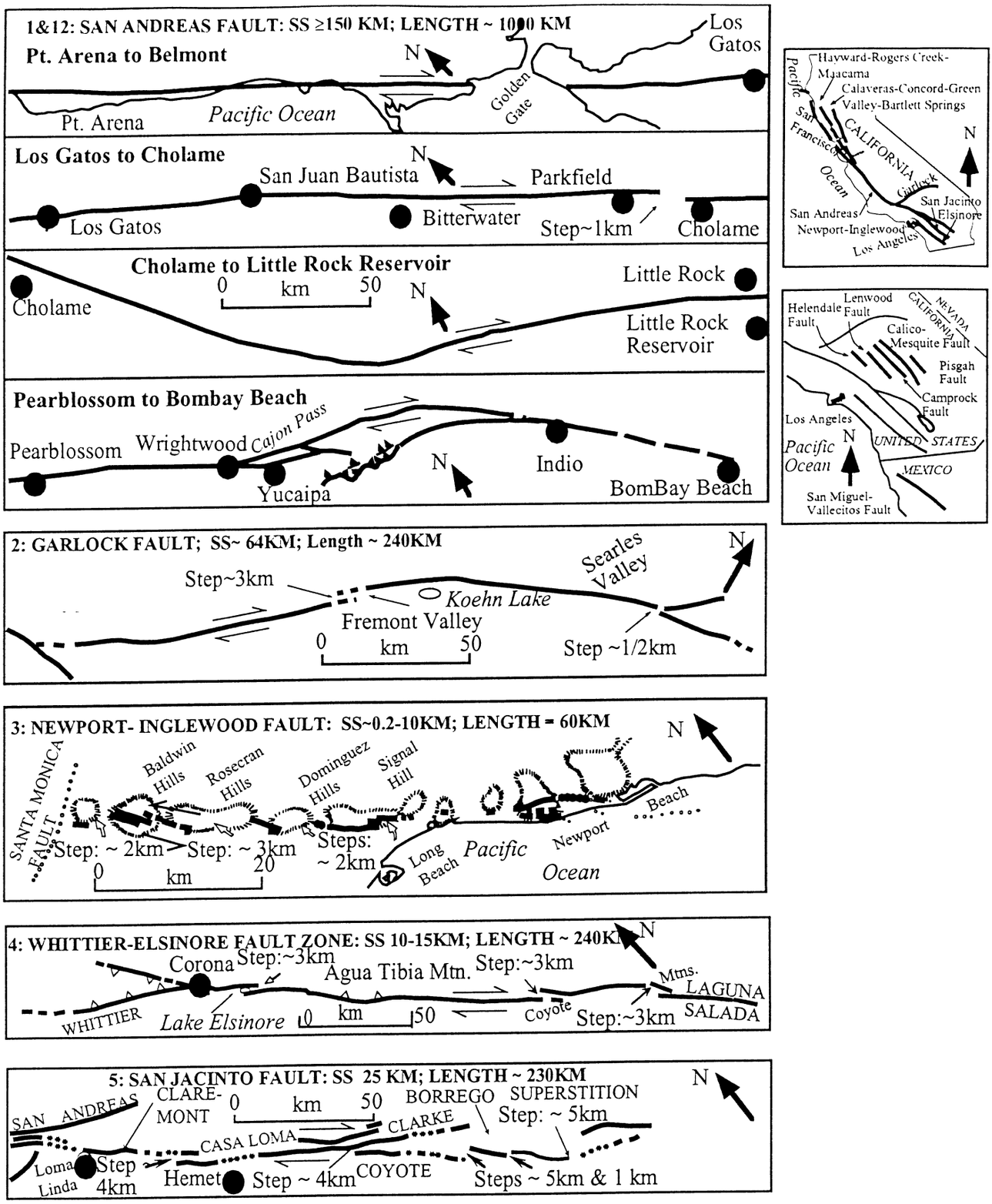
1&12: SAN ANDREAS FAULT: SS ≥150 KM; LENGTH ~ 1000 KM
Pt. Arena to Belmont
N
Los Gatos
Golden Gate
Pt. Arena
Pacific Ocean
Los Gatos to Cholame
N
San Juan Bautista
Parkfield
Los Gatos
Bitterwater
Step~1km
Cholame
Cholame to Little Rock Reservoir
0 km 50
N
Little Rock
Cholame
Little Rock Reservoir
Pearblossom to Bombay Beach
Pearblossom
Wrightwood
Cajon Pass
N
Indio
Yucaipa
BomBay Beach
2: GARLOCK FAULT; SS~ 64KM; Length ~ 240KM
Step~3km
Koehn Lake
Searles Valley
N
Fremont Valley
0 km 50
Step ~1/2km
3: NEWPORT- INGLEWOOD FAULT: SS~0.2-10KM; LENGTH = 60KM
N
SANTA MONICA FAULT
Baldwin Hills
Rosecran Hills
Dominguez Hills
Signal Hill
Step: ~ 2km
Step: ~ 3km
Steps: ~ 2km
0 km 20
Long Beach
Pacific Ocean
Newport Beach
4: WHITTIER-ELSINORE FAULT ZONE: SS 10-15KM; LENGTH ~ 240KM
N
Corona
Step:~3km
Agua Tibia Mtn.
Step:~3km
Mtns.
LAGUNA SALADA
WHITTIER
Lake Elsinore
0 km 50
Coyote
Step:~3km
5: SAN JACINTO FAULT: SS 25 KM; LENGTH ~ 230KM
N
SAN ANDREAS
CLARE-MONT
0 km 50
BORREGO
SUPERSTITION
Step: ~ 5km
CLARKE
CASA LOMA
Loma Linda
Step 4km
Hemet
Step ~ 4km
COYOTE
Steps ~ 5km & 1 km
Hayward-Rogers Creek-Maacama
Calaveras-Concord-Green Valley-Bartlett Springs
Pacific
San Francisco
CALIFORNIA
Ocean
N
Garlock
San Andreas
San Jacinto
Elsinore
Newport-Inglewood
Los Angeles
Lenwood Fault
NEVADA
CALIFORNIA
Helendale Fault
Calico-Mesquite Fault
Pisgah Fault
Camprock Fault
Los Angeles
N
UNITED STATES
Pacific Ocean
MEXICO
San Miguel-Vallecitos Fault

FIGURE A1

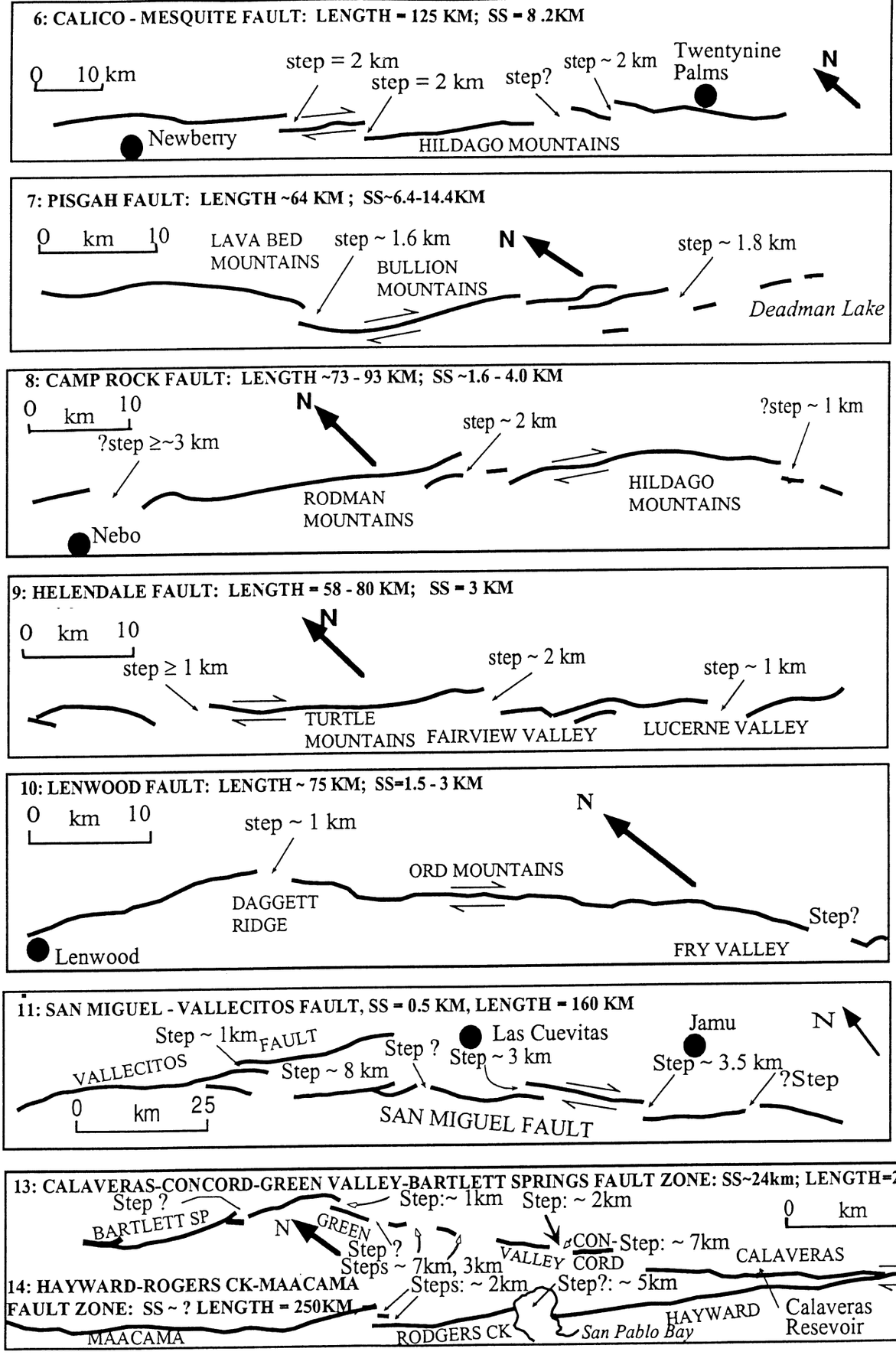
6: CALICO - MESQUITE FAULT: LENGTH = 125 KM; SS = 8 .2KM
0 10 km
step = 2 km
step = 2 km
step?
step ~ 2 km
Twentynine Palms
N
Newberry
HILDAGO MOUNTAINS
7: PISGAH FAULT: LENGTH ~64 KM ; SS~6.4-14.4KM
0 km 10
LAVA BED MOUNTAINS
step ~ 1.6 km
BULLION MOUNTAINS
N
step ~ 1.8 km
Deadman Lake
8: CAMP ROCK FAULT: LENGTH ~73 - 93 KM; SS ~1.6 - 4.0 KM
0 km 10
N
?step ≥~3 km
step ~ 2 km
?step ~ 1 km
RODMAN MOUNTAINS
HILDAGO MOUNTAINS
Nebo
9: HELENDALE FAULT: LENGTH = 58 - 80 KM; SS = 3 KM
0 km 10
N
step ≥ 1 km
step ~ 2 km
step ~ 1 km
TURTLE MOUNTAINS
FAIRVIEW VALLEY
LUCERNE VALLEY
10: LENWOOD FAULT: LENGTH ~ 75 KM; SS=1.5 - 3 KM
0 km 10
step ~ 1 km
N
ORD MOUNTAINS
DAGGETT RIDGE
Step?
Lenwood
FRY VALLEY
11: SAN MIGUEL - VALLECITOS FAULT, SS = 0.5 KM, LENGTH = 160 KM
Step ~ 1km
FAULT
Las Cuevitas
Jamu
N
VALLECITOS
Step ?
Step ~ 3 km
Step ~ 8 km
Step ~ 3.5 km
?Step
0 km 25
SAN MIGUEL FAULT
13: CALAVERAS-CONCORD-GREEN VALLEY-BARTLETT SPRINGS FAULT ZONE: SS~24km; LENGTH=220km
Step ?
Step:~ 1km
Step: ~ 2km
0 km 50
BARTLETT SP
N
GREEN
Step ?
CON-
Step: ~ 7km
VALLEY
CORD
CALAVERAS
Steps ~ 7km, 3km
14: HAYWARD-ROGERS CK-MAACAMA
FAULT ZONE: SS ~ ? LENGTH = 250KM
Steps: ~ 2km
Step?: ~ 5km
HAYWARD
Calaveras Resevoir
MAACAMA
RODGERS CK
San Pablo Bay

FIGURE A1

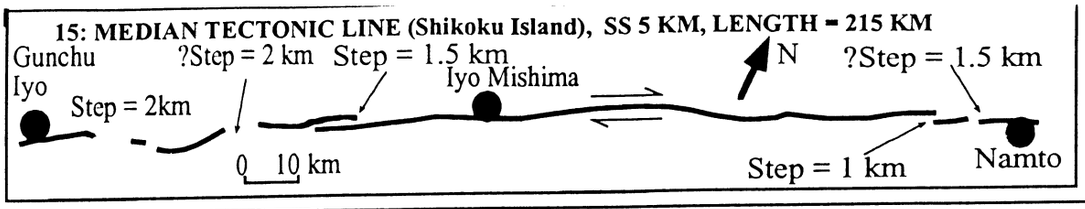
15: MEDIAN TECTONIC LINE (Shikoku Island), SS 5 KM, LENGTH = 215 KM
Gunchu
Iyo
?Step = 2 km
Step = 1.5 km
Iyo Mishima
N
?Step = 1.5 km
Step = 2km
0 10 km
Step = 1 km
Namto

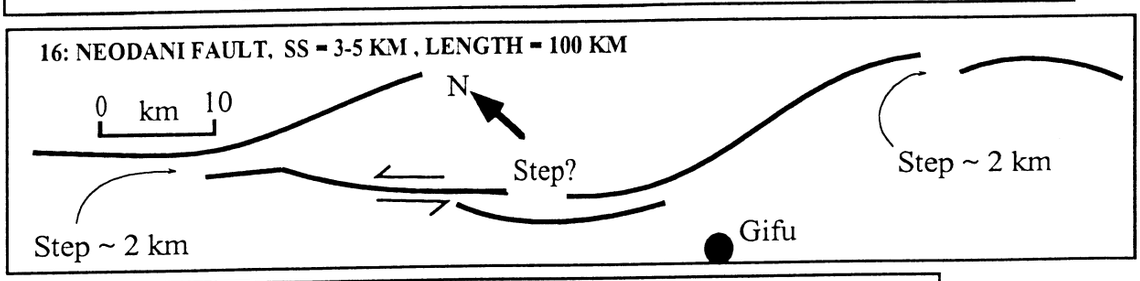
16: NEODANI FAULT, SS = 3-5 KM , LENGTH = 100 KM
0 km 10
N
Step?
Step ~ 2 km
Step ~ 2 km
Gifu

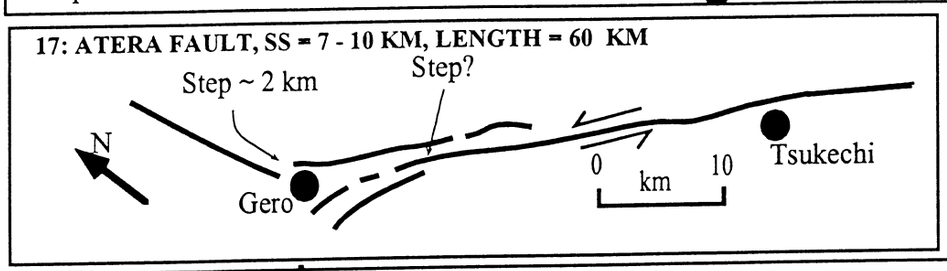
17: ATERA FAULT, SS = 7 - 10 KM, LENGTH = 60 KM
Step ~ 2 km
Step?
N
Gero
0 km 10
Tsukechi

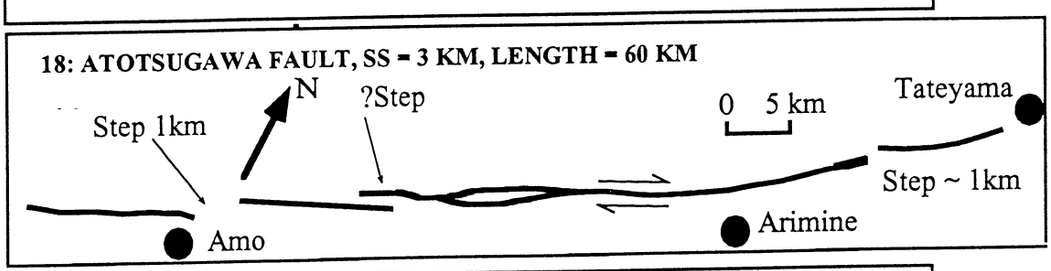
18: ATOTSUGAWA FAULT, SS = 3 KM, LENGTH = 60 KM
N
?Step
0 5 km
Tateyama
Step 1km
Step ~ 1km
Amo
Arimine

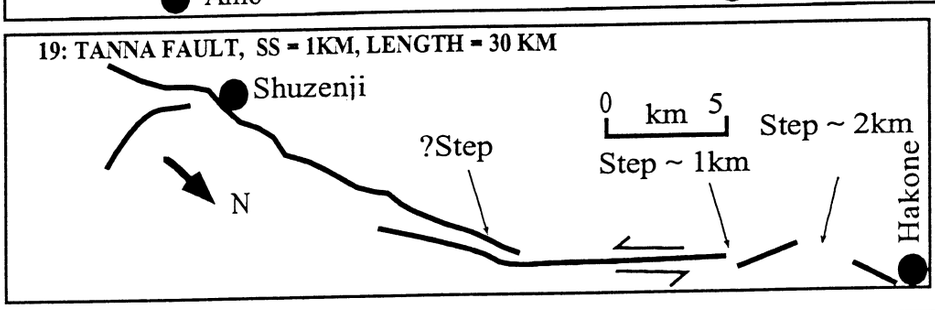
19: TANNA FAULT, SS = 1KM, LENGTH = 30 KM
Shuzenji
0 km 5
Step ~ 2km
?Step
Step ~ 1km
N
Hakone

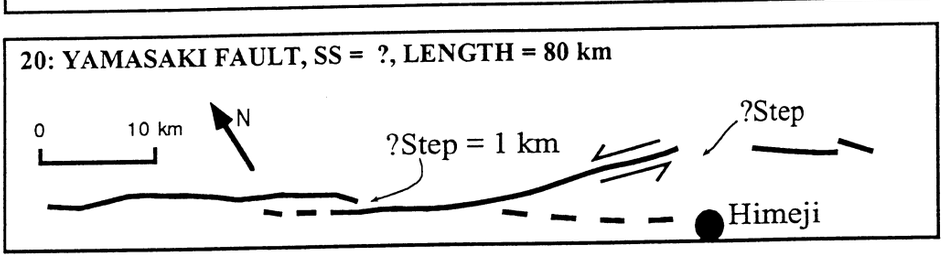
20: YAMASAKI FAULT, SS = ?, LENGTH = 80 km
0 10 km
N
?Step
?Step = 1 km
Himeji

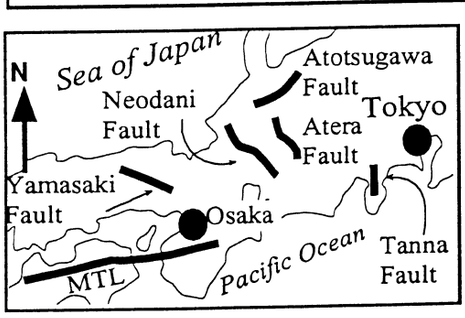
N
Sea of Japan
Atotsugawa Fault
Neodani Fault
Tokyo
Atera Fault
Yamasaki Fault
Osaka
MTL
Pacific Ocean
Tanna Fault

FIGURE A1

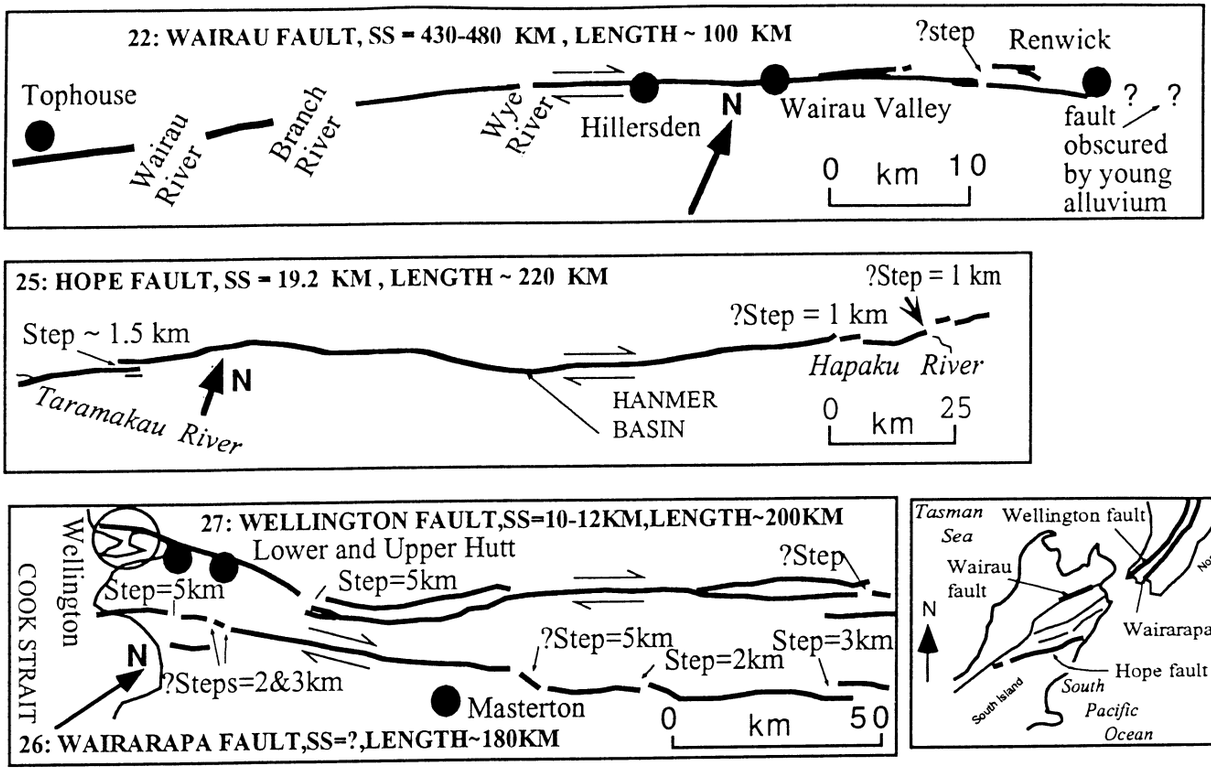
22: WAIRAU FAULT, SS = 430-480 KM , LENGTH ~ 100 KM
?step
Renwick
Tophouse
Wairau River
Branch River
Wye River
Hillersden
N
Wairau Valley
fault obscured by young alluvium
0 km 10
25: HOPE FAULT, SS = 19.2 KM , LENGTH ~ 220 KM
?Step = 1 km
?Step = 1 km
Step ~ 1.5 km
N
Hapaku River
Taramakau River
HANMER BASIN
0 km 25
27: WELLINGTON FAULT,SS=10-12KM,LENGTH~200KM
Lower and Upper Hutt
?Step
Step=5km
Step=5km
Wellington
COOK STRAIT
N
?Step=5km
Step=3km
Step=2km
?Steps=2&3km
Masterton
0 km 50
26: WAIRARAPA FAULT,SS=?,LENGTH~180KM
Tasman Sea
Wellington fault
Wairau fault
North Island
N
Wairarapa fault
Hope fault
South Island
South Pacific Ocean

FIGURE A1

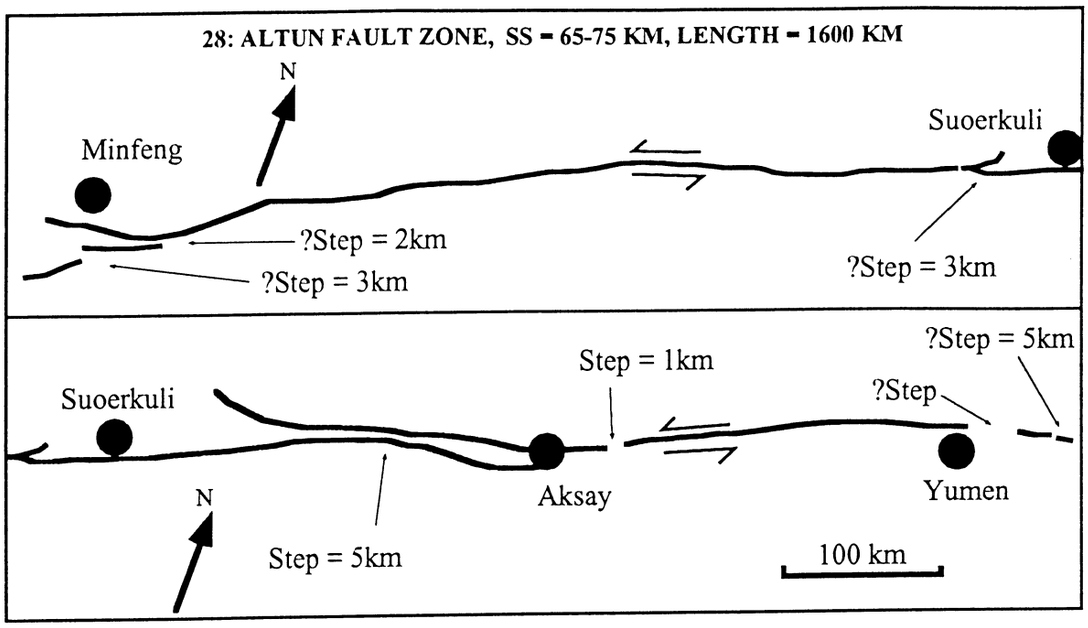
28: ALTUN FAULT ZONE, SS = 65-75 KM, LENGTH = 1600 KM
N
Minfeng
Suoerkuli
?Step = 2km
?Step = 3km
?Step = 3km
?Step = 5km
Step = 1km
?Step
Suoerkuli
Aksay
Yumen
N
Step = 5km
100 km

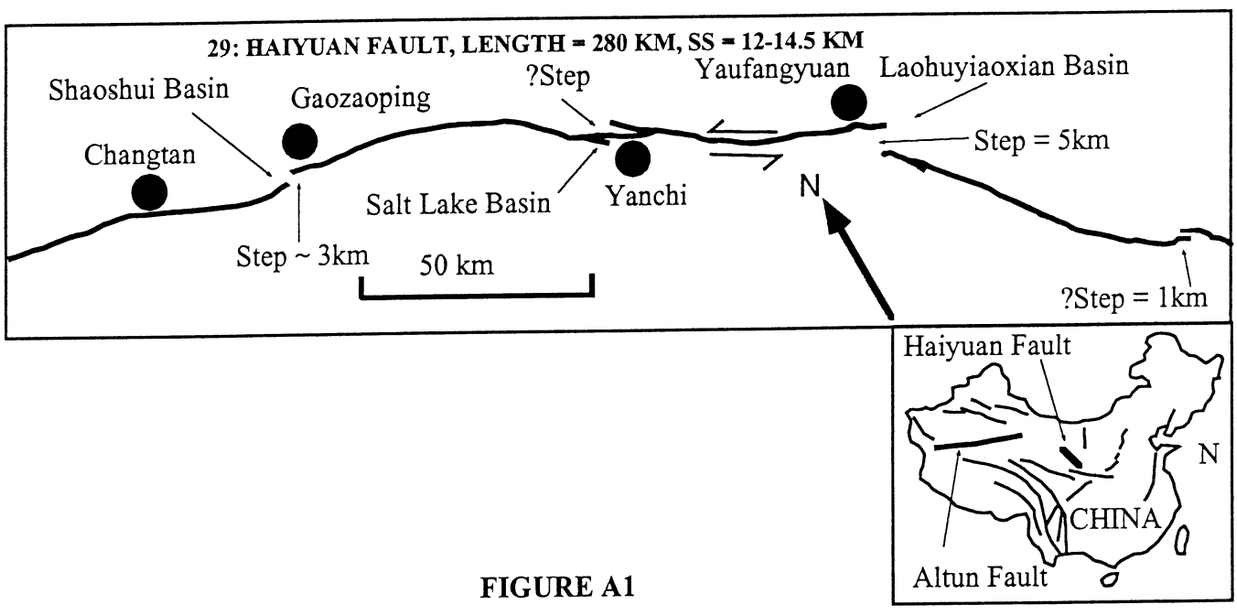
29: HAIYUAN FAULT, LENGTH = 280 KM, SS = 12-14.5 KM
Shaoshui Basin
Gaozaoping
?Step
Yaufangyuan
Laohuyiaoxian Basin
Changtan
Step = 5km
Salt Lake Basin
Yanchi
N
Step ~ 3km
50 km
?Step = 1km
Haiyuan Fault
N
CHINA
Altun Fault

FIGURE A1

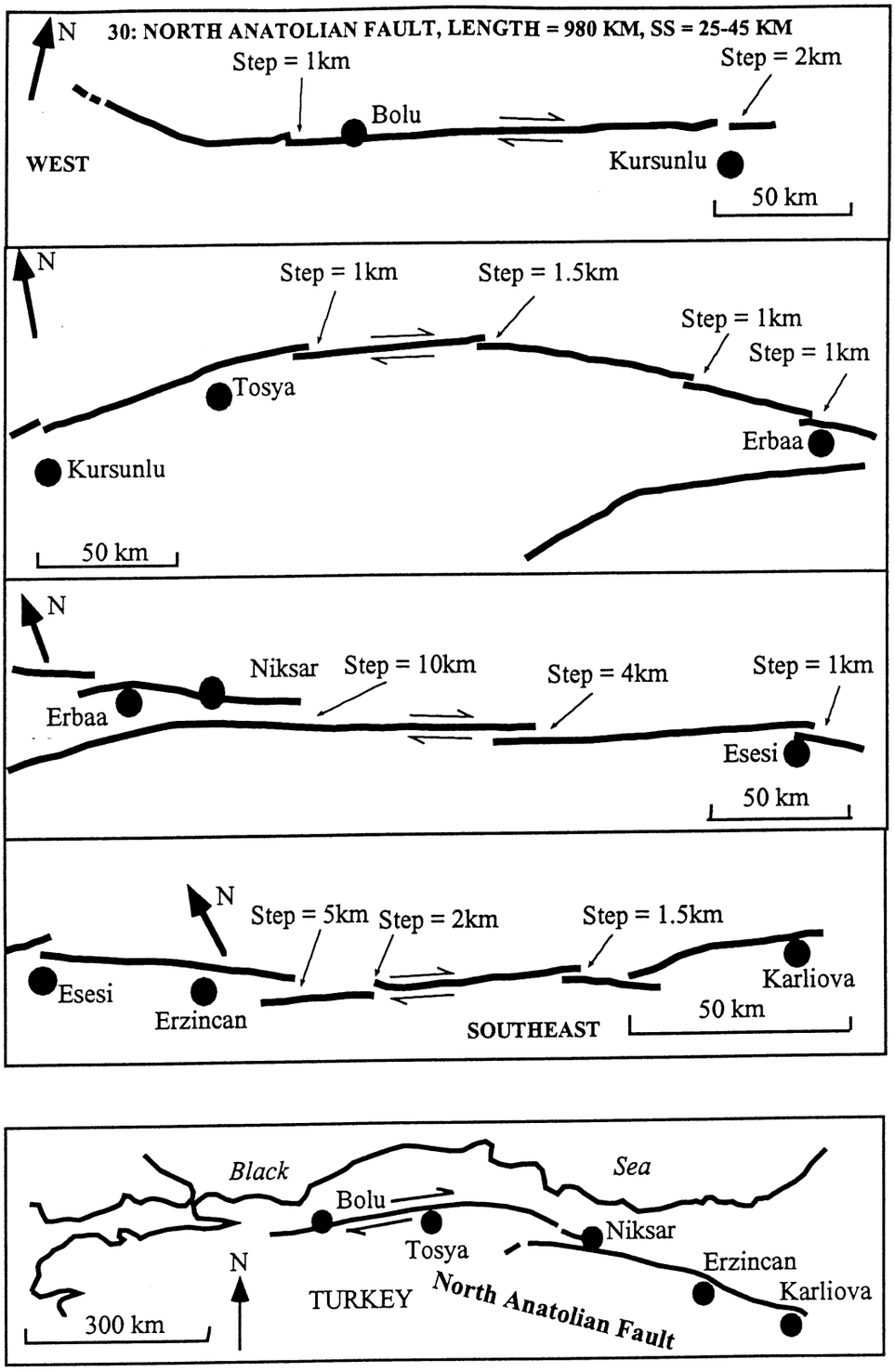
N
30: NORTH ANATOLIAN FAULT, LENGTH = 980 KM, SS = 25-45 KM
Step = 1km
Step = 2km
Bolu
WEST
Kursunlu
50 km
N
Step = 1km
Step = 1.5km
Step = 1km
Step = 1km
Tosya
Erbaa
Kursunlu
50 km
N
Niksar
Step = 10km
Step = 4km
Step = 1km
Erbaa
Esesi
50 km
N
Step = 5km
Step = 2km
Step = 1.5km
Karliova
Esesi
Erzincan
SOUTHEAST
50 km

Black
Sea
Bolu
Niksar
Tosya
N
Erzincan
TURKEY
North Anatolian Fault
Karliova
300 km

FIGURE A1